

# **Integrated Groundwater/Surface Water Model for the Little Spokane Watershed – Water Bank Modeling and Decision Support Tool**

## **Model Development and Application Report**

Report prepared for:  
Department of Water Resources  
Spokane County  
1004 North Freya Street  
Spokane WA 99202



Prepared by:  
WEST Consultants Incorporated  
Earthfx Incorporated



12509 Bel-Red Road, Suite 100  
Bellevue, WA 98005



3363 Yonge Street  
Toronto, Ontario M4N 2M6

December 2018

## DISCLAIMER

This report presents the results of data compilation and computer simulations of a complex physical setting. Data errors and data gaps are likely present in the information supplied to WEST/Earthfx, and it was beyond the scope of this project to review each data measurement and infill all gaps. Models constructed from these data are limited by the quality and completeness of the information available at the time the work was performed. All computer models represent a simplification of the actual hydrologic and hydrogeologic conditions. The applicability of the simplifying assumptions may or may not be suitable to a variety of end uses. The services performed by WEST/Earthfx Incorporated were conducted in a manner consistent with a level of care and skill ordinarily exercised by members of the environmental engineering and consulting profession.

This report does not exhaustively cover an investigation of all possible environmental conditions or circumstances that may exist in the study area. If a service is not expressly indicated, it should not be assumed that it was provided. It should be recognized that the passage of time affects the information provided in this report. Environmental conditions and the amount of data available can change. Any discussion relating to the conditions are based upon information that was provided at the time the conclusions were formulated.

This report was prepared by WEST Consultants Inc. and Earthfx Incorporated for the sole benefit of Spokane, Pend Oreille, and Stevens Counties. Any use that a third party makes of this report, any reliance thereon, or decisions made based on it, are the responsibility of such third parties. WEST/Earthfx accept no responsibility for damages, if any, suffered by any third party as a result of decisions made or actions taken based on this report.



Earth Science Information Systems

December 24, 2018

Mr. Mike Hermanson, Water Resources Manager  
Department of Water Resources  
1004 North Freya Street  
Spokane, WA 99202

RE: Integrated Groundwater/Surface Water Model for the Little Spokane Watershed – Model Development and Application Report

Dear Mr. Hermanson:

We are pleased to provide a copy of our final report titled: *Integrated Groundwater/Surface Water Model for the Little Spokane Watershed - Model Development and Application Report*. This report describes the physical setting, the conceptual hydrogeologic model, and the numerical model developed to simulate the surface water and groundwater systems in the Little Spokane Watershed. The model was calibrated to match observed streamflow and groundwater levels and has been tested on a series of water use and climate change scenarios. These applications were intended to demonstrate the usefulness of the integrated model as a decision-support tool for future water use management.

We trust this work report meets with your satisfaction, and we look forward to discussing it with you. If you have any questions, please call.

Yours truly,

**West Consultants Inc.,**

Henry Hu, Ph.D., P.H., D.WRE  
Vice President and Manager, Bellevue Office

Raymond Walton, Ph.D., P.E., D.WRE  
Lead Water Resources Engineer

**Earthfx Incorporated**

Dirk Kassenaar, M.Sc., P.Eng.  
President, Earthfx Inc.

E.J. Wexler, M.Sc, M.S.E., P.Eng.  
Director of Modelling Services

## Table of Contents

<b>TABLE OF CONTENTS .....</b>	<b>IV</b>
<b>LIST OF TABLES .....</b>	<b>V</b>
<b>LIST OF FIGURES .....</b>	<b>VI</b>
<b>1 INTRODUCTION .....</b>	<b>1</b>
1.1 BACKGROUND .....	1
1.2 PROJECT DESCRIPTION .....	1
1.3 PROJECT OBJECTIVES AND SCOPE .....	1
1.4 TECHNICAL APPROACH .....	2
1.5 STUDY AREA EXTENTS AND MODEL BOUNDARY .....	2
1.6 REPORT SCOPE AND STRUCTURE .....	3
1.7 PREVIOUS INVESTIGATIONS .....	3
1.8 ACKNOWLEDGEMENTS .....	4
1.1 FIGURES .....	5
<b>2 WATERSHED OVERVIEW .....</b>	<b>7</b>
2.1 TOPOGRAPHY AND PHYSIOGRAPHY .....	7
2.2 CURRENT LAND USE .....	8
2.3 AGRICULTURAL LAND USE .....	8
2.4 TABLES .....	1
2.5 FIGURES .....	3
<b>3 GEOLOGICAL AND HYDROGEOLOGIC SETTING .....</b>	<b>11</b>
3.1 KEY GEOLOGIC UNITS .....	11
3.2 HYDROGEOLOGIC UNITS .....	14
3.3 HYDROSTRATIGRAPHIC MODEL SURFACES .....	15
3.1 GROUNDWATER FLOW REGIMES .....	17
3.2 TABLES .....	20
3.3 FIGURES .....	22
<b>4 CLIMATIC AND HYDROLOGIC SETTING .....</b>	<b>59</b>
4.1 CLIMATE DATA .....	59
4.2 HYDROLOGIC SETTING .....	61
4.3 TABLES .....	64
4.4 FIGURES .....	67
<b>5 WATER USE MANAGEMENT .....</b>	<b>84</b>
5.1 BACKGROUND .....	84
5.2 WATER RIGHTS IN WASHINGTON STATE .....	85
5.3 WATER BANKING .....	86
5.4 FIGURES .....	87
<b>6 INTEGRATED MODEL DEVELOPMENT OVERVIEW .....</b>	<b>89</b>
6.1 INTRODUCTION .....	89
6.2 INTEGRATED MODELLING - OVERVIEW .....	89
6.3 USGS GSFLOW OVERVIEW .....	90
6.4 GSFLOW MODEL DEVELOPMENT PROCESS .....	95
<b>7 HYDROLOGIC SUBMODEL DEVELOPMENT .....</b>	<b>96</b>
7.1 INTRODUCTION .....	96
7.2 SUBMODEL DESCRIPTION .....	96
7.3 HYDROLOGIC PROCESSES .....	97
7.4 CLIMATE INPUTS .....	101
7.5 PARAMETER ASSIGNMENT FOR THE HYDROLOGIC SUBMODEL .....	101
7.6 TABLES .....	108
7.7 FIGURES .....	111
<b>8 GROUNDWATER FLOW SUBMODEL DEVELOPMENT .....</b>	<b>136</b>
8.1 GROUNDWATER FLOW EQUATION .....	136
8.2 SUBMODEL DESCRIPTION: MODFLOW-NWT .....	137
8.3 MODEL DISCRETIZATION .....	138

8.4	MODEL BOUNDARY CONDITIONS .....	138
8.5	SIMULATED SURFACE WATER AND GROUNDWATER WITHDRAWALS .....	142
8.6	MODEL PARAMETERIZATION .....	144
8.7	FIGURES .....	147
<b>9</b>	<b>INTEGRATED GSFLOW MODEL CALIBRATION .....</b>	<b>163</b>
9.1	CALIBRATION STRATEGY AND TARGETS .....	163
9.2	GSFLOW OUTPUTS .....	168
9.3	WATER BUDGET ASSESSMENT .....	169
9.4	LIMITATIONS .....	171
9.5	TABLES .....	174
9.6	FIGURES .....	178
<b>10</b>	<b>MODEL SCENARIOS .....</b>	<b>220</b>
10.1	INTRODUCTION .....	220
10.2	INCREASED DOMESTIC WATER USE .....	221
10.3	WATER RIGHTS RETIREMENT .....	222
10.4	AQUIFER RECHARGE PROJECTS .....	223
10.5	FUTURE CLIMATE CHANGE .....	224
10.6	FIGURES .....	227
<b>11</b>	<b>CONCLUSIONS .....</b>	<b>248</b>
<b>12</b>	<b>REFERENCES .....</b>	<b>251</b>

## List of Tables

TABLE 2.1: LAND USE WITHIN THE STUDY AREA (FROM NLCD, 2011).....	1
TABLE 2.2: CROP TYPES WITHIN THE STUDY AREA (FROM NLCD, 2011). .....	2
TABLE 3.1: SIMPLIFIED GEOLOGIC FRAMEWORK AND TIME SCALE (MODIFIED FROM KAHLE <i>ET AL.</i> , 2013).....	11
TABLE 3.2: SUMMARY OF TRANSIENT MONITORS. ....	18
TABLE 3.3: BRIEF DESCRIPTION OF GEOLOGIC UNITS (MODIFIED FROM KAHLE <i>ET AL.</i> , 2013).....	20
TABLE 3.4: BRIEF DESCRIPTION OF HYDROSTRATIGRAPHIC UNITS (MODIFIED FROM KAHLE <i>ET AL.</i> , 2013).....	21
TABLE 4.1: BASIN-AVERAGED ANNUAL PRECIPITATION WITH VARIOUS OBSERVATION PERIODS. ....	60
TABLE 4.2: CLIMATE STATIONS PROXIMAL TO THE STUDY WATERSHED. ....	64
TABLE 4.3: STREAMFLOW GAGES AND CATCHMENT SIZE. ....	66
TABLE 6.1: PROCESSES AND GSFLOW SUBMODELS. ....	90
TABLE 7.1: HYDROLOGIC SUBMODEL LOOKUP TABLE FOR PARAMETERS BASED ON LAND COVER (NLCD (2011)). ....	108
TABLE 7.2: HYDROLOGIC SUBMODEL LOOKUP TABLE FOR PARAMETERS BASED ON SURFICIAL GEOLOGY MAPPING. ....	109
TABLE 7.3: LOOKUP TABLE TO ASSIGN CN VALUES BASED ON LAND COVER AND SOIL CLASSES. ....	110
TABLE 8.1: SUMMARY OF MONTHLY AVERAGE SIMULATED GROUNDWATER PUMPING. ....	143
TABLE 8.2: SUMMARY OF MONTHLY AVERAGE SIMULATED SURFACE WATER DIVERSIONS. ....	144
TABLE 8.3: REPRESENTATIVE RANGES OF HYDRAULIC CONDUCTIVITY. ....	145
TABLE 8.4: FINAL CALIBRATED MODEL PARAMETER VALUES. ....	146
TABLE 9.1: STREAMFLOW CALIBRATION STATISTICS FOR THE GSFLOW MODEL. ....	174
TABLE 9.2: SUMMARY OF SPOT FLOW MEASUREMENTS AND AVERAGE SIMULATED FLOW. ....	175
TABLE 9.3: CALIBRATION STATISTICS FOR THE GROUNDWATER SUBMODEL. ....	176
TABLE 9.4: GROUNDWATER BUDGET FOR THE LITTLE SPOKANE RIVER WATERSHED, AS SIMULATED BY THE MODFLOW SUBMODEL, FOR WY2004 TO WY2017. ....	176
TABLE 9.5: GROUNDWATER BUDGET FOR THE LITTLE SPOKANE RIVER WATERSHED, AS SIMULATED BY GSFLOW, FOR WY2004 TO WY2017. ....	177
TABLE 10.1: SUMMARY OF MONTHLY AVERAGE SIMULATED GROUNDWATER PUMPING. ....	221
TABLE 10.2: RETIRED WATER RIGHTS FOR SCENARIO 2.....	222
TABLE 10.3: PROJECTED 2050 TEMPERATURE (°F) AND PRECIPITATION INCREASES (PERCENTAGE) FOR RCP 6.0 EAST OF THE CASCADES. ....	225

## List of Figures

FIGURE 1.1: LITTLE SPOKANE RIVER WATERSHED - WATER RESOURCE INVENTORY AREA - WRIA 55. ....	5
FIGURE 1.2: EXTENTS OF THE LITTLE SPOKANE RIVER (LSR) MODEL AREA. ....	6
FIGURE 2.1: STREAMS AND SUBWATERSHEDS DELINEATED IN THE STUDY AREA. ....	3
FIGURE 2.2: LAKES AND WETLANDS IN THE NORTHERN PART OF THE STUDY AREA. ....	4
FIGURE 2.3: LAKES AND WETLANDS IN THE SOUTHERN PART OF THE STUDY AREA. ....	5
FIGURE 2.4: LAND SURFACE TOPOGRAPHY IN THE STUDY AREA. ....	6
FIGURE 2.5: HYPSONETRIC PROFILE OF THE LITTLE SPOKANE RIVER WATERSHED. ....	7
FIGURE 2.6: ELEVATION PROFILE OF THE LITTLE SPOKANE RIVER AND PRINCIPAL TRIBUTARIES. ....	7
FIGURE 2.7: KEY PHYSIOGRAPHIC FEATURES OF THE STUDY AREA AND THE BEDROCK HIGHLANDS. ....	8
FIGURE 2.8: LAND COVER CLASSIFICATION FOR THE STUDY AREA BASED ON NLCD (2011). ....	9
FIGURE 2.9: SUMMARY OF LAND USE (TOP) AND CROP TYPE (BOTTOM) WITHIN THE WITHIN THE STUDY AREA (BASED ON NLCD (2011)). ....	10
FIGURE 3.1: EXTENT OF GLACIAL ICE AND GLACIAL LAKES IN NORTHEASTERN WASHINGTON, IDAHO, AND WESTERN MONTANA (MODIFIED FROM KAHLE <i>ET AL.</i> (2013) AND U.S. FOREST SERVICE (2010)). ....	13
FIGURE 3.2: SCHEMATIC SHOWING SIMPLIFIED CONCEPTUAL HYDROSTRATIGRAPHIC MODEL (MODIFIED FROM KAHLE <i>ET AL.</i> , 2013). ....	15
FIGURE 3.3: GEOLOGIC MAP (MODIFIED FROM KAHLE <i>ET AL.</i> , 2013). ....	22
FIGURE 3.4: BEDROCK TOPOGRAPHY, AS INTERPOLATED FROM BOREHOLE DATA. ....	23
FIGURE 3.5: INTERPRETED THICKNESS OF THE MIOCENE, PLEISTOCENE, AND RECENT DEPOSITS. ....	24
FIGURE 3.6: TOP OF THE GRANDE RONDE BASALT. ....	25
FIGURE 3.7: TOP OF THE WANAPUM BASALT AND TOP OF MIOCENE UNCONFORMITY. ....	26
FIGURE 3.8: INTERPRETED THICKNESS OF THE PLEISTOCENE AND RECENT DEPOSITS. ....	27
FIGURE 3.9: INTERPRETED THICKNESS OF THE UPPER AQUIFER WITHIN THE STUDY AREA. ....	28
FIGURE 3.10: INTERPRETED THICKNESS OF THE UPPER CONFINING UNIT WITHIN THE STUDY AREA. ....	29
FIGURE 3.11: INTERPRETED THICKNESS OF THE LOWER AQUIFERS WITHIN THE STUDY AREA. ....	30
FIGURE 3.12: INTERPRETED THICKNESS OF THE LOWER CONFINING UNIT WITHIN THE STUDY AREA. ....	31
FIGURE 3.13: INTERPRETED THICKNESS OF THE WANAPUM BASALT WITHIN THE STUDY AREA. ....	32
FIGURE 3.14: INTERPRETED THICKNESS OF THE UPPER LATAH FORMATION WITHIN THE STUDY AREA. ....	33
FIGURE 3.15: INTERPRETED THICKNESS OF THE GRANDE RONDE BASALT WITHIN THE STUDY AREA. ....	34
FIGURE 3.16: INTERPRETED THICKNESS OF THE LOWER LATAH FORMATION WITHIN THE STUDY AREA. ....	35
FIGURE 3.17: INTERPRETED THICKNESS OF THE PRE-LATAH SANDS WITHIN THE STUDY AREA. ....	36
FIGURE 3.18: INTERPRETED THICKNESS OF THE WEATHERED BEDROCK BASED ON BOREHOLE LOGS. ....	37
FIGURE 3.19: LOCATIONS OF CROSS SECTIONS FROM KAHLE <i>ET AL.</i> (2013) AND RIVER SECTIONS. ....	38
FIGURE 3.20: GEOLOGIC CROSS SECTION A-A'. ....	39
FIGURE 3.21: GEOLOGIC CROSS SECTION C-C'. ....	40
FIGURE 3.22: GEOLOGIC CROSS SECTION C-C' FROM KAHLE <i>ET AL.</i> (2013). ....	41
FIGURE 3.23: GEOLOGIC SECTION ALONG THE MAIN BRANCH OF THE LITTLE SPOKANE RIVER. ....	42
FIGURE 3.24: GEOLOGIC SECTION ALONG DRAGOON CREEK. ....	43
FIGURE 3.25: WELLS WITH STATIC WATER LEVELS COMPLETED IN KEY HYDROGEOLOGIC UNITS. ....	44
FIGURE 3.26: INTERPOLATED STATIC WATER LEVELS IN THE UPPER AQUIFER. ....	45
FIGURE 3.27: INTERPOLATED STATIC WATER LEVELS IN THE LOWER AQUIFERS. ....	46
FIGURE 3.28: INTERPOLATED STATIC WATER LEVELS IN THE GRANDE RONDE BASALT AQUIFER. ....	47
FIGURE 3.29: INTERPOLATED STATIC WATER LEVELS IN THE BEDROCK AQUIFER. ....	48
FIGURE 3.30: ESTIMATION VARIANCE FOR WATER LEVELS IN THE UPPER AQUIFER. ....	49
FIGURE 3.31: ESTIMATION VARIANCE FOR WATER LEVELS IN THE LOWER AQUIFERS. ....	50
FIGURE 3.32: ESTIMATION VARIANCE FOR WATER LEVELS IN THE GRANDE RONDE BASALT AQUIFER. ....	51
FIGURE 3.33: ESTIMATION VARIANCE FOR WATER LEVELS IN THE BEDROCK AQUIFER. ....	52
FIGURE 3.34: GROUNDWATER MONITORS WITH DATALOGGERS. ....	53
FIGURE 3.35: GROUNDWATER ELEVATION HYDROGRAPH FOR THE DOE-DEER PARK GRAND RONDE BASALT AQUIFER WELL. ....	54
FIGURE 3.36: GROUNDWATER ELEVATION HYDROGRAPH FOR THE DOE-CHATTAROY BEDROCK AQUIFER WELL. ....	54
FIGURE 3.37: GROUNDWATER ELEVATION HYDROGRAPH FOR THE WHITWORTH WATER-SHADY SLOPE LOWER AQUIFER WELL. ....	55
FIGURE 3.38: GROUNDWATER ELEVATION HYDROGRAPH AT SCWD#3 PINE RIVER. ....	55
FIGURE 3.39: GROUNDWATER ELEVATION HYDROGRAPH AT PINE RIVER PARK. ....	56
FIGURE 3.40: GROUNDWATER ELEVATION HYDROGRAPH FOR THE SCWD#3 RIVER ESTATES UPPER AQUIFER WELL. ....	56
FIGURE 3.41: GROUNDWATER ELEVATION HYDROGRAPH AT COLBERT LANDFILL. ....	57
FIGURE 3.42: GROUNDWATER ELEVATION HYDROGRAPH AT WHITWORTH WATER – NORTH MT. VIEW. ....	57
FIGURE 3.43: GROUNDWATER ELEVATION HYDROGRAPH FOR WHITWORTH WATER – RIVILLA. ....	58
FIGURE 4.1: CLIMATE STATIONS PROXIMAL TO THE STUDY AREA. ....	67
FIGURE 4.2: AVAILABLE PERIOD OF RECORD AT CLIMATE STATIONS PROXIMAL TO THE STUDY AREA (NOTE: SOME STATIONS DISCONTINUED PRIOR TO 1990). ....	68
FIGURE 4.3: ANNUAL AVERAGE INTERPOLATED PRECIPITATION (WY1892 THROUGH WY2016), HILL SHADED WITH THE 1000 FT DEM. ....	69
FIGURE 4.4: DAILY AVERAGE INTERPOLATED MEAN TEMPERATURE (WY1892 THROUGH WY2016), HILL SHADED WITH 1000 FT DEM. ....	70
FIGURE 4.5: BASIN AVERAGED TOTAL PRECIPITATION FROM WY1977 TO WY2016. ....	71
FIGURE 4.6: BASIN AVERAGED MAXIMUM (RED) AND MINIMUM (BLUE) DAILY TEMPERATURE FROM WY1977 TO WY2016. ....	72
FIGURE 4.7: MEAN ANNUAL PRECIPITATION (WY1895 - 2016). ....	73
FIGURE 4.8: WASHINGTON STATE PALMER DROUGHT SEVERITY INDEX. ....	73
FIGURE 4.9: BASIN-AVERAGED MEAN ANNUAL TEMPERATURE (WY1895 - 2016). ....	74
FIGURE 4.10: BASIN-AVERAGED MEAN ANNUAL TEMPERATURE AND PRECIPITATION (WY1895 - 2016). ....	74
FIGURE 4.11: ANNUAL SUMMARY OF BASIN-AVERAGED PRECIPITATION FORM (WY1895 - WY2016). ....	75
FIGURE 4.12: MEAN MONTHLY PRECIPITATION (WY1895 – WY2016). ....	75

FIGURE 4.13: MAXIMUM (ORANGE) AND MINIMUM (BLUE) MONTHLY TEMPERATURE (WY1895 - WY2016).....	76
FIGURE 4.14: BASIN-AVERAGED DAILY PRECIPITATION EXCEEDANCE PLOT (WY1895 THROUGH WY2016).....	76
FIGURE 4.15: PERENNIAL AND INTERMITTENT STREAMS (INCLUDES STREAMS CLASSIFIED AS "ARTIFICIAL").....	77
FIGURE 4.16: STREAMFLOW STATIONS WITH SEEPAGE RUN STATIONS, SPOT FLOW LOCATIONS WITH MULTIPLE MEASUREMENTS, AND GAGES WITH LONG-TERM DATA; AVERAGE FLOWS POSTED FOR GAGES.....	78
FIGURE 4.17: AVAILABLE PERIOD OF RECORD AT STREAMFLOW GAGES WITHIN THE STUDY AREA (USGS GAGES START PRIOR TO 1990)....	79
FIGURE 4.18: DAILY DISCHARGE OBSERVED AT THE USGS DARTFORD GAGE FOR WY1957 TO WY2016.....	80
FIGURE 4.19: ANNUAL AVERAGE STREAMFLOW AT THE USGS DARTFORD GAGE AND NUMBER OF DAYS PER YEAR WITH FLOW BELOW 115 CFS.....	81
FIGURE 4.20: BASIN-AVERAGED PRECIPITATION VERSUS STREAMFLOW AT THE DARTFORD GAGE.....	81
FIGURE 4.21: MONTHLY-AVERAGED DAILY STREAMFLOW FOR THE KEY GAGES.....	82
FIGURE 4.22: DAILY FLOW DURATION CURVES FOR STREAM GAUGES IN THE LITTLE SPOKANE RIVER WATERSHED.....	82
FIGURE 4.23: OBSERVED DAILY DISCHARGE AND ESTIMATED BASEFLOW DISCHARGE FOR WY2003 TO 2017 AT THE USGS GAUGE AT DARTFORD.....	83
FIGURE 5.1: POINTS OF WITHDRAWAL FROM THE WASHINGTON STATE GWIS.....	87
FIGURE 5.2: WATER RIGHT DOCUMENTATION ASSOCIATED WITH POINTS OF WITHDRAWAL.....	88
FIGURE 6.1: SCHEMATIC DIAGRAM OF THE GSFLOW PROCESS REGIONS.....	90
FIGURE 6.2: DIFFERENT GRID RESOLUTIONS ARE AVAILABLE FOR EACH PROCESS REGION WITHIN GSFLOW.....	91
FIGURE 6.3: GSFLOW PROCESS FLOWCHART.....	92
FIGURE 6.4: CHANGES IN THE SPRING AND SUMMER POSITION OF THE WATER TABLE INCREASING DUNNIAN RUNOFF AND THE SIZE OF THE "CONTRIBUTING AREA" (FROM MARKSTROM <i>ET AL.</i> , 2008).....	93
FIGURE 6.5: COMPUTATIONAL SEQUENCE FOR AN INTEGRATED PRMS/MODFLOW SIMULATION IN GSFLOW (MODIFIED FROM MARKSTROM <i>ET AL.</i> (2008)).....	95
FIGURE 7.1: PORTION OF THE PRMS GRID SHOWING THE 250 FT MESH.....	96
FIGURE 7.2: HYDROLOGICAL PROCESSES SIMULATED BY THE PRECIPITATION-RUNOFF MODELING SYSTEM (FROM MARKSTROM <i>ET AL.</i> , 2015).....	97
FIGURE 7.3: PRMS TWO-LAYER SNOWPACK CONCEPTUALIZATION AND THE COMPONENTS OF THE SNOWPACK ENERGY BALANCE, ACCUMULATION, SNOWMELT, AND SUBLIMATION ALGORITHMS (FROM MARKSTROM <i>ET AL.</i> , 2015).....	98
FIGURE 7.4: RUNOFF, ET, AND INTERFLOW PROCESSES IN THE SOIL ZONE AS A FUNCTION OF INCREASING MOISTURE CONTENT.....	99
FIGURE 7.5: AVERAGE DAILY GLOBAL SOLAR RADIATION FOR SPOKANE (1952-1976) (DATA FROM KNAPP, <i>ET AL.</i> , 1980) AND COMPOSITE (2001-2017) DATA.....	101
FIGURE 7.6: SOIL WATER ZONES IN PRMS AND GSFLOW (MODIFIED FROM MARKSTROM <i>ET AL.</i> , 2015).....	104
FIGURE 7.7: HRU ELEVATIONS (FROM USGS 23 FT DEM RESAMPLED TO PRMS GRID).....	111
FIGURE 7.8: DISTRIBUTION OF SLOPE (IN FT/FT). LARGE GREY AREAS WITH ZERO SLOPE ARE ARTIFACTS OF ORIGINAL DEM.....	112
FIGURE 7.9: DISTRIBUTION OF SLOPE ASPECT (VALUE OF 0 OR 360 INDICATES CELL IS FACING DUE NORTH).....	113
FIGURE 7.10: TOPOGRAPHY AND RESULTING CASCADE FLOW NETWORK NEAR ELOIKA LAKE.....	114
FIGURE 7.11: DISTRIBUTION OF SUMMER VEGETATION COVER DENSITY.....	115
FIGURE 7.12: DISTRIBUTION OF WINTER VEGETATION COVER DENSITY.....	116
FIGURE 7.13: DISTRIBUTION OF SUMMER RAIN INTERCEPTION STORAGE.....	117
FIGURE 7.14: DISTRIBUTION OF WINTER RAIN INTERCEPTION STORAGE.....	118
FIGURE 7.15: DISTRIBUTION OF WINTER SNOW INTERCEPTION STORAGE.....	119
FIGURE 7.16: DISTRIBUTION OF WINTER RADIATION TRANSMISSION COEFFICIENT.....	120
FIGURE 7.17: DISTRIBUTION OF SOIL ZONE THICKNESS (IN INCHES).....	121
FIGURE 7.18: DISTRIBUTION OF PERCENT IMPERVIOUSNESS (FROM NLCD, 2011).....	122
FIGURE 7.19: DISTRIBUTION OF SOIL ZONE POROSITY.....	123
FIGURE 7.20: DISTRIBUTION OF SOIL ZONE FIELD CAPACITY.....	124
FIGURE 7.21: DISTRIBUTION OF SOIL ZONE WILTING POINT.....	125
FIGURE 7.22: DISTRIBUTION OF MAXIMUM AVAILABLE SOIL MOISTURE FOR ET AND PLANT USE.....	126
FIGURE 7.23: SATURATION THRESHOLD (DRAINABLE POROSITY).....	127
FIGURE 7.24: DISTRIBUTION OF SOIL TYPE.....	128
FIGURE 7.25: DISTRIBUTION OF SCS SOIL CLASS (A-D).....	129
FIGURE 7.26: DISTRIBUTION OF SCS CN VALUES BASED ON LAND USE AND SOIL CLASS.....	130
FIGURE 7.27: DISTRIBUTION OF THE MAXIMUM DAILY SOIL ZONE PERCOLATION RATES (IN/D).....	131
FIGURE 7.28: LOCATION OF SNOW-DEPTH STATIONS AND SIMULATED DAILY SNOW DEPTH (INCHES) ON DECEMBER 30, 2004.....	132
FIGURE 7.29: OBSERVED AND SIMULATED SNOWPACK DEPTH (INCHES) AT (A) ELK AND (B) QUARTZ PEAK.....	133
FIGURE 7.30: FREQUENCY OF PRECIPITATION FORM WITH OBSERVED MAXIMUM DAILY TEMPERATURE AT CLIMATE STATIONS PROXIMAL TO THE STUDY AREA.....	134
FIGURE 7.31: FREQUENCY OF PRECIPITATION FORM WITH OBSERVED MINIMUM DAILY TEMPERATURE AT CLIMATE STATIONS PROXIMAL TO THE STUDY AREA.....	134
FIGURE 7.32: SIMULATED DAILY PET RATES CALCULATED BY PRMS USING THE MODIFIED JENSEN HAISE METHOD COMPARED WITH PET MEASUREMENTS AT CHAMOKANE AND DEER PARK USING THE PENMAN METHOD.....	135
FIGURE 8.1: STREAM NETWORK AND LAKE REPRESENTATION IN THE SFR2 AND LAK3 MODULES (MODIFIED FROM MARKSTROM, <i>ET AL.</i> , 2008).....	140
FIGURE 8.2: ESTIMATED CROSS-SECTIONS FOR THE SIX STRAHLER CLASSES.....	141
FIGURE 8.3: CUMULATIVE MUNICIPAL/COMMERCIAL MONTHLY WITHDRAWALS FROM 2005-2015.....	144
FIGURE 8.4: FINITE-DIFFERENCE GRID FOR THE LSR MODEL.....	147
FIGURE 8.5: BOUNDARY CONDITIONS FOR THE NUMERICAL GROUNDWATER FLOW SUBMODEL.....	148
FIGURE 8.6: SECTION C-C' SHOWING ASSIGNMENT OF AQUIFER UNITS TO NUMERICAL MODEL LAYERS.....	149
FIGURE 8.7: SECTION C-C' SHOWING ASSIGNMENT OF HYDRAULIC CONDUCTIVITY TO NUMERICAL MODEL LAYERS.....	150
FIGURE 8.8: STREAMBED HYDRAULIC CONDUCTIVITY.....	151
FIGURE 8.9: LOCATIONS OF GROUNDWATER WITHDRAWALS AND SURFACE WATER DIVERSIONS IN THE MODEL.....	152

FIGURE 8.10: HYDRAULIC CONDUCTIVITY DISTRIBUTION IN MODEL LAYER 1 .....	153
FIGURE 8.11: HYDRAULIC CONDUCTIVITY DISTRIBUTION IN MODEL LAYER 2 .....	154
FIGURE 8.12: HYDRAULIC CONDUCTIVITY DISTRIBUTION IN MODEL LAYER 3 .....	155
FIGURE 8.13: HYDRAULIC CONDUCTIVITY DISTRIBUTION IN MODEL LAYER 4 (GREY AREAS WITHIN THE MODEL BOUNDARY REPRESENT CELLS BENEATH THE UNWEATHERED BEDROCK UNIT) .....	156
FIGURE 8.14: HYDRAULIC CONDUCTIVITY DISTRIBUTION IN MODEL LAYER 5 .....	157
FIGURE 8.15: HYDRAULIC CONDUCTIVITY DISTRIBUTION IN MODEL LAYER 6 .....	158
FIGURE 8.16: HYDRAULIC CONDUCTIVITY DISTRIBUTION IN MODEL LAYER 7 .....	159
FIGURE 8.17: HYDRAULIC CONDUCTIVITY DISTRIBUTION IN MODEL LAYER 8 .....	160
FIGURE 8.18: HYDRAULIC CONDUCTIVITY DISTRIBUTION IN MODEL LAYER 9 .....	161
FIGURE 8.19: HYDRAULIC CONDUCTIVITY DISTRIBUTION IN MODEL LAYER 10 .....	162
FIGURE 9.1: GAGED CATCHMENTS WITHIN THE MODEL AREA USED IN THE LSR MODEL CALIBRATION .....	178
FIGURE 9.2: SIMULATED DAILY STREAMFLOW (RED) VERSUS OBSERVED (BLUE) AT ELK (USGS 12427000) FOR WY2009-WY2013, WITH SIMULATED RAIN AND SNOWMELT .....	179
FIGURE 9.3: SIMULATED DAILY LOG-TRANSFORMED STREAMFLOW (RED) VERSUS OBSERVED (BLUE) AT ELK (USGS 12427000) FOR WY2009-WY2013 .....	179
FIGURE 9.4: FLOW DURATION CURVES FOR SIMULATED DAILY STREAMFLOW (RED) AND OBSERVED STREAMFLOW (BLUE) AT ELK (USGS 12427000) FOR WY2009-WY2013 .....	179
FIGURE 9.5: SIMULATED DAILY STREAMFLOW (RED) VERSUS OBSERVED (BLUE) AT LSR TMDL-23 BELOW ELOIKA LAKE FOR WY2009-WY2013, WITH SIMULATED RAIN AND SNOWMELT .....	180
FIGURE 9.6: SIMULATED DAILY LOG-TRANSFORMED STREAMFLOW (RED) VERSUS OBSERVED (BLUE) AT LSR TMDL-23 BELOW ELOIKA LAKE FOR WY2009-WY2013 .....	180
FIGURE 9.7: FLOW DURATION CURVES FOR SIMULATED DAILY STREAMFLOW (RED) AND OBSERVED STREAMFLOW (BLUE) AT LSR TMDL-23 BELOW ELOIKA LAKE FOR WY2009-WY2013 .....	180
FIGURE 9.8: SIMULATED DAILY STREAMFLOW (RED) VERSUS OBSERVED (BLUE) AT DRAGOON CREEK AT E. CHATTAROY RD. FOR WY2009-WY2013, WITH SIMULATED RAIN AND SNOWMELT .....	181
FIGURE 9.9: SIMULATED DAILY LOG-TRANSFORMED STREAMFLOW (RED) VERSUS OBSERVED (BLUE) AT DRAGOON CREEK AT E. CHATTAROY RD. FOR WY2009-WY2013 .....	181
FIGURE 9.10: FLOW DURATION CURVES FOR SIMULATED DAILY STREAMFLOW (RED) AND OBSERVED STREAMFLOW (BLUE) AT DRAGOON CREEK AT E. CHATTAROY RD. FOR WY2009-WY2013 .....	181
FIGURE 9.11: SIMULATED DAILY STREAMFLOW (RED) VERSUS OBSERVED (BLUE) AT DEADMAN CREEK FOR WY2009-WY2013, WITH SIMULATED RAIN AND SNOWMELT .....	182
FIGURE 9.12: SIMULATED DAILY LOG-TRANSFORMED STREAMFLOW (RED) VERSUS OBSERVED (BLUE) AT DEADMAN CREEK FOR WY2009-WY2013 .....	182
FIGURE 9.13: FLOW DURATION CURVES FOR SIMULATED DAILY STREAMFLOW (RED) AND OBSERVED STREAMFLOW (BLUE) AT DEADMAN CREEK FOR WY2009-WY2013 .....	182
FIGURE 9.14: SIMULATED DAILY STREAMFLOW (RED) VERSUS OBSERVED (BLUE) AT DARTFORD (USGS 12431000) FOR WY2009-WY2013, WITH SIMULATED RAIN AND SNOWMELT .....	183
FIGURE 9.15: SIMULATED DAILY LOG-TRANSFORMED STREAMFLOW (RED) VERSUS OBSERVED (BLUE) AT DARTFORD (USGS 12431000) FOR WY2009-WY2013 .....	183
FIGURE 9.16: FLOW DURATION CURVES FOR SIMULATED DAILY STREAMFLOW (RED) AND OBSERVED STREAMFLOW (BLUE) AT DARTFORD (USGS 12431000) FOR WY2009-WY2013 .....	183
FIGURE 9.17: SIMULATED DAILY STREAMFLOW (RED) VERSUS OBSERVED (BLUE) AT LSR TMDL-1 FOR WY2003-WY2008, WITH SIMULATED RAIN AND SNOWMELT .....	184
FIGURE 9.18: SIMULATED DAILY STREAMFLOW (RED) VERSUS OBSERVED (BLUE) AT LSR TMDL-23 BELOW ELOIKA LAKE FOR WY2003-WY2008, WITH SIMULATED RAIN AND SNOWMELT .....	184
FIGURE 9.19: SIMULATED DAILY STREAMFLOW (RED) VERSUS OBSERVED (BLUE) AT LSR TMDL-2 FOR WY2003-WY2008, WITH SIMULATED RAIN AND SNOWMELT .....	184
FIGURE 9.20: SIMULATED DAILY STREAMFLOW (RED) VERSUS OBSERVED (BLUE) AT DRAGOON CREEK AT E. CHATTAROY RD. FOR WY2003-WY2008, WITH SIMULATED RAIN AND SNOWMELT .....	185
FIGURE 9.21: SIMULATED DAILY STREAMFLOW (RED) VERSUS OBSERVED (BLUE) AT DR9-(DRAGOON CREEK AT N. CRESCENT RD.) FOR WY2003-WY2008, WITH SIMULATED RAIN AND SNOWMELT .....	185
FIGURE 9.22: SIMULATED DAILY STREAMFLOW (RED) VERSUS OBSERVED (BLUE) AT DEADMAN CREEK FOR WY2003-WY2008, WITH SIMULATED RAIN AND SNOWMELT .....	185
FIGURE 9.23: SIMULATED DAILY STREAMFLOW (RED) VERSUS OBSERVED (BLUE) AT DARTFORD (USGS 12431000) FOR WY2003-WY2008, WITH SIMULATED RAIN AND SNOWMELT .....	186
FIGURE 9.24: SIMULATED DAILY STREAMFLOW (RED) VERSUS OBSERVED (BLUE) AT DARTFORD (USGS 12431000) FOR WY2003-WY2017, WITH SIMULATED RAIN AND SNOWMELT .....	186
FIGURE 9.25: FLOW DURATION CURVES FOR SIMULATED DAILY STREAMFLOW (RED) AND OBSERVED STREAMFLOW (BLUE) AT DARTFORD (USGS 12431000) FOR WY2003-WY2017 .....	186
FIGURE 9.26: AVERAGE OF SPOT FLOW OBSERVATIONS VERSUS LONG-TERM AVERAGE SIMULATED STREAMFLOW AT UNGAGED TRIBUTARIES .....	187
FIGURE 9.27: OBSERVED (BLUE) AND SIMULATED (RED) STAGE AT ELOIKA LAKE (WY2003-WY2017), IN FASL .....	188
FIGURE 9.28: AVERAGE SIMULATED HEAD IN THE UPPER AQUIFER (WY2003-WY2017) AND OBSERVED GROUNDWATER LEVELS .....	189
FIGURE 9.29: AVERAGE SIMULATED HEAD IN THE LOWER AQUIFER (WY2003-WY2017) AND OBSERVED GROUNDWATER LEVELS .....	190
FIGURE 9.30: AVERAGE SIMULATED HEAD IN THE GRANDE RONDE BASALT AQUIFER (WY2003-WY2017) AND OBSERVED GROUNDWATER LEVELS .....	191
FIGURE 9.31: AVERAGE SIMULATED HEAD IN THE BEDROCK AQUIFER (PRE-LATAH SANDS, WEATHERED BEDROCK, AND UNWEATHERED BEDROCK) (WY2003-WY2017) AND OBSERVED GROUNDWATER LEVELS .....	192
FIGURE 9.32: SCATTERPLOT OF RESIDUALS FOR THE (A) UPPER AQUIFER; (B) LOWER AQUIFER; (C) GRANDE RONDE BASALT AQUIFER; AND (D) BEDROCK AQUIFER .....	193

FIGURE 9.33: DISTRIBUTION OF RESIDUALS (OBSERVED - SIMULATED) IN THE UPPER AQUIFER. ....	194
FIGURE 9.34: DISTRIBUTION OF RESIDUALS (OBSERVED - SIMULATED) IN THE LOWER AQUIFER. ....	195
FIGURE 9.35: DISTRIBUTION OF RESIDUALS (OBSERVED - SIMULATED) IN THE GRANDE RONDE BASALT AQUIFER. ....	196
FIGURE 9.36: DISTRIBUTION OF RESIDUALS (OBSERVED - SIMULATED) IN THE BEDROCK AQUIFER. ....	197
FIGURE 9.37: HYDROGRAPH FOR THE DOE-CHATTAROY BEDROCK AQUIFER WELL SHOWING SIMULATED (RED) AND OBSERVED (BLUE) GROUNDWATER LEVELS. ....	198
FIGURE 9.38: HYDROGRAPH FOR THE DOE-DEER PARK GRAND RONDE BASALT WELL SHOWING SIMULATED (RED) AND OBSERVED (BLUE) GROUNDWATER LEVELS. ....	198
FIGURE 9.39: HYDROGRAPH FOR THE WHITWORTH WATER-SHADY SLOPE LOWER AQUIFER WELL SHOWING SIMULATED (RED) AND OBSERVED (BLUE) GROUNDWATER LEVELS. ....	199
FIGURE 9.40: HYDROGRAPH FOR THE SCWD#3 RIVER ESTATES UPPER AQUIFER WELL SHOWING SIMULATED (RED) AND OBSERVED (BLUE) GROUNDWATER LEVELS. ....	199
FIGURE 9.41: AVERAGED PRECIPITATION (IN/YR) FOR THE SIMULATION PERIOD AVERAGED OVER EACH GAGED CATCHMENT. ....	200
FIGURE 9.42: SIMULATED AVERAGE MARCH HEADS IN THE BEDROCK AQUIFER (FASL) AND SIMULATED STREAMFLOW (CFS). ....	201
FIGURE 9.43: SIMULATED AVERAGE AUGUST HEADS IN THE BEDROCK AQUIFER (FASL) AND SIMULATED STREAMFLOW (CFS). ....	202
FIGURE 9.44: AVERAGE ANNUAL PRECIPITATION (IN/YR), BASED ON PRISM DATA. ....	203
FIGURE 9.45: AVERAGE ANNUAL CANOPY INTERCEPTION (IN/YR). ....	204
FIGURE 9.46: AVERAGE ANNUAL HORTONIAN RUNOFF FROM IMPERVIOUS SURFACES (IN/YR). ....	205
FIGURE 9.47: AVERAGE ANNUAL HORTONIAN RUNOFF FROM IMPERVIOUS AND PERVIOUS SURFACES (IN/YR). ....	206
FIGURE 9.48: AVERAGE ANNUAL UPSLOPE DUNNIAN (SATURATION EXCESS) RUNOFF (IN/YR). ....	207
FIGURE 9.49: AVERAGE ANNUAL UPSLOPE INTERFLOW (IN/YR). ....	208
FIGURE 9.50: AVERAGE ANNUAL GENERATED OVERLAND RUNOFF AND INTERFLOW (IN/YR). ....	209
FIGURE 9.51: AVERAGE ANNUAL INFILTRATION THROUGH THE SOIL SURFACE (IN/YR). ....	210
FIGURE 9.52: AVERAGE ANNUAL POTENTIAL EVAPOTRANSPIRATION (IN/YR). ....	211
FIGURE 9.53: AVERAGE ANNUAL ACTUAL EVAPOTRANSPIRATION (IN/YR). ....	212
FIGURE 9.54: AVERAGE ANNUAL EVAPOTRANSPIRATION FROM THE SOIL ZONE (IN/YR). ....	213
FIGURE 9.55: AVERAGE DISTRIBUTION OF ANNUAL GROUNDWATER RECHARGE (IN/YR) FROM THE HYDROLOGIC SUBMODEL (PRMS). ....	214
FIGURE 9.56: AREAS WHERE STREAMFLOW IS LOST TO THE AQUIFER (RED) AND WHERE THE AQUIFER DISCHARGE TO STREAMS (BLUE) BASED ON THE LONG-TERM SIMULATION (VALUES IN CFS). ....	215
FIGURE 9.57: AREAS WITH SURFACE LEAKAGE (GROUNDWATER DISCHARGE TO STREAM, VALUES IN CFS). ....	216
FIGURE 9.58: ANNUAL GROUNDWATER BUDGET FOR THE LSR WATERSHED (WY2003 WAS NOT USED IN THE ANALYSIS). ....	217
FIGURE 9.59: AVERAGE MONTHLY GROUNDWATER BUDGET FOR THE LSR WATERSHED UNDER BASELINE CLIMATE. ....	217
FIGURE 9.60: ANNUAL AVERAGE WATER BUDGET FROM THE GSFLOW BASIN-WIDE DAILY FLOW BALANCE. ....	218
FIGURE 9.61: ANNUAL AVERAGE WATER BUDGET FOR STUDY AREA STREAMS FROM THE GSFLOW BASIN-WIDE DAILY FLOW BALANCE. ....	218
FIGURE 9.62: ANNUAL AVERAGE WATER BUDGET FOR STUDY AREA LAKES FROM THE GSFLOW BASIN-WIDE DAILY FLOW BALANCE. ....	219
FIGURE 10.1: 2050 CLIMATE CHANGE PREDICTIONS FOR THE FALL, EAST OF THE CASCADES (FROM THE CIG WEBSITE) ....	224
FIGURE 10.2: INCREASE IN WITHDRAWALS FOR PERMIT-EXEMPT SELF-SUPPLY. ....	227
FIGURE 10.3: SIMULATED DECREASE IN AVERAGE HEADS (FT) IN THE UPPER AQUIFER WITH INCREASED DOMESTIC SELF-SUPPLY WITHDRAWALS. ....	228
FIGURE 10.4: SIMULATED DECREASE IN AVERAGE HEADS (FT) IN THE BEDROCK AQUIFER WITH INCREASED DOMESTIC SELF-SUPPLY WITHDRAWALS. ....	229
FIGURE 10.5: SIMULATED FLOW AT THE DARTFORD GAGE – BASELINE (BLUE) VERSUS INCREASED DOMESTIC USE SCENARIO (RED) AND CHANGE IN FLOW (GREEN). ....	230
FIGURE 10.6: SIMULATED FLOW AT THE DEADMAN GAGE – BASELINE (BLUE) VERSUS INCREASED DOMESTIC USE SCENARIO (RED) AND CHANGE IN FLOW (GREEN). ....	230
FIGURE 10.7: SIMULATED FLOW AT THE DRAGON GAGE – BASELINE (BLUE) VERSUS INCREASED DOMESTIC USE SCENARIO (RED) AND CHANGE IN FLOW (GREEN). ....	230
FIGURE 10.8: SIMULATED INCREASE IN AVERAGE HEADS (FT) IN THE UPPER AQUIFER WITH FOUR RETIRED WATER RIGHTS. ....	231
FIGURE 10.9: SIMULATED INCREASE IN AVERAGE HEADS (FT) IN THE BEDROCK AQUIFER WITH FOUR RETIRED WATER RIGHTS. ....	232
FIGURE 10.10: SIMULATED FLOW AT THE DARTFORD GAGE – BASELINE (BLUE) VERSUS RETIRED WATER RIGHTS SCENARIO (RED) AND CHANGE IN FLOW (GREEN). ....	233
FIGURE 10.11: SIMULATED FLOW AT THE DRAGON CREEK GAGE – BASELINE (BLUE) VERSUS RETIRED WATER RIGHTS SCENARIO (RED) AND CHANGE IN FLOW (GREEN). ....	233
FIGURE 10.12: SIMULATED FLOW AT DRAGON CREEK AT HWY. 395 BELOW DEER PARK – BASELINE (BLUE) VERSUS RETIRED WATER RIGHTS SCENARIO (RED) AND CHANGE IN FLOW (GREEN). ....	233
FIGURE 10.13: PERCENT OF AVAILABLE RISE LEFT IN CELL AFTER INJECTION OF 1 CFS FOR 1 MONTH. ....	234
FIGURE 10.14: LOCATION OF ALTERNATE STREAM DIVERSION AND ARTIFICIAL RECHARGE INFILTRATION SITES REPRESENTED BY INJECTION WELLS IN LAYER 1. ....	235
FIGURE 10.15: SIMULATED INCREASE IN AVERAGE HEADS (FT) IN THE BEDROCK AQUIFER WITH TEN AQUIFER RECHARGE PROJECTS. ....	236
FIGURE 10.16: SIMULATED FLOW AT THE DARTFORD GAGE – BASELINE (BLUE) VERSUS RECHARGE PROJECTS SCENARIO (RED) AND CHANGE IN FLOW (GREEN). ....	237
FIGURE 10.17: SIMULATED FLOW AT DARTFORD CREEK NEAR HIGHWAY 395 – BASELINE (BLUE) VERSUS RECHARGE PROJECTS SCENARIO (RED) AND CHANGE IN FLOW (GREEN). ....	237
FIGURE 10.18: SIMULATED FLOW AT LITTLE DEEP CREEK NEAR HIGHWAY 2 – BASELINE (BLUE) VERSUS RECHARGE PROJECTS SCENARIO (RED) AND CHANGE IN FLOW (GREEN). ....	237
FIGURE 10.19: SIMULATED RAIN AND SNOW FOR BASELINE AND MEAN CLIMATE CHANGE CONDITIONS. ....	238
FIGURE 10.20: SIMULATED AVERAGE MONTHLY SNOWPACK DEPTH (IN INCHES) AND MONTHLY SNOWMELT VOLUMES (IN IN/D OVER THE MODEL AREA) FOR THE BASELINE AND MEAN CLIMATE CHANGE CONDITIONS. ....	238
FIGURE 10.21: PERCENT REDUCTION IN THE JANUARY SNOWPACK DEPTH (INCHES) UNDER FUTURE CLIMATE CONDITIONS. ....	239
FIGURE 10.22: SIMULATED REDUCTION IN THE JANUARY SNOWPACK DEPTH (INCHES) UNDER FUTURE CLIMATE CONDITIONS. ....	240

FIGURE 10.23: SIMULATED INCREASE IN THE LONG-TERM AVERAGE PET (INCHES) FOR THE STUDY AREA (IN/YR) UNDER FUTURE CLIMATE CONDITIONS.....	241
FIGURE 10.24: AVERAGE MONTHLY GROUNDWATER RECHARGE FOR THE BASELINE AND FUTURE CLIMATE SCENARIOS, IN INCHES/MONTH.....	242
FIGURE 10.25: SIMULATED LONG-TERM AVERAGE CHANGE IN GROUNDWATER RECHARGE (IN/YR) UNDER FUTURE CLIMATE CONDITIONS...	243
FIGURE 10.26: SIMULATED LONG-TERM AVERAGE DECREASE IN BEDROCK AQUIFER HEADS (FT) UNDER FUTURE CLIMATE CONDITIONS. ....	244
FIGURE 10.27: AVERAGE ANNUAL GROUNDWATER BUDGET FOR THE LSR WATERSHED UNDER FUTURE CLIMATE CONDITIONS .....	245
FIGURE 10.28: AVERAGE MONTHLY GROUNDWATER BUDGET FOR THE LSR WATERSHED UNDER FUTURE CLIMATE CONDITIONS: .....	245
FIGURE 10.29: FLOW AT THE DARTFORD GAGE – BASELINE (BLUE) VERSUS MEAN FUTURE (2050) CLIMATE CHANGE SCENARIO (RED). ....	246
FIGURE 10.30: SIMULATED FLOW AT THE DARTFORD GAGE – BASELINE (BLUE) VERSUS MEAN FUTURE (2050) CLIMATE CHANGE SCENARIO (RED) AND DIFFERENCE IN FLOW (GREEN) FOR WY2008-WY2013 (WY2048-WY2053).....	246
FIGURE 10.31: SIMULATED AVERAGE DAY FLOW AT THE DARTFORD GAGE – BASELINE (BLUE) VERSUS MEAN FUTURE (2050) CLIMATE CHANGE SCENARIO (RED).....	247
FIGURE 10.32: SIMULATED FLOW AT THE DARTFORD GAGE – BASELINE (BLUE) VERSUS MEAN FUTURE (2050) CLIMATE CHANGE SCENARIO (RED) AND HIGH RANGE FUTURE (2050) CLIMATE CHANGE SCENARIO (GREEN) FOR WY2008-WY2013 (WY2048-WY2053). ....	247
FIGURE 10.33: SIMULATED FLOW AT THE DARTFORD GAGE – BASELINE (BLUE) VERSUS MEAN FUTURE (2050) CLIMATE CHANGE SCENARIO (RED) AND LOW RANGE FUTURE (2050) CLIMATE CHANGE SCENARIO (GREEN) FOR WY2008-WY2013 (WY2048-WY2053). ....	248

# **1 Introduction**

## **1.1 Background**

Spokane County, in coordination with Pend Oreille and Stevens Counties, is in the process of developing an institutional and scientific framework to support water management decisions in the Little Spokane River basin, also referred to as Water Resource Inventory Area 55 (WRIA 55). The ongoing project is funded by a grant from the Washington Department of Ecology and is overseen by a Policy Advisory Group (PAG) comprised of elected officials and technical staff from each of the participating counties.

As part of the institutional and scientific framework, Spokane County applied for and received a grant from the US Bureau of Reclamation to fund a project titled: "Little Spokane River Basin Water Bank - Modeling and Decision Support Tools". The primary objective of this project was to develop a basin-wide integrated groundwater/surface water model that could serve as the scientific framework for the water bank including support for reallocation of banked water rights and assignment of mitigation value to water storage and retiming projects. The team of WEST Consultants Incorporated and Earthfx Incorporated (the Study Team) were selected to carry out this work.

## **1.2 Project Description**

The project required construction and calibration of an integrated groundwater/surface water flow model to use as a tool to simulate changes in surface water flows and groundwater reservoirs resulting from reallocation of existing water rights or development of new water supplies. Outputs from the model would be utilized to assign mitigation value within the Little Spokane Water Bank to proposed reallocation of existing water rights or development of new supplies. The model was to also be capable of representing future climate change and simulating the impacts to groundwater and surface water flows under these conditions. This will allow the model to be used for consideration of future climate change and evaluation of approaches to drought management.

Use of GSFLOW, an integrated surface water flow/groundwater flow model code developed by the U.S. Geological Survey (Markstrom *et al.*, 2008), was recommended for this study. The code couples the USGS Precipitation-Runoff Modeling System (PRMS) and the USGS Modular groundwater flow model (MODFLOW). The Study Team utilized the GSFLOW code as the foundation for this study.

Integrated surface water flow/groundwater flow models are quite complex and required considerable data compilation, analysis, and synthesis prior to model construction and calibration. Model construction and calibration proceeded with development of the input data sets for the PRMS and MODFLOW models and calibration of the integrated GSFLOW model. Once calibrated, a set of model scenarios were developed in consultation with Spokane County and the stakeholder Technical Advisory Committee. Data sets were created for each scenario and model outputs were compared to baseline conditions to determine change in streamflow and groundwater levels.

## **1.3 Project Objectives and Scope**

As noted, the primary objective of this study was to develop, calibrate, and apply a basin-wide integrated groundwater/surface water model that could serve as the scientific framework for the Little Spokane watershed including support for reallocation of banked water rights and assignment of mitigation value to water storage and retiming projects.

Several tasks were involved in model development including: compilation and analysis of geologic, hydrogeologic, climate, and hydrologic data; development of conceptual geologic and hydrostratigraphic models; preparation of three-dimensional model surfaces; assignment of model parameters; creation of model input data sets for the PRMS and MODFLOW models; model integration; and calibration of the integrated GSFLOW model.

The GSFLOW integrated groundwater/surface water model was constructed to represent hydrologic and hydrogeologic processes in the Little Spokane River watershed with an emphasis on the interaction and feedback between surface and subsurface processes. The model was calibrated to best match observed streamflow, lake levels, and groundwater potentials over a 5-year period with the best data coverage (Water Years 2008 to 2013). The model was validated by extending the simulation period back to WY2003 and comparing against observed streamflow, lake levels, and groundwater potentials. The simulation period was then extended to WY2017 to provide a baseline to compare against additional simulations of water use management and climatic change scenarios. Model outputs were compared against the baseline simulation to quantify the likely effects on groundwater and surface-water resources. Hydrographs and maps were produced to illustrate changes in streamflow and groundwater levels at key locations. Monthly and annual average water budgets were created to show how the changes affected each part of the hydrologic cycle.

Finally, this report was prepared to summarize the available data, describe the construction and calibration of the integrated groundwater/surface-water flow model, and present results from simulations of the different climate and water use scenarios. Model uncertainty and limitations are also discussed.

## **1.4 Technical Approach**

The hydrologic and hydrogeologic conditions in the Little Spokane Watershed are highly variable and previous studies indicated that there is significant interaction between the groundwater and surface water systems. The interactions are complex, non-linear, and highly transient in nature. Characterizing the underlying physical setting (i.e., climate, geology, hydrology, and hydrogeology) is essential to developing an understanding the function of the watershed.

Development of a fully-integrated surface and groundwater model which represented hydrologic, hydraulic (streamflow), and groundwater flow process, is the best method to quantitatively represent the complexity of the watershed and interaction between the groundwater and surface water systems. The USGS GSFLOW code used in this study couples two proven USGS submodels: MODFLOW and PRMS. The components and linkage of these models is described in detail in Section 0. The integrated model represents the soil zone, all surface water bodies (streams, wetlands, lakes, and ponds), as well as the subsurface geologic and hydrogeologic features in the study area. The model simulates the response and interactions of the surface water and groundwater systems on a daily basis and provides output in terms of groundwater potentials, streamflows, and lake and wetland levels. It also provides daily values for all components of the water budget including precipitation, interception, snowmelt, evapotranspiration, overland runoff, infiltration, and groundwater recharge. These daily values were aggregated over time to provide monthly, seasonal, and annual water budgets. Values were also aggregated spatially to provide water budgets at the subwatershed scale and for particular areas of interest.

## **1.5 Study Area Extents and Model Boundary**

The study was focused on the Little Spokane River Watershed contributing to the USGS gage (USGS 12431000) at Dartford (Figure 1.1). The study area was extended north to the Pend Oreille River to account for possible groundwater inflows or outflows across the northern watershed boundary. Other study area boundaries coincide with the topographic divides that delineate the watershed. Lateral groundwater inflows and outflows across these boundaries were assumed to be

negligible relative to other components of the groundwater balance. Hydrologic and hydrogeologic data were collected within these boundaries. Additional data sets, particularly climate data, were collected from outside the study area boundaries.

Flows between the USGS gage at Dartford and the USGS gage near Dartford (USGS 12431500) are known to be strongly influenced by groundwater discharge from the Spokane Valley Rathdrum Prairie (SVRP) aquifer which underlies the Spokane River (see Kahle *et al.*, 2013, for example). The SVRP aquifer, which extends into neighboring Idaho, has been the subject of numerous investigations. Modeling of regional groundwater flow within the SVRP aquifer and its extension into the Little Spokane River area was beyond the scope of the current study. Accordingly, the study does not include the southern portion of the Little Spokane Watershed which contributes flow below the gage at Dartford.

The model boundary encompasses 688 square miles (mi<sup>2</sup>) or 1,780 square kilometers (km<sup>2</sup>), as shown in Figure 1.1. Approximately 620 mi<sup>2</sup> of the LSR Model area contributes to the USGS gage at Dartford. The LSR Model boundaries are discussed further in Section 8.4.

## **1.6 Report Scope and Structure**

The objective of this report is to document the development, calibration, application of the integrated model for the Little Spokane River watershed. The report broadly consists of four parts. The first, in Sections 1 through 5, presents a detailed discussion of the hydrologic and geologic setting of the study area. Section 6 introduces the GSFLOW model code and provides an overview of the model behavior. Sections 7 through 9 present the model representation of the study area and the calibration of the model to field observations. Section 10 discusses the application of the model and the results of the simulated scenarios.

## **1.7 Previous Investigations**

Numerous investigations have contributed to the understanding of the hydrogeologic framework in all, or parts, of the Little Spokane River Basin. Several key documents that were relied on heavily in this study are listed below. Others can be found in the references cited.

First and foremost is the study of the hydrogeologic framework of the Little Spokane River Basin by Kahle *et al.* (2013). This study described the geologic and stratigraphic setting, identified eight principal hydrogeologic units in the study area, and presented estimates of their hydraulic characteristics. It also discussed factors controlling groundwater movement, which generally follows the surface-water drainage pattern of the basin, moving from the topographically high tributary-basin areas toward the topographically lower valley floor. The study provided maps of surficial geology and well locations, maps showing the principal hydrogeologic units, and sections showing the units and groundwater levels. Tables provided information on wells used to interpret the geology and hydrogeology and wells with long-term water level information. The USGS provided the mapping and well data from this report in digital format for use in this study, which is greatly appreciated.

Kahle *et al.* identified several studies upon which they relied. These were obtained for this study and provided additional background information. These included a study by Cline (1969) of the groundwater resources of northern Spokane County and southeastern Stevens County that covers the southern half of the LSR watershed. The study described the physiographic setting, the geologic units, their hydrogeologic properties, and the storage and movement of groundwater. A study by Chung (1975) was foundational for water resource management within the watershed and established in-stream flow rules for key streams and restrictions on water use still imposed today. A Ph.D. thesis by Conners (1976) was particularly useful for providing a geologic history of the LSR area. Local investigations include a study by EMCON (1992) of the Deer Park Basin, a study by Landau Associates (1991) of the Colbert Landfill, a study of the hydrogeology of the Green Bluff

plateau by Ader (1996), and a study of the hydrogeology of the Peone Prairie by Boleneus and Derkey (1996). Dames and Moore, Inc. (1995) reviewed the surface and groundwater resources in the Little Spokane River Basin (WRIA 55) including data on water quantity, hydrogeology, water demand, water quality, and status of aquatic habitat and fish stocks. They identified increasing trends in groundwater rights, declining trends in streamflow, and an increase in the number of days where baseflow fell below a minimum. They provided groundwater level data at wells, maps of water use, and identified gaps in the data available for the watershed.

Golder (2003) provides a data compilation for WRIA 55 and adjacent watershed WRIA 57 (which includes part of the SVRP). These data were used by Golder (2004) to develop an integrated model of the watersheds using the Mike SHE code Version 5.44 (Danish Hydrologic Institute, 2004). The two-layer model represented the shallow aquifer system composed of unconsolidated sediments and a deeper aquifer within the basalt units. They did not simulate flow in the granitic bedrock. Golder (2004) subdivided the groundwater system into several aquifer units: the Deer Park, Little Spokane River, Green Bluff, Peone Prairie, Orchard Prairie, and Diamond Lake aquifers. The Diamond Lake aquifer was not hydraulically connected to the other units.

Ely and Kahle (2012) developed an integrated model of the nearby Chamokane Creek watershed in southwestern Stevens County using the USGS GSFLOW code. The basin is similar in several respects to the LSR study area. Their modeling approach and range of parameter values used in the model provided a good starting point for this study.

Spokane County has also conducted a number of studies to augment the groundwater and hydrologic data available for the study area. A number of annual data reports have been produced (e.g., Spokane County, 2009). The streamflow, water level, and seepage data presented in these studies were incorporated into the project database for this study and used as calibration targets for the integrated model.

There are a large number of publications on the hydrogeology of the SVRP. A modeling study by Hsieh *et al.* (2007) helped develop a better understanding of the interaction between the LSR and the SVRP and to set boundary conditions for the model in this study. Paul Hsieh of the USGS provided copies of the SVRP model data sets. An early study of the SVRP by Bolke and Vaccaro (1981) was the first model that one of the authors of this study worked on as a research hydrologist at the USGS.

## **1.8 Acknowledgements**

The Study Team would like to acknowledge the support of the Spokane County Water Resources Department and Mike Hermanson, in particular, for his assistance in this study and for the provision of the high-quality data used in these analyses.

## **2 Watershed Overview**

The Little Spokane River (LSR) watershed is located in northeast Washington State, north of the City of Spokane and adjacent to the Washington-Idaho border (Figure 1.1). The watershed is designated by the Washington State Department of Ecology (Ecology) as Water Resources Inventory Area (WRIA) 55. The part of the LSR watershed considered in this study contributes to the USGS gage at Dartford (USGS 12341000) and drains an area of about 620 mi<sup>2</sup> and covers parts of Spokane, Pend Oreille, and Stevens counties. The study area was extended further north to the Pend Oreille River to include this feature as a hydrologic boundary for the integrated model.

Seven subwatersheds were analyzed within this study (Figure 2.1) and include:

1. Otter Creek
2. West Branch of the LSR
3. Beaver Creek
4. Deer Creek
5. Dragoon Creek (Main and West Branches)
6. Little Deep Creek; and
7. Deadman Creek

Subwatersheds were also delineated to define the contributing areas to active and historic stream gages in the study area. These were used in model calibration and are discussed further on in Section 9.1.2.

The headwaters of the Little Spokane River are in the northeastern part of the watershed, west of the city of Newport. The eastern branch of the Little Spokane River joins with Otter Creek in the Otter Creek subwatershed. The West Branch of the LSR also has its headwaters in the northeastern part of the watershed, flows west through a series of lakes, joins up with Buck Creek, flows south-southeast and through Eloika Lake, and then meets the eastern branch of the river north of Milan (Figure 2.2). The main stem continues to flow south where it meets up with Dragoon Creek (Figure 2.3) which drains the west-central part of the watershed and with several streams that drain the east side.

The Dartford Creek subwatershed includes the reach of the Little Spokane River extending from the USGS gage at Dartford to the confluence with the Spokane River. As was noted earlier, baseflow in this reach is known to increase significantly due to groundwater discharge from the regionally-extensive SVRP aquifer. It was assumed in this study that bedrock outcrops and subcrops along the northern boundary of the Dartford Creek subwatershed separate the groundwater systems above and below the gage at Dartford and minimize the interaction between them. Only the upper portion of the Dartford Creek subwatershed was included in this study.

There are several large lakes in the study area, including Diamond, Eloika, Horseshoe, and Sacheen lakes (Figure 2.2 and Figure 2.3). Smaller lakes are also present, mostly in the northern part of the watershed. There are also numerous wetlands of various sizes, many within the riparian zones of streams. Representation of these features within the model is discussed further in Section 8.4.2.

### **2.1 Topography and Physiography**

Land surface topography for the study area, based on a 23.75 ft (7.24 m) digital elevation model (DEM), is shown in Figure 2.4. The minimum elevation is 1570 feet above sea level (fasl) and occurs in the Little Spokane River stream valley at the Dartford gage. The maximum elevation, 5847 fasl, occurs at the top of Mt. Spokane located in the southeast portion of the watershed (Figure 2.5).

Relief in the study area is highly variable, with steeply sloping bedrock in upland areas and a large gently-sloping plain in the center of the study area. A hypsometric profile for the watershed (Figure 2.5) confirms that most elevations (80%) lie between 1900 and 2800 ft. Elevation profiles of the Little Spokane River and the key tributaries are presented in Figure 2.6. Deer Creek, Little Deep Creek, and Deadman Creek have very steep profiles in their headwaters which drain the bedrock highland in the vicinity of Mt. Spokane. The main branches of the Little Spokane River, as well as Dagoon Creek and its tributaries, mainly drain the central plain and have flatter profiles.

Key physiographic features for the area are shown in Figure 2.7 which is based on earlier mapping by Cline (1969). The Little Spokane River watershed can be characterized as a broad basin surrounded by the Okanogan foothills to the west and the Selkirk bedrock highlands to the east. The hills and highlands are formed primarily by metasedimentary (argillite, siltite, and quartzite) and granitic rocks with relatively thin or absent soil cover. Bedrock is exposed or near surface in parts of the basin and can create isolated groundwater subbasins such as in the Diamond Lake area. The central basin is relatively flat but can be hilly in places and contains several mesas, such as Orchard Bluff, Green Bluff, Peone Foothills, Pleasant Prairie, Orchard Prairie, and Five Mile Prairie (Cline, 1969). These mesas are formed by the remnants of extensive flood basalts which serve as cap rocks over more erodible sediments.

## **2.2 Current Land Use**

Current land use and coverage within the Little Spokane Watershed was evaluated based on the 2011 National Land Class mapping (Homer *et al.*, 2015). NLCD (2011) is a national land cover product created by the Multi-Resolution Land Characteristics (MRLC) Consortium using 16 land cover classes at a spatial resolution of 30 meters and is based on 2011 Landsat satellite data. The data were resampled to a 250 ft grid for use in the hydrologic model.

The percent coverage for the major land use classes is provided in Figure 2.8 and clearly shows the dominance of evergreen forest (55%). Shrub and scrub land and grassland/herbaceous classes cover 27% of the area and are mostly natural but can be used for grazing or occasional cultivation. More intensive agricultural land use, including cultivated crops and pasture/hay fields comprise 10.6% of the watershed. Open developed areas, predominantly single family lots with less than 20% impervious cover and low-intensity development (20 to 49% impervious cover) cover 4.2% of the study area. Medium and high intensity development covers less than 0.5% of the area mainly in the Deer Park area and in the southern part of the study area along Highway 2 and Highway 395. Other land use types cover less than 1% of the watershed each and are too small to show in Figure 2.9. Detailed breakdowns, along with descriptions of the land use classes, are provided in Table 2.1.

## **2.3 Agricultural Land Use**

Agricultural land usage was also obtained from the NLCD (2011) data set and is shown in Figure 2.9. Alfalfa is the largest crop (33%), covering 22,805 of 68,580 acres. The second largest crop classification is grassland and pasture (26%). Other primary crops are spring and winter wheat, other hay, rye, peas, and barley. About 8% of the crop land is classified as fallow or idle. Current crop distributions may vary from the 2011 Landsat data. A detailed breakdown of all crop types is also summarized in Table 2.2.

## 2.4 Tables

Table 2.1: Land use within the study area (from NLCD, 2011).

NLC ID	Name	Area (mi <sup>2</sup> )	% of Study Area
11	<b>Open Water</b> - areas of open water, generally with less than 25% cover of vegetation or soil.	7.68	1.12
21	<b>Developed, Open Space</b> - areas with a mix of some constructed materials, but mostly vegetation in the form of lawn grasses. Impervious surfaces account for less than 20% of total cover. Commonly includes large-lot single-family housing units, parks, golf courses, and vegetation planted in developed settings for recreation, erosion control, or aesthetic purposes.	12.9	1.88
22	<b>Developed, Low Intensity</b> - areas with a mixture of constructed materials and vegetation. Impervious surfaces account for 20% to 49% percent of total cover. These areas most commonly include single-family housing units.	15.9	2.31
23	<b>Developed, Medium Intensity</b> - areas with a mixture of constructed materials and vegetation. Impervious surfaces account for 50% to 79% of the total cover. These areas most commonly include single-family housing units.	2.93	0.43
24	<b>Developed High Intensity</b> - highly developed areas where people reside or work in high numbers. Examples include apartment complexes, row houses, and commercial/industrial. Impervious surfaces account for 80% to 100% of the total cover.	0.13	0.02
31	<b>Barren Land</b> (Rock/Sand/Clay) - areas of bedrock, desert pavement, scarps, talus, slides, volcanic material, glacial debris, sand dunes, strip mines, gravel pits, and other earthen material. Generally, vegetation accounts for less than 15% of total cover.	0.19	0.03
41	<b>Deciduous Forest</b> - areas dominated by trees generally greater than 5 m tall, and greater than 20% of total vegetation cover. More than 75% of the tree species shed foliage simultaneously in response to seasonal change.	0.32	0.05
42	<b>Evergreen Forest</b> - areas dominated by trees generally greater than 5 m tall, and greater than 20% of total vegetation cover. More than 75% of the tree species maintain their leaves all year. Canopy is never without green foliage.	377.3	54.87
43	<b>Mixed Forest</b> - areas dominated by trees generally greater than 5 m tall, and greater than 20% of total vegetation cover. Neither deciduous nor evergreen species are greater than 75% of total tree cover.	0.002	0.0003
52	<b>Shrub/Scrub</b> - areas dominated by shrubs; less than 5 m tall with shrub canopy typically greater than 20% of total vegetation. This class includes true shrubs, young trees in an early successional stage or trees stunted from environmental conditions.	112.4	16.35
71	<b>Grassland/Herbaceous</b> - areas dominated by graminoid or herbaceous vegetation, generally greater than 80% of total vegetation. These areas are not subject to intensive management such as tilling, but can be utilized for grazing.	74.2	10.79
81	<b>Pasture/Hay</b> - areas of grasses, legumes, or grass-legume mixtures planted for livestock grazing or the production of seed or hay crops, typically on a perennial cycle. Pasture/hay vegetation accounts for greater than 20% of total vegetation.	8.86	1.29
82	<b>Cultivated Crops</b> - areas used for production of annual crops, such as corn, and also perennial woody crops such as orchards and vineyards. Crop vegetation accounts for greater than 20% of total vegetation. Includes all land being actively tilled.	63.9	9.29
90	<b>Woody Wetlands</b> - areas where forest or shrubland vegetation accounts for greater than 20% of vegetative cover and the soil or substrate is periodically saturated with or covered with water.	2.64	0.38
95	<b>Emergent Herbaceous Wetlands</b> - areas where perennial herbaceous vegetation accounts for greater than 80% of vegetative cover and the soil or substrate is periodically saturated with or covered with water.	8.23	1.20

Table 2.2: Crop types within the study area (from NLCD, 2011).

NLC ID	Name	Area (acres)	% of Study Area
6	Sunflower	182	0.36
21	Barley	1029	1.50
23	Spring Wheat	7010	10.2
24	Winter Wheat	6964	10.2
28	Rye	2485	3.62
31	Canola	352	0.513
35	Mustard	90	0.132
36	Alfalfa	22806	33.3
37	Other Hay/Non Alfalfa	2552	3.72
42	Dry Beans	428	0.623
51	Chick Peas	11	0.017
52	Lentils	20	0.029
53	Peas	1274	1.85
59	Sod/Grass Seed	126	0.184
60	Switchgrass	168	0.245
61	Fallow/Idle Cropland	5408	7.89
68	Apples	33	0.048
69	Grapes	3	0.004
70	Christmas Trees	32	0.046
176	Grassland/Pasture	17584	25.6
205	Triticale	16	0.023
224	Vetch	6	0.008

### 3 Geological and Hydrogeologic Setting

Development of a three-dimensional integrated model started with the compilation and synthesis of existing physiographic, geologic, hydrologic, and hydrogeologic data for the study area. Much of the key information on the geology and hydrogeology of the Little Spokane River watershed can be found in the USGS report by Kahle *et al.* (2013). This section summarizes the information that was relied on in model construction. The reader is referred to Kahle *et al.* (2013) for more detail. Another excellent reference for the geologic history of the area is Conners (1976).

#### 3.1 Key Geologic Units

Kahle *et al.* (2013) divided the geologic history of the study area into three major time periods: the pre-Tertiary, the Tertiary, and the Quaternary. Table 3.1 (modified from Kahle *et al.* (2013)) presents a simplified geologic time scale showing approximately when the key geologic units in the study area were formed. The geologic units, shown in the right hand side of Table 3.1, are mapped in Figure 3.3. This geologic map is a simplified version of those produced by the USGS and Washington Department of Natural Resources (e.g. Miller, 1974) at smaller scales. In particular, the wide varieties of pre-Tertiary and Tertiary rocks have been amalgamated into just two units. It should be noted that the map by Kahle *et al.* (2013) did not cover the northern part of the study area. Earthfx extended the geologic interpretation for this area based on the more detailed geologic mapping.

Table 3.1: Simplified geologic framework and time scale (modified from Kahle *et al.*, 2013)

Eon	Era	Period	Epoch	Geologic Unit
Phanerozoic (542 Mya to present)	Cenozoic (66 Mya to present)	Quaternary (2.6 Mya to present)	Holocene (11,700 ya to present)	Stream deposits; <b>Qs</b>
				Mass wasting deposits; <b>Qmw</b>
				Eolian deposits, <b>Qe</b>
			Pleistocene (2.6 Mya to 11,700 ya)	Fine-grained glacial deposits; <b>Qgf</b>
				Coarse-grained glacial deposits; <b>Qgc</b>
				Glacial till, <b>Qgt</b>
		Tertiary (66 to 2.6 Mya)	Pliocene	
			Miocene (23 to 5.3 Mya)	Wanapum Basalt; <b>Mw</b>
				Grande Ronde Basalt; <b>Mgr</b>
				Latah Formation; <b>MI</b>
			Oligocene	
	Mesozoic (251 to 65 Mya)	Cretaceous	Eocene	Intrusive igneous rocks; <b>TKg</b>
			Paleocene	
	Paleozoic (542 to 251 Mya)	Jurassic (200 to 146 Mya)		
		Triassic		
		Permian		
		Pennsylvanian		
		Mississippian		
		Devonian		
		Silurian		
		Ordovician		
		Cambrian		
Proterozoic (2,500 to 542 Mya)	Neoproterozoic			Metasedimentary rocks; <b>pEm</b>
	Mesoproterozoic			
	Paleoproterozoic			

The following sections are condensed from Kahle *et al.* (2013). Brief descriptions of the geologic units, modified from Kahle *et al.* (2013), are presented in Table 3.3.

**Pre-Tertiary Units:** The oldest rocks in the study area are metamorphosed, fine-grained sedimentary rocks that originally were deposited in a large, shallow north-south-trending marine basin during the Precambrian. These rocks are present in outcrop today as low-grade metasedimentary rocks, including argillite, siltite, and quartzite, which grade locally into more highly metamorphosed schists and gneisses. These rocks primarily outcrop in the headwater areas of the west branch of the Little Spokane River, northwest of Eloika Lake, as well as forming an east-west-trending ridge of mountains (Bare and Lone Mountains and Mt. Pisgah) between Diamond Lake and Chain Lakes and Elk.

Following deposition and metamorphism, as much as 20,000 ft of the Precambrian rocks were eroded before the Paleozoic Era began (Conners, 1976). During the Paleozoic, additional sedimentation occurred in shallow seas that resulted in shale, limestone, and sandstone being deposited over the Precambrian rocks. However, from near the end of the Paleozoic to the present, the region mostly has been emergent, and much of the post-Cambrian sediments have been eroded from the area leaving few surface exposures.

Emplacement of various granitic intrusive bodies, along with associated metamorphism and deformation, occurred during a long period of time between the Jurassic and Tertiary; with the largest volume of granitic rocks emplaced during the Cretaceous. The granitic rocks occur at land surface over much of the study area and comprise most of the highland areas along the perimeter of the basin. They include biotite-muscovite (two-mica) granite that forms Dunns and Lookout Mountains on the southwest part of the study area and the southern end of the Selkirk Mountains, including Mt. Spokane, on the eastern side (Stoffel *et al.*, 1991). Much smaller outcrops of Cretaceous biotite granite form Dart Hill and the northern side of Five Mile Prairie (Boese, 1996). Younger granitic rocks (hornblende-biotite monzogranite and granodiorite), emplaced during the Eocene, occur in the north of the study area in the Diamond and Sacheen Lake areas (Miller, 2000).

**Tertiary Geology:** Basalt lava flowed from eastern Washington, northeastern Oregon, and western Idaho during the Miocene Epoch, mantling much of the pre-existing landscape and filling in low-lying areas. The study area is on the northeastern edge of the Columbia Plateau and only a few flows of two formations of the Columbia River Basalt Group reached the area. The oldest flows are part of the Grande Ronde Formation. The stratigraphically higher and younger flows are part of the Wanapum Formation. The Grande Ronde Basalt underlies north parts of the Wild Rose and Half Moon Prairies, and other areas west of the Little Spokane River. The Wanapum Formation has been mostly eroded away in the west but forms basalt mesas or bluffs on the east side of the LSR valley, including Green Bluff, Orchard Bluff, Pleasant Prairie, Orchard Prairie, and Five Mile Prairie.

During the Miocene, the basalt flows blocked existing drainages to the southwest and caused the formation of lakes and swamps that covered the lowlands areas. Large thicknesses of sand, silt, and clay were deposited in large basalt-dammed lakes along the perimeter of the flows. The resulting deposits are known as the Latah Formation. Repeated cycles of basalt flows and continued damming of the stream network resulted in inter-layered Latah sediment and basalt.

A period of slow down-cutting occurred from the Late Miocene to the Early Pleistocene which removed as much as 590 ft of Latah Formation from the region (Anderson, 1927). Accurate estimates of the thickness and extent of the remaining Latah Formation sediments are difficult to determine because of the cover of Pleistocene drift and the difficulty in distinguishing it from younger glacial lake sediment. A few surface exposures of deeply weathered, yellow to orange silt and clay of the Latah Formation can be found below the basalt cap on Five Mile and Orchard Prairies, and Green Bluff and Orchard Bluff.

**Quaternary Geology:** During the Pleistocene Epoch, the study area was subjected repeatedly to the erosional and depositional processes associated with glacial and interglacial periods (Kiver and Stradling, 1982, 2001; Kiver *et al.*, 1989). At the maximum extent of the most recent Pleistocene glaciation (about 15,000 years ago), much of northern Washington, Idaho, and westernmost Montana was covered by lobes of the Cordilleran ice sheet [Conners (1976) notes that there is little evidence that the main Little Spokane Valley was occupied by ice. The maximum extent of the ice was likely the low mountains south of Diamond Lake. Glacial till deposits are found within the study area along the Pend Oreille River and to the north.]. For thousands of years, lobes of the Cordilleran ice sheet modified the pre-existing landscape through erosion and deposition related to glacial and meltwater action. Pre-existing river or melt water drainages were often blocked, creating ice-age lakes that covered large areas and resulted in thick accumulations of sediment.

Glacial Lake Missoula was created when the Purcell Trench ice lobe in northern Idaho (Figure 3.1) blocked the drainage of the ancestral Clark Fork in northwestern Montana. Catastrophic floods occurred over a 2,000-year period when the ice dam periodically failed, sending floodwaters to the west and southwest. The larger of the Missoula floods overwhelmed local drainage patterns, topped the 2,400-ft divide west of Spokane, and creating the Channeled Scablands. When glaciers were at their maximum extent, Missoula outburst floods were mostly routed through the Spokane Valley, then north through the Hillyard trough to the southern portion of the Little Spokane River Basin, and then west through the Long Lake area.

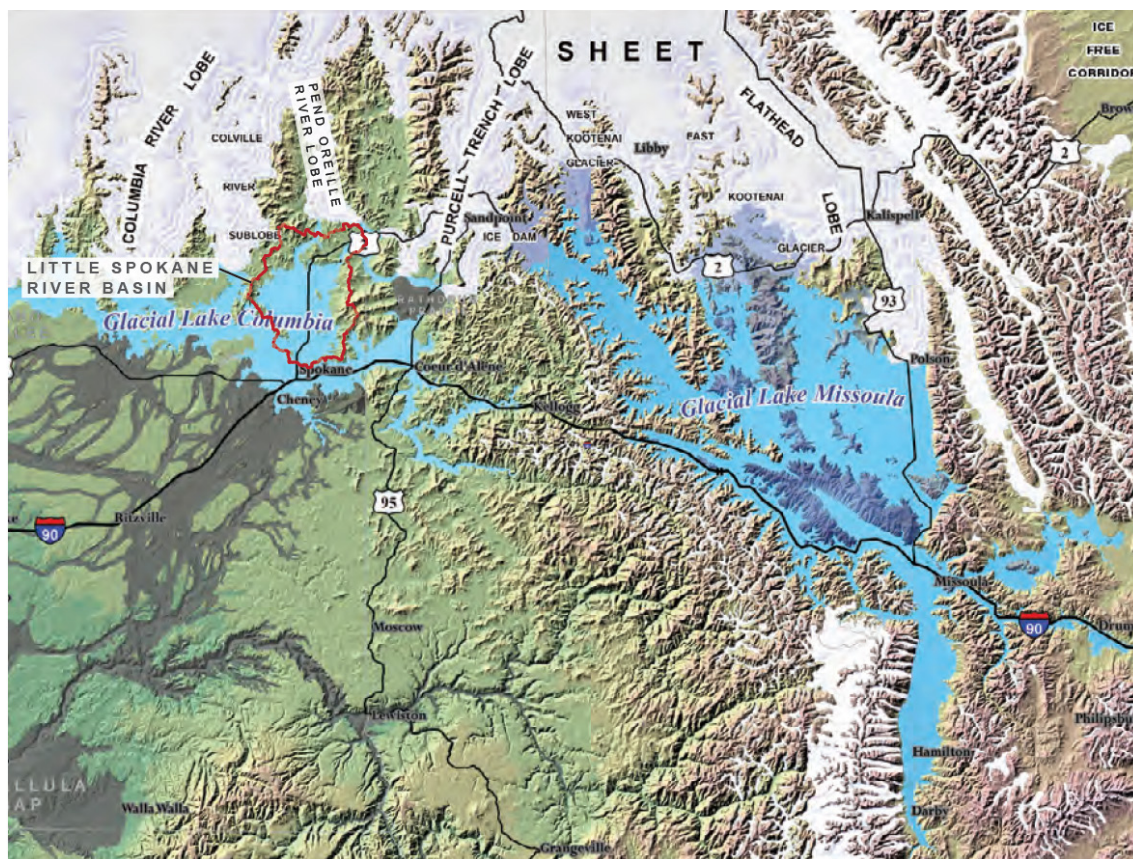


Figure 3.1: Extent of glacial ice and glacial lakes in northeastern Washington, Idaho, and western Montana (modified from Kahle *et al.* (2013) and U.S. Forest Service (2010)).

The Pend Oreille River lobe occupied the Pend Oreille River valley and reached its most recent southernmost extent near the northeast extent of the Little Spokane Basin (Carrara *et al.*, 1995). This was swept by Lake Missoula floodwaters that followed more northern flood routes through a network of channels south and west of Newport, including Scotia and Camden Gaps (Bjornstad and

Kiver, 2012), before eventually emptying into the Deer Park area and the Little Spokane River. Most of the coarse-grained deposits from the catastrophic floods are along the channel of the Little Spokane River, where depositional bars and terraces of sand and gravel hundreds of feet thick were emplaced (Boese, 1996).

The Okanogan and Columbia River lobes affected the study area by blocking westward drainage of the ancestral Columbia and Spokane Rivers and creating vast ice-age lakes that resulted in thick accumulations of clay and silt (Waite and Thorson, 1983). Glacial Lake Columbia, impounded by the Okanogan lobe, was the largest glacial lake in the path of the Missoula floods. At the higher level of Glacial Lake Columbia (2,350 ft), the glacial lake flooded most of the Little Spokane River Basin covering what is now Deer Park and extending to near the top of the basalt bluffs. The long-lived and sediment-rich nature of glacial lakes led to vast thicknesses of mostly fine-grained material being deposited throughout much of the region's lower elevation areas.

Wind-blown sediments were deposited over much of the Columbia Plateau during the Pleistocene (McDonald and Busacca, 1992). The eolian material, composed of fine sand to silt-sized particles, is informally known as the Palouse loess. The Little Spokane River Basin is at the northern edge of the Palouse deposition area and thicknesses are generally less than 25 ft (Boese, 1996). In the southern part of the basin, the unit mantles the basalt bluffs and locally overlies the bedrock.

Following the Pleistocene, rivers and streams eroded the glacial deposits in many places as well as depositing alluvium along their flood plains. Sand deposited by wind also covers parts of the western side of Peone Prairie and areas around Mead (Boese, 1996).

### **3.2 Hydrogeologic Units**

The hydrogeologic setting in the study area is strongly related to the local geology. The individual hydrostratigraphic units were classified as aquifers or aquitards based on the ability of the geologic units to transmit groundwater or limit its movement. In general, this study followed the hydrogeologic classification by Kahle *et al.* (2013); although some modifications were made to subdivide some of the units. For example, the granitic bedrock was subdivided into a weathered shallow unit and a deeper, unweathered unit. The Latah formation was subdivided into an upper unit between the Wanapum and Grande Ronde basalt and a lower unit below the Grande Ronde basalt. A discontinuous sand unit, found between the lower Latah Unit and the weathered bedrock, was separated from the lower aquifers unit and is referred to as the Pre-Latah Sands. Brief descriptions of the hydrostratigraphic units, modified from Kahle *et al.* (2013), are presented in Table 3.4.

The primary aquifers within the Little Spokane River Basin are formed by coarse-grained glacial outwash and flood deposits. Fine-grained glacial deposits form the aquitards and may occur at surface or form semi-confining units between shallow and deeper aquifers. It should be recognized that the upper aquifer and the lower aquifers, in particular, are not continuous due to the complex depositional environment and due to outcropping and subcropping of the bedrock within the basin.

The basalt and weathered bedrock have hydraulic properties that are highly variable. The weathered bedrock and Grande Ronde basalt units serve as aquifers in areas where granular deposits are absent. The Wanapum Basalt can sometimes be above the regional water table, and is not a reliable source of water. The basalt units and the Latah formation are also discontinuous due to erosional processes that occurred post-deposition.

A simplified conceptual model of the hydrologic system of the Little Spokane River Basin (Figure 3.2) was presented by Kahle *et al.* (2013) to illustrate the series of unconsolidated sedimentary deposits and basalt layers (together referred to as basin fill) overlying the "basin" of crystalline bedrock. The figure is representative of the southern half of the Little Spokane River Basin where basin-fill deposits are composed mostly of low permeability fine-grained material overlain or interbedded with

coarse-grained material (sand and gravel) or basalt, in places. Farther north in the basin, the basin-fill deposits are generally thinner and the basalt does not extend beyond the Eloika Lake area.

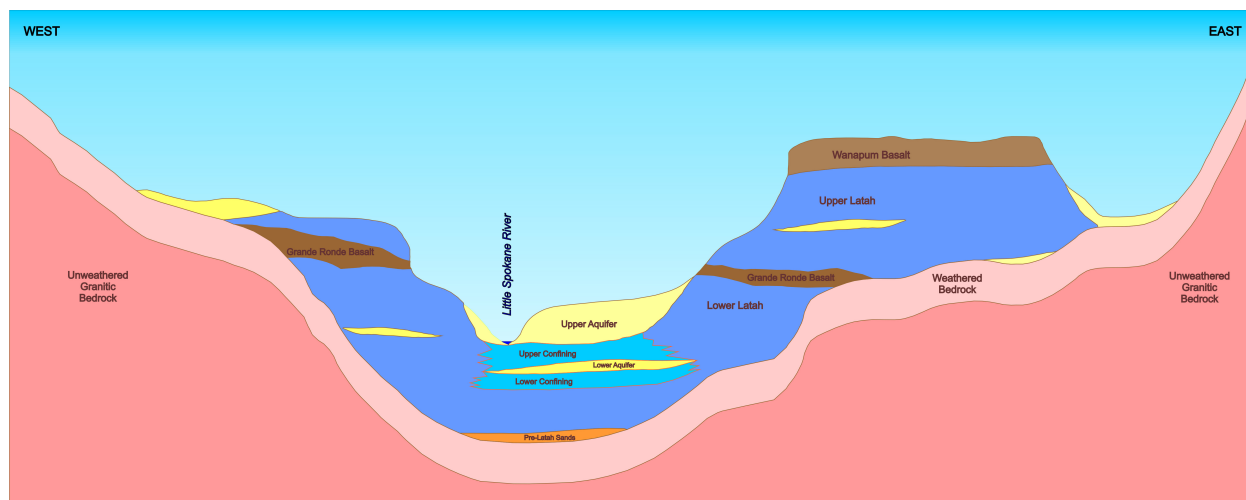


Figure 3.2: Schematic showing simplified conceptual hydrostratigraphic model (modified from Kahle *et al.*, 2013).

Kahle *et al.* (2013) found adequate data to map the approximate thickness and extent of the Upper Aquifer, the Lower Aquifers, and the Grande Ronde Basalt aquifer. As noted, the hydrogeologic units are heterogeneous and discontinuous. In addition, the upper confining unit, lower confining unit, and the Latah unit are similar in nature and were difficult to distinguish in drillers' logs. Generally, the first or upper confining material detected during drilling was considered part of the upper confining unit. If a deeper confining unit was detected below a lower aquifer, it was considered part of the lower confining unit. Confining beds (with or without associated sandy zones) either below or associated with basalt were considered part of the Latah unit.

To construct a numerical model, all hydrostratigraphic surfaces needed to be defined. Earthfx staff reviewed the geologic logs and other information to extend the work of Kahle *et al.* (2013) and create a set of three-dimensional (3-D) hydrostratigraphic model surfaces for all surfaces and covering the entire study area, as described below. Estimates of hydraulic properties of the units are discussed further on in Section 8.6.

### 3.3 Hydrostratigraphic Model Surfaces

A continuous multi-layer hydrostratigraphic model of the LSR Model area was developed from borehole log layer "picks", formation outcrop elevations, and 3-D interpolation constraint lines drawn on multiple cross-sections. The hydrostratigraphic model area extends a little beyond the study area boundaries in places and went through three major revisions during the course of this study. The conceptual hydrostratigraphic layers used in the numerical model are based on that presented in Kahle *et al.* (2013) which, in turn, relied on earlier work including Cline (1969), Carrara *et al.* (1995), Boese (1996), and Kiver and Stradling (1982).

The VIEWLOG GIS software (Kassenaar, 2013) was used to aid in the creating the continuous surfaces representing the tops of each hydrostratigraphic unit. First, an east-west cross-section line was drawn in the plan view map window at the southern end of the study area. Lithologic logs were extracted from the project database for each borehole within a selected offset distance and posted on the section map. The borehole data were analyzed and geologic picks were made recording the tops of each unit present, automatically entering the layer picks into the project database. The section was pushed northward, a set distance, and the process repeated until the northern boundary was reached. Borehole data included the 631 well records with geology compiled by the USGS

along with 469 new geologic logs for water wells added by Earthfx at critical locations within the study area. Interpretive polylines were drawn on the cross sections to add virtual points to guide the interpolation in areas with limited or inconsistent data. Lines representing bedrock valley thalwegs were also added to aid in the interpolation. Other picks, referred to as “push down points”, were used to constrain the surfaces where the mapped unit was known to lie below the base of borehole.

The geologic picks and constraint line vertices were interpolated to a grid with 100-foot square cells to create seamless surfaces using a geostatistical technique known as “kriging”. After interpolation, the surfaces were corrected for crossovers. For example, the interpolation process may fit a surface passing between two geologic picks on either side of a valley. By forcing the interpolated surface to not cross the upper surface (i.e., land surface topography), outcrops are created along the valley walls. The process was then repeated, posting the interim interpolated surfaces on the sections, so that borehole picks and interpretive polylines could be refined, as needed.

Figure 3.4 presents a map of the interpolated top of pre-Tertiary bedrock and shows the location of data points. This surface was checked to ensure it did not exceed land surface topography in areas of exposed bedrock. This considered to be a high confidence surface because drillers can accurately identify the granite or metasedimentary rock, however, the number of deep holes are limited in areas where there is thick water-bearing granular deposits. The thickness of all units above the Pre-Tertiary bedrock (pEm metasedimentary and TKg granite) was determined by subtracting the top of bedrock from land surface and is presented in Figure 3.5. The thickness includes the Grande Ronde and Wanapum basalt units and Latah Formation as well as younger Pleistocene and Recent deposits.

Two other high-confidence surfaces are the top of the Grande Ronde Basalt (Figure 3.6) and Wanapum Basalt (Figure 3.7). The figures show the locations of data points used to generate the surfaces. While the surfaces appear continuous, they follow the top of the underlying unit if the unit is locally absent. The Wanapum Basalt surface also represents the erosional top of the Miocene unconformity. The thickness of the Pleistocene and Recent deposits above the Miocene unconformity was determined by subtracting the top of the Wanapum surface from land surface and is presented in Figure 3.8.

While surface elevation maps can be generated for each overlying hydrostratigraphic model unit, the extent and significance of the units is better presented as a series of isopach (unit thickness) maps. Figure 3.9 through Figure 3.18 present the isopach maps of each identified unit. Note that the contour range and color scale can vary between the different maps. As evident in all these maps, the thicknesses are highly variable and the units tend to be discontinuous through much of the study area. This is a result of the complex geologic history of the area.

One new map of particular note is the map of the thickness of weathered or decomposed granite (Figure 3.18). This moderately permeable unit, which was previously not considered separately, was identified from driller’s descriptions (e.g., “decomposed granite”) that were entered into the database during the data compilation task. The surface was mapped from borehole logs to determine if there was a characteristic thickness or patterns in the depth of weathering. No consistent depth of weathering was identified; however the groundwater flow model turned out to be very sensitive to the properties assigned to this unit and that of the underlying unweathered bedrock. The initial interpolated surface was modified to assign a minimum weathered bedrock thickness (25 ft), mostly in areas where borehole data were lack or insufficiently detailed.

### 3.3.1 Comparison with USGS Conceptual Cross Sections

A series of section lines and conceptual cross sections through the study area were presented in Plate 2 of the USGS study (Kahle et al, 2013). Locations of the cross sections are shown on Figure 3.19. To facilitate the analysis and review of the continuous three-dimensional hydrostratigraphic models, a series of cross sections were generated along the same section lines. For example,

Figure 3.20 shows geologic section A-A' and Figure 3.21 shows geologic section C-C'. Figure 3.22 shows the corresponding conceptual sections from Kahle *et al.* (2013) at the same scale, for comparison. It should be noted that the USGS sections are schematic in nature, while the sections shown in Figure 3.20 and Figure 3.21 represent slices through the continuous stratigraphic model. The USGS sections, for example, include interpreted lenses and unknown surface elevations denoted as dashed lines and question marks where information was lacking. Gaps do not exist within the continuous surfaces of the hydrostratigraphic model. Borehole logs for wells along or close to the section line are shown on the Earthfx sections.

In general, there is good agreement between the USGS conceptual sections and the sections through the LSR continuous hydrostratigraphic model. The continuous surfaces show a higher level of refinement that was achieved through the review of the previous information, adjustment of layer picks, and nearly doubling the number of borehole logs interpreted.

### 3.3.2 River Profile Sections

Cross sections were prepared along the main branch of the Little Spokane River and the major creeks in the watershed to assess the nature of geologic materials underlying the key streams. The river profile cross sections lines are shown on Figure 3.19. A geologic section along the main branch of the Little Spokane River from the headwaters north of Diamond Lake to the gage at Dartford is shown on Figure 3.23. Dramatic changes in subsurface materials are observed along the direction of flow. Note that in many areas, the river has eroded through the overburden and is flowing directly on weathered granite bedrock. Dragoon Creek is somewhat unique, as can be seen in Figure 3.24, in that for much of its profile it is flowing on exposed Grand Ronde Basalt below the Wild Rose and Half Moon Prairies.

## 3.1 Groundwater Flow Regimes

### 3.1.1 Static Water Levels

Regional water level patterns were evaluated using well information imported from the Washington State Department of Ecology's (Ecology) Water Well database, USGS data, and data from the Counties and various municipalities within the LSR watershed. Groundwater level data for each of the key aquifer units, the Upper Aquifer, Lower Aquifers, Grande Ronde Basalt aquifer, and bedrock aquifer, were assembled by analyzing available borehole logs. Well screens were assigned to hydrogeologic units based on screen setting (Figure 3.25). Water level data include static water levels collected at the time of well installation and average water levels at wells where continuous water level data are collected. Data from wells in a buffer zone outside the study area boundary were also used in the analysis.

The groundwater-level data were interpolated to a 100 ft square grid using kriging to determine general patterns of groundwater flow. Figure 3.26 to Figure 3.29 show the locations of the water level data points and results of the kriging of the water levels within the extents of each key aquifer. Additional constraint points representing stream stage were added along the stream channels for the Upper Aquifer. The additional data points ensured that the interpolated water levels intersected the streams. The other units were not constrained.

The kriging analysis also produces a map of estimation variance. These maps, shown in Figure 3.30 to Figure 3.33, highlight where uncertainty is greatest and where having additional water levels would reduce the uncertainty in the water level maps.

### 3.1.2 Regional Water Level Trends

The interpolated potentiometric surface maps can be used to infer patterns of groundwater flow. Because most of the aquifers are thin relative to their areal extent, flow can be treated as being

predominantly horizontal (Bear, 1979). Vertical flow can dominate in some local areas such as in the immediate vicinity of partially penetrating wells, springs, and streams.

Flow patterns in the Upper and Lower Aquifers are difficult to discern because of the discontinuous nature of these units. The Grande Ronde Basalt aquifer is more continuous, especially in the Deer Park Basin/Dragon Creek subwatershed. Groundwater flow in the Deer Park Basin is generally from northwest to southeast toward the main branch of the Little Spokane River, then down the valley to the south, consistent with Kahle *et al.* (2013).

Granitic bedrock underlies the entire study area and regional groundwater flow patterns can be readily distinguished. In general, groundwater flow occurs from areas of high topographic relief in the bedrock highlands, towards the center of the watershed and down the Little Spokane River valley. Water levels in the bedrock appear to be heavily influenced by surface water features where overburden is thinnest in the east-central portion of the watershed. Locally, groundwater flow directions are similar to that of the upper aquifers, where present. As such, groundwater flow in the Deer Park Basin is generally from northwest to southeast toward the main branch of the Little Spokane River, then down the valley to the south. Down-valley flow from east-to-west toward the Little Spokane River also appears to occur in the Deadman Creek subwatershed.

In the northeast, flow is complex, especially around the subwatershed and watershed divides and is directed towards either Diamond Lake, the main branch of the Little Spokane River, or towards the Pend Oreille River to the north. There was discussion in earlier studies (Dames and Moore, 1995 and Golder, 2004) regarding inflows to the LSR watershed across the northeastern boundary near Newport. This cross-basin groundwater flow was assumed to supply baseflow to the main stem (east branch) of the LSR. The interpolated water levels (Figure 3.29) and the results of the groundwater model (discussed further on) do not support that conclusion.

### 3.1.3 Transient Water Level Data

Transient groundwater level data were obtained from Spokane County at nine locations within the watershed (Figure 3.34) to assess the temporal behaviour of the groundwater system and to aid in model calibration (discussed further on). Well construction details are summarized in Table 3.2. Continuous long-term transient monitoring data are sparsely distributed across the watershed and many of the monitoring wells are near municipal pumping wells making it difficult to discern the natural seasonal response from the seasonal variation in pumping. There are also 41 wells with more than 12 water level measurements in the database. About half have data from the 1960s and 1970s, the rest have monthly data from 2012 to 2013.

Table 3.2: Summary of transient monitors.

Monitoring Well Name	Top of Casing (fsl)	Depth (fbgs)	Hydrogeologic Unit	Period of Record
Deer Park	2180	350	Grande Ronde	2009 - 2016
Chattaroy	1989	242	Bedrock	2005 - 2016
Shady Slope	1639	245	Lower Aquifer	2005 - 2016
Whitworth North Mt. View	1958	90	Upper Aquifer/ Upper Confining	2009 - 2012
Whitworth Rivilla	1585	30	Upper Aquifer	2009 - 2016
SCWD#3 River Estates	1722	122	Upper Aquifer	2009 - 2014
SCWD#3 Pine River	1619	208	Pre-Latah Sands	2009 - 2016
Colbert Landfill - North Glen	1672	44	Lower Aquifer	2009 - 2013

Pine River Park	1603	70	Pre-Latah Sands	2014 - 2016
-----------------	------	----	-----------------	-------------

Hydrographs at each of the nine monitoring location with continuous data are presented in Figure 3.35 through Figure 3.43. Water levels at the Deer Park monitor (Figure 3.35), completed in the Grand Ronde Basalt, exhibit daily fluctuations on the order of inches; however, large seasonal fluctuations are observed on the order of 10-15 feet. Water levels tend to decline gradually starting in May, followed by a sharp drop in July, and recover through the fall and winter in an exponential manner. This behaviour, typical of pumping-induced drawdown and recovery, is likely driven by the seven Deer Park municipal pumping wells, located slightly over one mile to the northeast and southeast. The wells are screened across multiple aquifer units including the Upper Aquifer, Lower Aquifers, and Grande Ronde Basalt aquifers. Very little seasonal lag occurs between the timing of the pumping wells and the response at the Deer Park monitor, suggesting that the systems are reasonably well connected. Water levels annually return to approximately 2,143 fsl through the winter and spring with only a few feet of inter-annual variability. Overall, the large annual pumping induced drawdown, followed by relatively rapid recovery are indicative of a high degree of confinement and suggests that the storage capacity of the screened unit is likely limited.

Water levels at the Chattaroy monitor (Figure 3.36), completed in the bedrock, fluctuate annually by only a few feet on either side of 1950 fsl; however, the trends suggest that it is influenced by seasonal pumping – possibly due to irrigation wells within 0.5 miles of the Chattaroy monitoring well, Deer Park wells (located about 4.0 miles to the west) or a Spokane County Water District #3 well (located 2.5 miles to the east). Water levels drop sharply in late June and early July and begin to recover in the fall. The recovery is slow and only on occasion do water levels flatten or begin to exhibit a natural response. The relatively small annual fluctuations and slower recovery are indicative of less confined conditions and greater aquifer storage in this area.

The Whitworth Shady Slope monitor is located near the confluence of Deadman Creek with the Little Spokane River and immediately adjacent to Whitworth Pumping Well 8 (Figure 3.37). Despite its close proximity to a pumping well, the Shady Slope monitor does not appear to be as heavily influenced by seasonal pumping, where a sharp drop in water levels through the summer is often followed by exponential-type recovery through the fall, as described above and as observed at the Pine River and Pine River Park monitors (Figure 3.38, Figure 3.39). While this behaviour is seen during certain years (e.g., early 2011, 2012 and 2015), the annual variability follows a more symmetrical seasonal pattern. This suggests that either the pumping at this location is uniform year-round, the magnitude of the natural variability dominates over the seasonality of the pumping rates, or more likely, a combination of both. Water levels fluctuate seasonally by 10 to 15 feet, consistently reaching a maximum in May or June and a minimum in November or December.

Shallow groundwater monitors located close to the main branch of the Little Spokane River include the Pine River Park monitor (Figure 3.39), SCWD#3 River Estates (Figure 3.40), Colbert Landfill (Figure 3.41), and Whitworth Rivilla (Figure 3.43). These wells, with the exception of Pine River Park, all exhibit hydrographs that appear analogous to streamflow. Sharp increases in water levels on the order of 2 to 3 feet occur in the spring, followed by a slow decline through the summer at all three locations. It is likely that the wells are screened in a geologic unit that is in good connection to the Little Spokane River and are influenced by stream-aquifer interaction. On the other hand, the Pine River Park monitor (Figure 3.39) behaves more like the deeper SCWD#3 Pine River monitor (Figure 3.38) and is influenced by municipal pumping, following a similar drawdown and recovery trend on the order of 15 to 20 feet annually. This suggests that there is likely a degree of vertical connectivity between the shallow and deeper aquifer units in this area. On a technical note, the data logger in Whitworth Rivilla was replaced by Spokane County staff in 2014 and the method for correcting for atmospheric pressure was changed; these factors are responsible for the difference in the appearance of the post-2014 data.

### 3.2 Tables

Table 3.3: Brief description of geologic units (modified from Kahle et al, 2013)

Geologic Unit	Description
Stream deposits <b>Qs</b>	Includes channel, overbank, and alluvial-fan deposits of rivers and streams. Consists mostly of stratified silt and sand with some gravel and minor amounts of clay deposited by flowing water. Also includes peat deposits in low-lying, poorly-drained areas.
Mass wasting deposits <b>Qmw</b>	Includes poorly-sorted angular rock fragments deposited as talus at the base of steep slopes and heterogeneous mixtures of unconsolidated surficial material and rock fragments deposited by landslides. Commonly occurs at the base of the basalt uplands, where the unit is composed mostly of Latah Formation and basalt fragments.
Eolian deposits <b>Qe</b>	Includes loess—wind-blown silt and fine sand, with minor amounts of clay, blanketing basalt uplands, and dune sand overlying glacial outburst flood deposits
Fine-grained glacial deposits <b>Qgf</b>	Includes clay, silt, and sand lake sediments deposited in ice-marginal lakes and sand and silt outwash and distal outburst flood deposits. Unit includes coarse-grained lenses in places
Coarse-grained glacial deposits <b>Qgc</b>	Includes glacial-outburst flood deposits that consist of sand with gravel, cobbles, and boulders deposited by catastrophic draining of Glacial Lake Missoula and reworked outwash and till deposited by the Pend Oreille lobe. Includes local areas and lenses of fine-grained material.
Glacial till <b>Qgt</b>	Includes mostly poorly sorted and unstratified clay, silt, sand, and gravel deposited by the Pend Oreille River lobe.
Wanapum Basalt <b>Mw</b>	Composed of fine- to coarse-grained basalt flows with olivine and plagioclase phenocrysts. Forms prominent rim rock and steep cliffs, commonly with well-developed columnar jointing.
Upper Latah <b>Mul</b>	Includes lacustrine and fluvial deposits of gray to tan to yellow orange siltstone, claystone, and minor sandstone that underlie and are interbedded with the Grande Ronde Basalt and Wanapum Basalt.
Grande Ronde Basalt <b>Mgr</b>	Composed of black to dark gray, fine-grained, dense to slightly vesicular flows composed of dark-brown glass, plagioclase, pyroxene, and minor olivine. Flows are commonly pillowed, indicating the basalt flowed into water. Overlies or is invasive into the lower Latah Formation or older crystalline rocks.
Lower Latah <b>Mll</b>	Similar to upper Latah Formation.
Pre-Latah Sands <b>Mpls</b>	Patchy granular unit found overlying crystalline rocks.
Intrusive igneous <b>TKg</b>	Granite and includes fine- to coarse-grained, equigranular to porphyritic, muscovite-biotite granite, hornblende-biotite granite, granodiorite, and quartz monzonite.
Metamorphic <b>pEm</b>	Includes strongly foliated and layered, fine- to coarse-grained gneiss, schist, and quartzite; minor amphibolite and hornfels; meta-argillite and metasiltite, and metadolomite.

Table 3.4: Brief description of hydrostratigraphic units (modified from Kahle et al, 2013)

Unit	Name	Description
UA	Upper aquifer	Unconfined sand and gravel aquifer with some fine-grained lenses. Mostly composed of glacial outwash, outburst flood deposits, and stream deposits. Unit consists of sand, gravel, and cobbles along the Little Spokane River and in much of the Diamond Lake area. Generally finer grained, consisting mostly of sand, in the Deer Park area. Unit is thickest along former outwash channels including that now occupied by the Little Spokane River.
UC	Upper confining unit	Low-permeability unit consisting mostly of silt and clay with some sand. Contains coarse grained material in places. Composed mostly of glaciolacustrine material deposited in ice dammed lakes and the distal and fine-grained part of Missoula flood deposits. Contains mass-wasting deposits at the base of steep slopes and bluffs. Unit contains some lithologically similar but older deposits of the Latah Formation
LA	Lower aquifers	Localized confined aquifers consisting of sand and some gravel. Occurs at depth in various places in the basin; appears to be fairly continuous at depth below the lower reaches of the Little Spokane River. Unit is commonly overlain by UC and underlain by other low permeability sedimentary units (LC, LT), basalt, or bedrock.
LC	Lower confining unit	Low-permeability unit consisting mostly of silt and clay that, in places, underlies the Lower aquifers. Composed of glaciolacustrine sediment and (or) older Latah Formation sediment.
WB	Wanapum Basalt	Wanapum Basalt of the Columbia River Basalt Group; includes thin sedimentary interbeds in places and overlying loess. Generally not a reliable water-bearing unit.
ULT	Upper Latah	Mostly low-permeability unit consisting of the Latah Formation silt, clay, and sand that underlies and is interbedded with the Grande Ronde and Wanapum Basalts. Includes thin or broken basalt and coarse grained lenses. Sandy or gravelly parts of this unit can provide sufficient water for domestic use. Unit may contain lithologically similar but younger glaciolacustrine deposits.
GRB	Grande Ronde Basalt	Unit includes the Grande Ronde Basalt of the Columbia River Basalt Group and sedimentary interbeds in places. Provides sufficient water to numerous domestic wells in the west central part of the study area.
LLT	Lower Latah	Same as Upper Latah
PLS	Pre Latah Sands	Discontinuous sand unit found in places to overly crystalline bedrock.
WBR	Weathered Bedrock	Includes granite, quartzite, schist, and gneiss. Locally yields usable quantities of water where rocks are fractured. Yields are generally small and assumed to decrease with depth.
UBR	Unweathered Bedrock	

## **4 Climatic and Hydrologic Setting**

### **4.1 Climate Data**

Eastern Washington State has a unique climate due to the relative proximity to the Pacific Ocean and the position of the Coastal and Cascades mountain ranges in western Washington. These ranges cause orographic lifting and remove much of the moisture from the air masses moving eastward from the Pacific Ocean, causing the low annual rainfall observed in the Spokane area (16.7 inches at the Spokane Airport). Orographic lifting occurs again as air rises along the western foothills of the Rocky Mountains at the eastern state boundary, causing higher rates of precipitation over Mt. Spokane. The air is relatively dry year-round and convective storms are relatively rare compared to frontal storms.

Golder (2003) discusses the effect of the changes in the surface temperature and winds of the Pacific Ocean on local climate, in particular, the El Nino Southern Oscillation (ENSO) and the Pacific Decadal Oscillation (PDO). The ENSO recurs on a 2 to 7 year time scale while the PDO is a pattern that reverses on a 20 to 30-year time scale. The El Nino (a warm phase ENSO) generally causes unusually warm and dry weather while the La Nina (a cool phase ENSO) generally causes unusually cool and wet weather. ENSO phases usually last 6 to 18 months with strongest impacts in October and March. The PDO is like a more persistent ENSO, where a warm PDO increases temperature and precipitation; while a cool PDO decreases them.

#### **4.1.1 Precipitation and Temperature Data**

Climate data from stations within and nearby the study area were obtained and analyzed to better understand historical climate patterns and to create a continuous high-quality set of daily climate. Key data sets were obtained from the Global Historical Climate Network (GHCN) archives maintained by the National Oceanic and Atmospheric Administration (NOAA) and the Cooperative Agricultural Weather Network (AgriMet) archives. The NOAA archives contain data from the National Weather Service and data collected by volunteers in the Community Collaborative Rain, Hail, and Snow (CoCoRHAS) network. SNOTEL data were obtained for the Elk and Quartz Peak stations. Station locations are shown in Figure 4.1.

Station information for 49 stations is presented in Table 4.2. The available period of record for the stations, based on months with available data, is illustrated on Figure 4.2. Spokane and Deer Park airports go back to the 1890s but the Deer Park station was discontinued in 1977 and restarted in 1988. The number of stations prior to 2008 is limited, however, as can be seen in Figure 4.2. Many additional stations, primarily in the CoCoRHAS network, became operational in 2008 although there is less continuity in the data.

To assess the spatial distribution of precipitation and temperature, daily climate data at the 49 climate stations were interpolated to a 1000 ft square grid using an inverse-distance-squared weighting technique. Grids of daily precipitation (total precipitation, rain, and snow) were prepared for the period from WY1892 to WY2016. Daily temperature (minimum, mean, and maximum) data were also gridded for the period. Lapse corrections were applied to both precipitation and temperature to account for the elevation differences between climate stations.

Average annual precipitation for the period of record was calculated from the daily grids. Average annual precipitation is as high as 50 inches atop Mt. Spokane in the east and Boyer Mountain in the northwest of the study area and is as low as 15 inches at lower elevations of the Little Spokane River valley (Figure 4.3). Precipitation at Deer Park was estimated to be approximately 20 inches, slightly less than the 22 inches stated in Chung (1975). The bedrock highlands receive more precipitation than the more permeable overburden sediments found at lower elevations. Annually-averaged daily temperature (Figure 4.4) has an inverse relationship with elevation, with average

temperature ranging between 35°F and 50°F. Figure 4.3 and Figure 4.4 are both hill-shaded with a 1000 ft DEM to illustrate the correlation of precipitation and temperature with topography.

#### 4.1.2 Basin Averaged Daily Precipitation and Temperature

The daily gridded climate data were averaged over the Little Spokane River watershed to generate a daily time series of basin-averaged precipitation and temperature. A forty-year portion of this daily basin-average dataset is presented in Figure 4.5 and Figure 4.6 for the period from WY1977 to WY2016. The following analysis of climate trends was undertaken with this interpolated, basin-averaged time series.

Figure 4.7 presents the annual average precipitation observed over the study area for a 122-year period showing long-term trends and the number of stations used in the interpolation. Estimated average annual precipitation between WY1895 and WY2016 was 23.1 inches per year (in/yr) over the watershed; while over the past 50 years (WY1967-WY2016) annual precipitation averaged 25 in/yr (Table 4.1). The precipitation trends follow the general pattern observed in the Washington State Palmer Drought Severity Index (Figure 4.8), which is a measure of relative wetness and dryness. Periods of observed wet and dry climate correspond well to years with above and below average precipitation, respectively. Prolonged periods of drought in the observed record occur in the late 1920s, early 1930s, and mid-to-late 1980s.

Table 4.1: Basin-averaged annual precipitation with varying observation periods.

Period	Watershed Average Precipitation (in/yr)
Total Record	23.1
Past 100 years	23.8
Past 50 Years	25
Past 30 Years	24.8
Past 10 Years	27

Figure 4.9 presents the basin-average annual temperature observed in the study area between WY1895 and WY2016. Figure 4.10 overlays the annual mean temperature with the annual precipitation totals. Some years of reduced precipitation correspond to years with a higher than normal mean temperature (e.g., the late 1980s to early 1990s) and vice-versa (e.g., the mid-1970s). Figure 4.11 presents a breakdown of annual precipitation volumes by rain and snow. On average, rain makes up 77% of total annual precipitation but has been as low as 53% and as high as 96%.

Figure 4.12 presents a histogram of average monthly precipitation. Median monthly precipitation falls from January to August and increases during the fall. The mid-summer months have very low median precipitation and in extreme cases (5<sup>th</sup> percentile), there are months with no precipitation at all (e.g., July, 1930). Precipitation tends to be higher and more variable in the winter months. Figure 4.13 presents monthly histograms of daily minimum and maximum temperature. Daily values range from extreme minimums of -35°F in January to maximums exceeding 100°F in July.

Figure 4.14 presents the daily precipitation exceedance probability function (EPF) for the period of record. Daily precipitation totals exceed 0.05 in for 60% of days with measured precipitation. Only 0.5% of daily precipitation events exceed 1 in.

#### 4.1.3 PRISM Data

Initial runs with the integrated model using the interpolated data showed some anomalous results that were traced back to the precipitation inputs. These occurred primarily in the years with few

stations. The number of stations with separately measured rainfall and snowfall, the preferred input for the model, are even more limited and the interpolation often used only one or two stations.

An alternative climate data set is available from the PRISM Climate Group at Oregon State University (<http://prism.oregonstate.edu/>). The group gathers climate observations from a wide range of monitoring networks. While many of the stations used are identical, the PRISM Climate Group applies sophisticated quality control measures and lapse correction techniques to develop high-quality spatial climate datasets covering the period from 1895 to the present.

PRISM data sets containing daily minimum and maximum temperature and daily precipitation for the period 2002 through 2017 were obtained by WEST for the Little Spokane River watershed. The ASCII file data included daily total rainfall in millimeters and daily minimum and maximum temperature in degrees Celsius. The PRISM day is defined as 1200 UTC-1200 UTC and uses a day-ending naming convention (e.g., a day ending at 1200 UTC on 1 January is labeled 1 January). Data were downloaded from the official PRISM website (<http://www.prism.oregonstate.edu/explorer/>) in Tiff file format. The original Tiff files are gridded data with a resolution of 4 km (about 2 mi by 3 mi, when re-projected to the study area). The Geospatial Data Abstraction Library (GDAL) was used to clip the data to the study area, re-project the grid, and then resample to a regular 1000 ft square grid covering the study area. A Python program was used by WEST to automate this process and generate gridded ASCII air temperature and precipitation data for each day. Earthfx converted the ASCII gridded data into a format compatible with the GSFLOW model.

As noted above, the previous calibration runs used snow and rain measurements directly from the climate data sets rather than total precipitation. Methods built into the PRMS code were used to partition the PRISM precipitation data into rain and snow based on the daily temperature. The methods were tested against the available observed snow and rain data and initially overpredicted rainfall and underpredicted snow in mixed snow/rain events. The threshold temperatures for defining all-snow, all rain, and mixed events were adjusted to improve the match to the observed data. Further discussions regarding precipitation form can be found in Section 7.5.4.

#### 4.1.4 Other Climate Data

Spokane has about 174 days classified as sunny or partly sunny. Solar radiation is an important input to the hydrologic model and is used to estimate snowmelt and actual evapotranspiration. Data were obtained for the closest station (Deer Park) but were available only for 2014 and onward. Supplemental data were obtained from the Chamokane station for 2007 to the present. An analysis of data from the overlapping period showed very high correlation. Data prior to 2007 were obtained from a University of Oregon network station in Cheney, WA. While the data were not as well correlated, they provided the necessary coverage.

Potential evaporation estimates using the Penman method were obtained from stations in Chamokane and Deer Park. The Chamokane covered the WY2009-WY2013 calibration period and correlated well to the Deer Park data starting in July 2014. Snowpack depth and water equivalent data were obtained from a station in Elk and a SNOTEL site on Quartz Peak. These data are discussed further in Section 7.5.4.

## 4.2 Hydrologic Setting

Along with climate, the hydrologic setting of the Little Spokane River watershed is controlled by the physiography, surficial geology, and drainage pathways. The study area can be generally divided into several broad hydrologic regions based on these factors:

- **Bedrock uplands:** This area forms the boundary of the LSR watershed and is dominated by intermittent streams that drain the relatively thin or absent soil zone mantling the mostly granitic bedrock.

- **Diamond Lake – East Deer Valley area:** This area is isolated from the rest of the LSR watershed by an east-west trending line of bedrock hills (Lone Mt., Bare Mt., and an unnamed hill to the west). The area is drained by Moon Creek which flows into Sacheen Lake and then to the West Branch of the Little Spokane River.
- **Deer Park Basin:** This central area is drained mainly by Dragon Creek and its many tributaries and to a lesser degree by tributaries to Eloika Lake and the West Branch of the Little Spokane River. The basin is mantled by finer-grained flood deposits. The central part of the basin is underlain by the basalt units while the deposits in the uplands to the south (Wild Rose Prairie and Half Moon Prairie) are underlain by granitic bedrock.
- **East Side of the Little Spokane River Watershed:** This area is dominated by streams that drain Mt. Spokane. These include Dry Creek, Deer Creek, Little Deep Creek, and Deadman Creek. The creeks are separated by mesas (Green Bluff, Orchard Bluff, and an unnamed feature to the north) and Peone Prairie.
- **Little Spokane River Valley:** The valley containing the main branch of the Little Spokane River is dominated by coarser-grained flood and outwash deposits that form the upper aquifers and provide baseflow to the stream. The Little Spokane River has few artificial controls on its flow and the hydrograph shows sharp responses to seasonal effects such as snowmelt (Golder, 2003).
- **Newport - West Deer Valley area:** This area is outside the LSR watershed and contains several short north-flowing streams that drain to the Pend Oreille River (Bracket Creek, Kent Creek, and McCloud Creek).

#### 4.2.1 Streamflow Measurement

The major streams that drain the Little Spokane River Watershed are shown on Figure 1.1. The streams have been classified as perennial and intermittent, as shown on Figure 4.15. Locations of stream gages maintained by the USGS and Ecology are shown on Figure 4.16. Table 4.3 presents a summary of the properties and streamflow characteristics of the gages within the study area. A gage on Eloika Lake monitors lake stage except during the winter months. Spot flow locations with multiple measurements and seepage run locations are also posted on Figure 4.16.

#### 4.2.2 Flow at Dartford

The USGS gage at Dartford (12431000) measures flow at the outlet of the portion of the LSR watershed within the study area and is of prime significance to this investigation. The gage started in May 1929 but there was a gap from October 1932 until December 31, 1946. Streamflow has been monitored continuously at this site since January 1947. A hydrograph of the observed record at the gauge is presented in Figure 4.18. Annual average streamflow for WY1966 to WY 2017 is shown in Figure 4.19. Other gages in the area have shorter periods of record and many have significant gaps. These gages were used in the model calibration and are discussed further in Section 9.1.4.

Average annual discharge at the Dartford gage is 292 cubic feet per second (cfs) with a maximum of 625 cfs and a minimum of 152 cfs. Daily flow at the gage rarely drops below 100 cfs. Extreme low-flow events (less than 80 cfs) in the Little Spokane River watershed were observed in the early 1930s, the mid-1990s and in WY2015. Since 1976, 115 cfs was set as a trigger to notify all junior water rights holders in the basin to stop withdrawals (Spokane County, 2006). The number of days per year where flow fell below 115 cfs is shown on Figure 4.19. Dames and Moore (1995) noted an increasing trend in the number of these occurrences; however, the timing of their study coincided with a dry series of years.

Flows can be converted into an equivalent depth over the watershed by dividing the annual flow volume by the contributing area. These values can be compared to total precipitation over the area to compare trends as well as estimate the losses due to evaporation. Results using the interpolated

precipitation data from study area stations are shown in Figure 4.20. Flow and precipitation depths appear to be generally well correlated on an annual basis. The precipitation-to-flow ratio for the period shown is 25.5% and indicates that losses to ET should average about 18.6 in/yr.

#### 4.2.3 Flow Duration Curves

The flow-duration curve (FDC) is an analysis plot that characterizes the relationship between magnitude and frequency of flows at a gauge station (Searcy, 1959). In the method, each flow rate is plotted against the percentage of time that flow rate is equalled or exceeded. FDCs represent an empirical approximation of the cumulative distribution function of stream flow record at a gaging station (Maidment, 1992). These curves offer a simple and effective method to characterize catchment runoff properties and flow regimes from gage data.

Flow duration curves are plotted for the gage at Dartford and for four other key gages. A separate scale (left-hand axis) is used for the Dartford gage because of the large difference in the magnitude of the flows. The steep slopes at the high end for all gages except Elk indicate that flow is highly variable and the system is likely affected by overland runoff in this range. Very flat slopes for the rest of the range suggest a damped runoff response where flow is dominated by groundwater discharge, seepage from wetlands, and/or gradual snowmelt. One might expect the response at TMDL23 to be different than the others; it is downstream of Eloika Lake which should attenuate high flows but does not appear to do so in a significant manner. On the other hand, the flat response at the Elk gage is a bit surprising. The presence of Chain Lake, wetlands, and blockages upstream of the gage are likely factors in attenuating the flows. The local geology is also a factor; the high permeability soils and the isolation of the basin by bedrock hills allow the basin to act as a large storage reservoir and attenuate flows.

Monthly-averaged daily streamflow at Dartford for WY1947 to WY2017 is presented in Figure 4.21 to illustrate general seasonal patterns. Flows increase from January to April as a result of rainfall and snowmelt. Flows decrease consistently from May to August and then recover from September to December.

#### 4.2.4 Baseflow Estimates

Hydrograph separation techniques were applied to the continuous flow data to split the two components of streamflow: (1) overland runoff and (2) baseflow. Baseflow is often assumed to be primarily composed of groundwater discharge. It should be noted that the separation methods cannot, by themselves, distinguish between groundwater discharge and other relatively steady flows such as discharge from large wetlands or gradual melting and runoff from the snowpack at high elevations. Numerous techniques are available to estimate baseflow including curve processing and statistical techniques. Ten methods were investigated, all giving comparable results. Figure 4.23 presents estimated baseflow using the local minimum method (Sloto and Crouse, 1996).

The baseflow index (BFI) is the ratio between baseflow discharge ( $Q_{BF}$ ) and total discharge ( $Q$ ). The BFI can serve as an initial estimate into the overall groundwater contribution to flow. BFIs were very high; ranging from 0.86 to 1.0 for the Dartford gage and from 0.95 to 0.99 for the USGS gage at Elk. The local minimum method yielded 0.934 and 0.973, respectively, for the two gages.

#### 4.2.5 Spotflows

Flows are measured at additional locations, primarily on ungaged tributaries, to supplement the available long-term record. Seepage runs, where flows are measured synoptically along a section of stream, have been carried out to estimate the contribution from groundwater discharge or loss to the aquifer along the section. Spotflow measurements supplemented the flow calibration targets for the integrated model. These are discussed further in Section 9.1.4

### 4.3 Tables

Table 4.2: Climate stations proximal to the study watershed.

Name	Station ID	Data Source	Easting (ft)	Northing (ft)	Elevation (ft)	Start Date	End Date	Water Years with Data	Average Days with Data per Water Year
Deer Park, WA	drpw	AgriMET	366623	2473218	2174.0	Jun 2014	Feb 2017	4	237
Chamokane, WA	chaw	AgriMET	391434	2397267	1950.0	Nov 2007	Feb 2017	10	335
Priest River 2.0 ENE	US1IDBR0009	GHCN	462960	2605539	2395.0	Jun 1998	Nov 2009	3	79
Oldtown 6.0 S	US1IDBR0025	GHCN	422475	2566834	2287.1	Jun 2015	Oct 2016	3	73
Post Falls 2.1 NNW	US1IDKT0002	GHCN	294196	2592253	2150.9	Dec 2008	Aug 2011	3	163
Rathdrum 1.4 SSW	US1IDKT0005	GHCN	314081	2606241	2208.0	Jun 1998	Jan 2017	11	156
Elk 5.6 NE	US1WAPO0001	GHCN	413432	2530102	2594.2	Jun 2008	Feb 2017	10	302
Elk 5.2 NW	US1WAPO0002	GHCN	404786	2486786	2272.0	Oct 2008	Nov 2016	9	65
Newport 0.4 W	US1WAPO0004	GHCN	453112	2560780	2182.1	Nov 2008	Jun 2014	6	261
Newport 5.5 W	US1WAPO0009	GHCN	452049	2533500	2544.9	Jul 2009	Jan 2016	8	279
Spokane 5.2 SSE	US1WASP0001	GHCN	241956	2498635	2377.0	May 2008	Sep 2009	2	135
Spokane 4 SE	US1WASP0002	GHCN	246179	2494321	2440.0	May 2008	Mar 2012	5	233
Spokane 6.6 NW	US1WASP0003	GHCN	289550	2463676	1984.9	Jun 2008	Apr 2012	5	223
Spokane 5.5 S	US1WASP0004	GHCN	234379	2483564	2171.9	Jun 2008	Feb 2017	10	294
Spokane 8.9 E	US1WASP0006	GHCN	256275	2530410	2067.9	Jun 2008	Jul 2012	5	265
Spokane 5.1 NNW	US1WASP0010	GHCN	280529	2466952	1987.9	Jun 2008	May 2014	7	246
Fairwood 1.1 ENE	US1WASP0012	GHCN	299805	2485900	1813.0	Jun 2008	Nov 2009	3	153
Spokane 1.3 SSW	US1WASP0013	GHCN	257833	2478920	1896.0	Jun 2008	Oct 2012	6	182
Deer Park 2.1 WSW	US1WASP0014	GHCN	365667	2462620	2123.0	Jul 2008	Feb 2017	10	246
Spokane 5.7 SSE	US1WASP0016	GHCN	237472	2496368	2392.1	Jun 1998	Feb 2017	11	264
Spokane 3.8 SSE	US1WASP0017	GHCN	245036	2489188	2344.2	Sep 2008	Dec 2011	5	21
Airway Heights 0.5 N	US1WASP0021	GHCN	254783	2441333	2381.9	Jun 2009	Oct 2014	7	115
Nine Mile Falls 8.7 NW	US1WASP0022	GHCN	333232	2416621	1557.1	Sep 2009	Feb 2017	9	233
Spokane 6.0 SE	US1WASP0023	GHCN	244751	2507890	2598.1	Jan 2010	Jul 2012	3	229

Name	Station ID	Data Source	Easting (ft)	Northing (ft)	Elevation (ft)	Start Date	End Date	Water Years with Data	Average Days with Data per Water Year
Chattaroy 6.3 NE	US1WASP0024	GHCN	365540	2518065	2207.0	Feb 2010	Feb 2017	8	315
Spokane 1.7 SSE	US1WASP0025	GHCN	256007	2487118	2000.0	Apr 2010	Jun 2013	4	227
Mead 1.9 NNE	US1WASP0027	GHCN	309172	2498496	1903.9	Sep 2010	Sep 2014	4	77
Spokane 5.0 N	US1WASP0030	GHCN	290584	2481362	1941.9	May 2011	Feb 2017	7	57
Deer Park 3.7 NE	US1WASP0032	GHCN	384040	2486666	1938.0	Jul 2011	Sep 2015	5	235
Spokane Valley 4.2 ESE	US1WASP0033	GHCN	257928	2546027	2064.0	Sep 2011	Jun 2014	4	201
Spokane 3.5 NNW	US1WASP0034	GHCN	279137	2471867	2047.9	Dec 2011	Jan 2017	6	46
Liberty Lake 1.4 WNW	US1WASP0035	GHCN	263137	2557151	2278.9	Dec 2011	Sep 2015	4	208
Elk 2.6 WNW	US1WASP0036	GHCN	397691	2498640	2116.1	Jan 2012	Feb 2017	6	283
Colbert 3.1 WNW	US1WASP0037	GHCN	328941	2483417	2039.0	Jan 2013	Jun 2013	1	129
Spokane 14.6 NW	US1WASP0043	GHCN	310443	2420854	2386.2	Jun 2014	Feb 2017	4	207
Clayton 2.6 SW	US1WASP0001	GHCN	372295	2430655	2304.1	Jun 2008	Feb 2017	10	219
Falls Ranger Station	USC00103117	GHCN	491964	2585517	2295.9	Mar 1928	Feb 1936	9	273
Deer Park Airport	USC00452066	GHCN	371019	2473078	2201.1	May 1911	Mar 1977	67	353
Mt. Spokane	USC00455673	GHCN	356191	2547369	5282.2	Oct 1934	Nov 1951	14	195
Mt. Spokane Summit	USC00455674	GHCN	356387	2551435	5892.1	Jul 1953	Dec 1972	21	330
Newport	USC00455844	GHCN	454674	2563585	2162.1	Oct 1909	Jan 2017	103	352
Spokane	USC00457933	GHCN	261876	2481997	1879.9	Nov 1953	Oct 1983	31	347
Spokane WFO	USC00457941	GHCN	264899	2430082	2392.1	Aug 1996	Feb 2017	22	341
Flowery Trail WA	USR0000WFLO	GHCN	491890	2474897	2600.1	Oct 1995	Feb 2017	22	304
Quartz Peak	USS0017B04S	GHCN	343333	2558626	4700.1	Jun 1986	Feb 2017	32	348
Ragged Mountain	USS0017B06S	GHCN	336647	2571240	4210.0	Sep 2006	Feb 2017	12	313
Fairchild AFB	USW00024114	GHCN	247239	2425069	2438.0	Jan 1949	Dec 1970	23	348
Spokane Intl Airport	USW00024157	GHCN	244279	2455279	2353.0	Aug 1889	Feb 2017	129	361
Deer Park Airport	USW00094119	GHCN	373807	2474180	2190.9	Nov 1998	Feb 2017	19	351
Spokane Felts Field	USW00094176	GHCN	268909	2505182	1953.1	Oct 1998	Feb 2017	19	352

Table 4.3: Streamflow gages and catchment size.

Station Name	Location	Easting (ft)	Northing (ft)	Period of Record	Status	Catchment Area (mi <sup>2</sup> )	Mean Discharge (cfs)	Median Discharge (cfs)
USGS 12427000	LSR at Elk	2511634	393039	1948-2016	Active	84.5	54.4	49.0
USGS 12431000	LSR at Dartford	2483374	305031	1929-2016	Active	619	298	201
USGS 12431500	LSR near Dartford	2460850	302722	1948-2016	Active	677	570	473
LSR at Chattaroy	LSR at Bridge at Chattaroy Rd	2493276	343661	1975-2001		273	145	108
Deadman Creek at Mouth	after confluence with Little Deep Creek	2488681	309241	1999-2016	Active	122	40.0	18.7
DR9	at mouth	2489076	338762	1999-2004		166	54.1	37.1
Dragoon Creek	at E Chattaroy Rd	2486689	342671	1999-2016	Active	165	50.1	32.7
LSRTMDL-1	LSR at Scotia Rd.	2539250	424897	2004-2006		44.5	24.7	23.7
LSRTMDL-2	LSR at Bridge Crossing - E. Deer Park Milan Rd.	2497338	373131	2004-2006		246	116	85.0
LSRTMDL-23	LSR at outlet of Eloika Lake	2489633	386292	2007-2016	Active	99.0	53.1	30.5

## **5 Water Use Management**

### **5.1 *Background***

The groundwater resources along with the tributary streams and creeks of the Little Spokane River watershed have been developed as a water source for public supply, self-supply, and agricultural purposes for decades. Water use in the watershed is governed by “water rights” (discussed further below) entitling the right-holder to utilize a defined water resource. However, much of water within the watershed is now appropriated (i.e., “spoken for”), limiting available water rights for future users. This presents a problem for a growing population with an increased demand for water. It has prompted the need for better management of water resources and an improved understanding of the importance of groundwater-surface water interaction.

The first major water resource assessment for WRIA 55 was conducted by the Washington State Department of Ecology (herein referred to as Ecology) and documented in Chung (1975). As a result of this study, many rivers in WRIA 55 are now regulated under an in-stream flow rule (WAC 173-555). Ecology, has established minimum flow requirements to preserve fish, wildlife, scenic, aesthetic and other environmental values of the rivers of WRIA 55. Water use in the basin, both groundwater and surface water, is regulated by the requirement that it will not impact the established flow requirements, nor will it impact more senior water users. As a result of the Ecology study, many tributaries of the Little Spokane River were closed for future water right appropriation, including Dry Creek, Otter Creek, Bear Creek, Deer Creek, Dagoon Creek, Deep Creek, Deadman Creek, Little Creek, and the West Branch of the Little Spokane River. All natural lakes in WRIA 55 were also closed to future appropriation (Chung, 1975).

A basin-wide water resources inventory was completed for WRIA 55 by Dames and Moore and Cosmopolitan (1995). This is one of the first studies to quantify water use in the basin using water-rights documentation. The primary groundwater use was municipal-domestic at 39% of the allocated groundwater rights in the basin. Irrigation was the largest surface water use category making up 75% of allocated surface water rights. An updated inventory was completed by Golder (2003) as part of a preliminary analysis for an integrated modeling study for WRIA 55 and 57 (Middle Spokane River Watershed). They estimated the allocated water use in WRIA 55, excluding non-consumptive activities, was approximately 187,000 acre-feet per year (af/yr). The largest water use category was municipal-domestic accounting for 47% of the allocated water-rights, followed by agricultural irrigation and commercial/industrial use at 39% and 11%, respectively. However, this study suggested that estimated actual withdrawals may be considerably less than the allocated quantities.

There has been considerable effort to improve the understanding of water demand in Spokane County and WRIA 55 through the development of a water demand forecast model. The model considers different types of urban development (e.g., single-family residential housing, multi-family residential housing, and commercial), acreage of urban and crop irrigation, and livestock (Spokane County Water Resources, 2011, 2013). Estimates of consumptive and non-consumptive water use and return flows (i.e., septic, sewage, irrigation) have been calculated for public and self-supplied domestic, commercial, and agricultural water users making it a useful tool to provide estimates of water demand for the integrated model developed for this study. Withdrawals used in the model are described further on in Section 8.5.

A feasibility study for the use of a water bank to manage water resources in WRIA 55, under existing and future regulatory constraints, was completed recently by Aspect Consulting (Aspect, 2015). One concern motivating the water bank feasibility study is that Ecology is no longer issuing any new water rights in WRIA 55 under current conditions. Their report addressed many of the legal and economic factors that influenced the perception and success of other water banks in Washington

State. The findings suggest that water banking may be a feasible option and, accordingly, highlights the need for a water bank management model.

## **5.2 Water Rights in Washington State**

In the State of Washington, withdrawals are governed by a legal authorization known as a water right. State law requires any user of streams, lakes, springs, and other surface waters to be permitted through a water right. Users of groundwater are also legally required to obtain a water right unless they are: (1) providing water for livestock; (2) watering a non-commercial lawn or garden less than one-half acre in size; or (3) providing less than 5000 gallons per day (GPD) of water to single or multiple households or for industrial purposes, including irrigation.

Ecology maintains a database of water rights information, referred to as the Geographic Water Rights Information System (GWIS). The distribution of known points of withdrawal (POW), with and without associated water-right documentation, is shown in

Figure 5.1. A total of 5,876 points are found within the WRIA 55 boundary. It is possible to have multiple POWs associated with a single water right. As such, the 5,876 POWs correspond to 5,791 unique water rights. No distinction, however, is made in the dataset to allocate withdrawals to a specific POW. Rather, each POW is linked to the total withdrawal associated with the water right. How the user decides to allocate withdrawal to multiple POWs is at their discretion, as long as the instantaneous and annual withdrawals specified in the water right are not exceeded.

There are three primary documents that govern water rights: claims, permits, and certificates. The distribution of the POWs based on their form of documentation is shown in

Figure 5.2 and discussed further below.

### **5.2.1 Claims**

A claim, as the name suggests, is a claim to a water right that predates the State Surface Water Code (1917) and the State Groundwater Code (1945). There have only been three periods since the water right legislation was implemented for surface water and groundwater users to register water right claims. Claims were submitted on either a long-form, which includes detailed domestic and irrigation uses, or on a short-form for single domestic use with up to one-half acre of non-commercial lawn and garden.

Claims make up the majority of the documents in the GWIS (

Figure 5.1); however, the validity of a claim can only be confirmed through an adjudication process, in which it is converted into a certificate. In the interim, water users may use water to which they “claim” to have a perfected right; however, it does not guarantee the security of this water indefinitely. Previous work by Golder (2003) suggests that using water right claims to estimate water use presents several challenges. For instance, many claims appear to have duplicate and triplicate records. Furthermore, many claims are unrealistically large, outdated, or are no longer active.

### **5.2.2 Water Right Applications Permits and Certificates**

For new water users, water rights may be obtained through transfer or through opening an application. A permit may be issued during the application process after a successful Report of Examination (ROE) review. A permit allows the user to proceed with construction of the water system and start putting the water to use in accordance with the terms of the permit. A water right certificate is the final piece of documentation confirming all of the conditions of the permit have been met. To obtain a certificate, a permitted water user must go through a Proof of Appropriation process and prove they are using the water that they are permitted. The spatial

distribution of the different forms of water right documentation associated with applications, permits, and certificates is shown in

Figure 5.2 . It should be noted that several water right applications are associated with amendments to an active water system. For instance, several municipal wells, located in Spokane and Deer Park, are associated with change applications to their current certificates.

### 5.2.3 Permit-Exempt Wells

As mentioned above, permit-exempt uses include domestic or industrial withdrawals of less than 5,000 GPD, irrigation of a lawn or non-commercial garden (less than one half acre in size), and livestock watering. However, these types of withdrawals have recently come under legal scrutiny (see *Whatcom County vs. Hirst, Futurewise et al.* decision) and have spurred new legislation imposing tighter restrictions on permit exempt wells. Under the newly imposed regulations, the owner of any well drilled after January 19, 2018 must either pay a \$500 fee and be restricted to 3,000 GPD, or purchase a Streamflow Mitigation Certificate from the WRIA 55 water bank, discussed further below.

## 5.3 Water Banking

A water bank is an accounting system that allows for the transfer of water rights between buyers and sellers. Water banking is a means of changing or moving water use to a new location in support of new development or stream flows. Water banking is common in many of the western states. While each state employs a different approach, all water banks operate under the common goal of reallocating water to where it is needed most (Washington State Department of Ecology and WestWater Research, 2004).

In Washington State, water banking is regulated under the Trust Water Right Program (TWRP). In 2009, legislation was passed to allow for implementation of water banks state-wide. Water rights may be retired or acquired by the state and held in trust, either permanently or temporarily, while preserving the seniority, the place of use, instantaneous and annual quantity, and period of use (Aspect, 2015). The water-right is also not subject to relinquishment while in trust.

Spokane County has developed a water bank for WRIA 55 to mitigate the impacts of new water use on streamflow. While a water bank has proven to be an excellent accounting tool for managing water resources, it does not offer quantitative insight into the local impacts of water-right relocation. This study is meant to provide a decision-making tool (i.e., a model) to aid in the process of water-right relocation by providing a framework to quantitatively assess impacts to streams, groundwater, and the interaction between the two regimes.

## 5.4 Figures

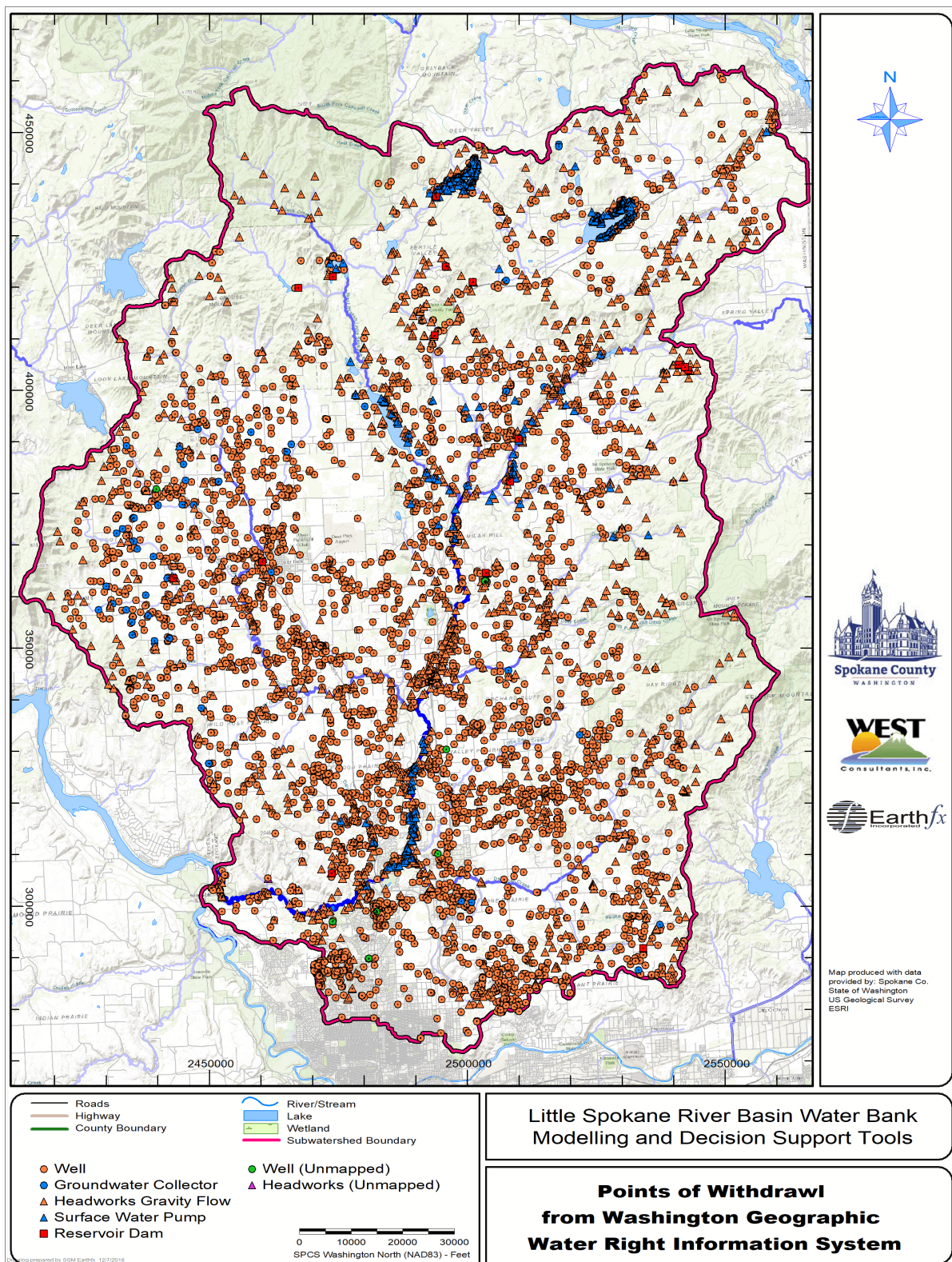


Figure 5.1: Points of withdrawal from the Washington State GWIS.

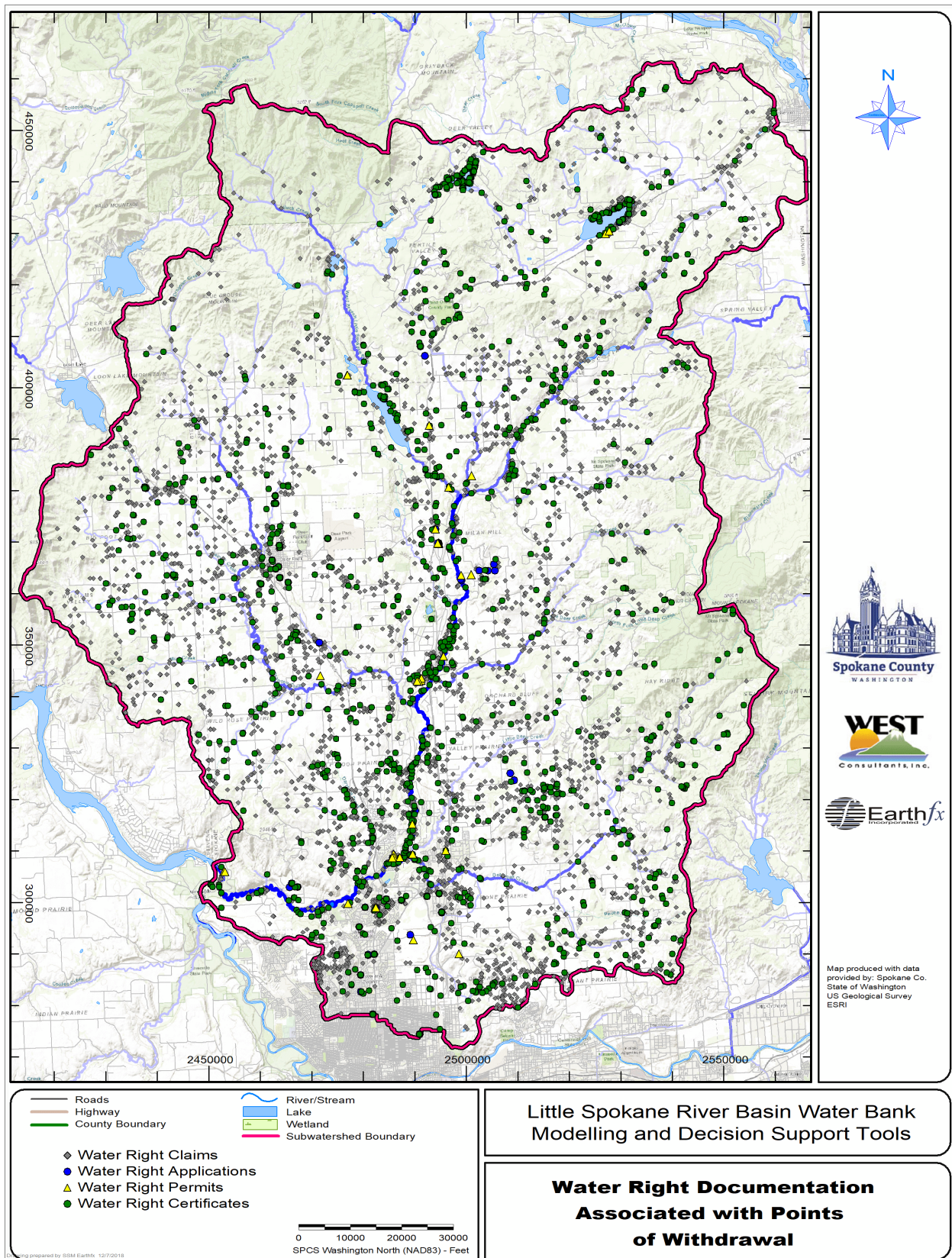


Figure 5.2: Water Right documentation associated with points of withdrawal.

## **6 Integrated Model Development Overview**

### **6.1 *Introduction***

Many of the technical readers of this report will be familiar with the concepts of surface water and groundwater modelling. As integrated modelling is less commonly applied, the purpose of this chapter is to address the following:

1. What is integrated modelling?
2. What are the benefits and possible disadvantages of integrated modelling as it applies to the objectives of this study and the unique features of this watershed?
3. How is the movement of water between the surface and groundwater systems (dynamic feedback) represented in the integrated model?
4. What is the approach to the development and calibration of the integrated model?

The final part of this chapter provides the reader with an overview of the process of developing and calibrating the integrated model. This overview will help the reader understand how each of the sub-model components are developed, pre-calibrated, and then coupled and “final calibrated”. With this high-level overview of the model development process, the reader will better understand the technical details presented in subsequent model construction chapters.

### **6.2 *Integrated Modelling - Overview***

#### **6.2.1 *Integrated Modelling***

The basic definition of an integrated model is one that represents the entire hydrologic cycle in a comprehensive, complete, and coupled manner. The hydrologic cycle includes:

- Hydrologic processes (e.g., precipitation, interception, snow accumulation and melt, overland runoff, interflow, evapotranspiration (ET), and groundwater recharge)
- Hydraulic processes (e.g., streamflow, wetland and lake water balance)
- Groundwater processes (i.e., saturated and unsaturated subsurface flow)

*A comprehensive and complete representation* of the hydrologic cycle is one in which the overall water budget is tracked through both the surface water and groundwater systems and where water cannot be created or lost. The term “integrated” is used to describe how the transfer of water between the surface water and groundwater domains is simulated and how feedback mechanisms are represented. In general, integrated models determine the flows in the groundwater and surface water systems at the same instant in time by solving the governing equations simultaneously or in an iterative manner.

An integrated approach also provides additional benefits that are related to the development and calibration of the model. When independent surface water and groundwater models are developed, simplifying assumptions must be made in each model to account for processes that occur in the other model domain. For example, groundwater recharge must be independently estimated and applied to a groundwater model. Similarly, multi-aquifer systems with complex hydrostratigraphy are often represented as simple linear reservoirs accepting excess water and whose discharge to streams must be estimated and incorporated in the calibration of a surface water model. Little dynamic feedback is provided between the systems. Transfer of groundwater across the watershed divides must be estimated but is often not considered. These simplified assumptions may not be valid when using the models to evaluate variable climate and water use conditions. With an integrated model, the sub-models are often “pre-calibrated” using a traditional model development

processes, but final calibration is undertaken without the need to rely on simplifying assumptions and estimates.

### 6.3 USGS GSFLOW Overview

The USGS GSFLOW code (Markstrom *et al.*, 2008) used in developing the integrated groundwater/surface water model for the LSR watershed, is an open-source, well-documented code that can be obtained at no cost from the USGS. The code is well-tested and has been used to investigate groundwater/surface water interaction in a number of recent peer-reviewed studies (e.g., Huntington and Niswonger, 2012; Hunt *et al.*, 2013; Ely and Kahle, 2012; Tanvir Hassan *et al.*, 2014; and Niswonger *et al.*, 2014).

GSFLOW was developed from two widely-recognized USGS submodels: the Precipitation Runoff Modelling System (PRMS, Leavesly *et al.*, 1986) and the modular groundwater flow model MODFLOW-NWT (Niswonger *et al.*, 2011). The MODFLOW-NWT code has the add-on USGS UZF unsaturated flow module (Niswonger *et al.*, 2006) and the SFR2 and LAK3 surface water modules (Niswonger and Prudic, 2005 and Merritt and Konikow, 2000). The different processes and submodels in GSFLOW are listed in Table 6.1 and are shown schematically in Figure 6.1. The submodels include numerical representations of the complete physical system and the processes that occur within each submodel domain.

Table 6.1: Processes and GSFLOW submodels.

Zone	Process Component	GSFLOW Submodel
1	Hydrology – Soil Water Processes	PRMS Hydrologic Submodel
2	Streamflow	SFR2 module for MODFLOW
	Lakes, and Wetlands	LAK3 module for MODFLOW
3	Unsaturated Flow	UZF module for MODFLOW
	Groundwater flow	MODFLOW-NWT Groundwater Submodel

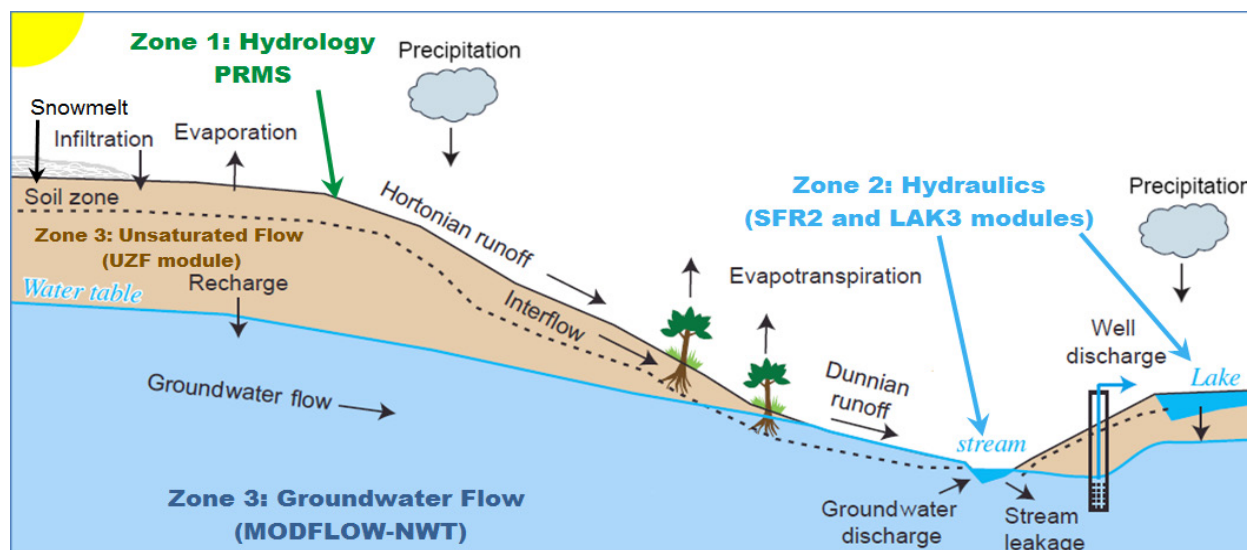


Figure 6.1: Schematic diagram of the GSFLOW process regions.

### 6.3.1 Spatial Representation

The MODFLOW groundwater flow submodel in GSFLOW is fully-distributed model, meaning that groundwater processes are simulated using a cell-based representation of the study area. The PRMS hydrology sub-model can be run using either subcatchments (lumped-parameter mode) or in a fully-distributed manner where the hydrologic response units (HRUs) are small cells rather than subcatchments, with each cell having unique physical properties. For this study, PRMS is being run in the fully distributed mode. Cells are assigned spatially variable soil and land cover properties as part of model construction. During a simulation, cells receive spatially-variable inputs, such as daily rainfall, snowfall, temperature, and solar radiation. Overland runoff and interflow are routed between cells and to the receiving streams or lakes through a topographically-drive cascade flow network.

The spatial representation in GSFLOW is particularly flexible. Three different grid resolutions can be used for the climate, surface hydrology, and subsurface groundwater processes (Figure 6.2), respectively. This allows for different levels of refinement in each of the three regions to meet the accuracy requirements associated with those processes and the type and spatial distribution of property and observation data available in the study area. The grids in this study share a common origin and have spacing so that the grids are generally aligned.

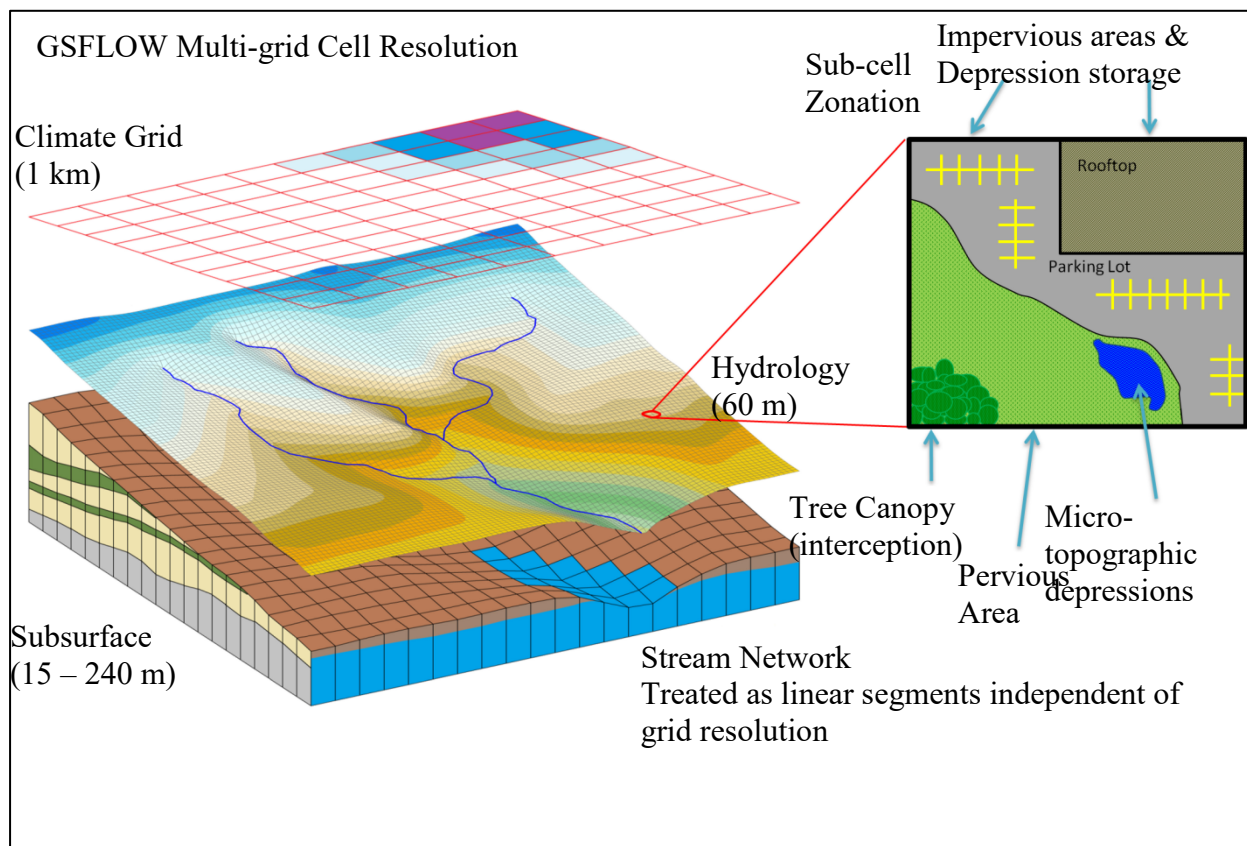


Figure 6.2: Different grid resolutions are available for each process region within GSFLOW.

Topography, soil properties, and land use can vary widely across the study area, so a fine resolution is typically used to represent local-scale natural features and anthropogenic modifications such as agricultural land use and urban development (Figure 6.2). Sub-cell hydrologic processes are also represented, where each cell in the PRMS submodel is divided into pervious (grass or soil) and impervious (roads, parking lots, buildings) zones (Figure 6.2, right side enlargement), with different processes, storage properties, and interactions simulated in each sub-cell zone.

Rivers and streams in GSFLOW are represented as a network of one-dimensional line elements with open-channel flow routing through the network. The storage associated with small wetlands can be represented in the PRMS soil zone, while larger lakes and wetlands are represented with the LAK3 module and can be incised into one or more groundwater layers.

Groundwater flow processes can generally be represented at a coarser scale. The MODFLOW submodel allows a variable cell size grid to represent variation in aquifer/aquitard thickness and the grid can be locally refined in the vicinity of wellfields, lakes, and streams.

Finally, climate inputs, such as climate station or PRISM precipitation data, are typically only available on a coarser resolution. GSFLOW allows a separate grid resolution optimised for climate inputs to be used to represent spatially variable temperature and precipitation.

### 6.3.2 GSFLOW Process and Region Integration

A complete description of the GSFLOW code can be found in Markstrom *et al.* (2008). The submodels and the how processes were represented in the LSR Model are described in subsequent sections. A key aspect of the integrated model is the representation of processes that move water between the three main model domains, as shown in Figure 6.3. The next sections provide a brief description of the key inter-region processes.

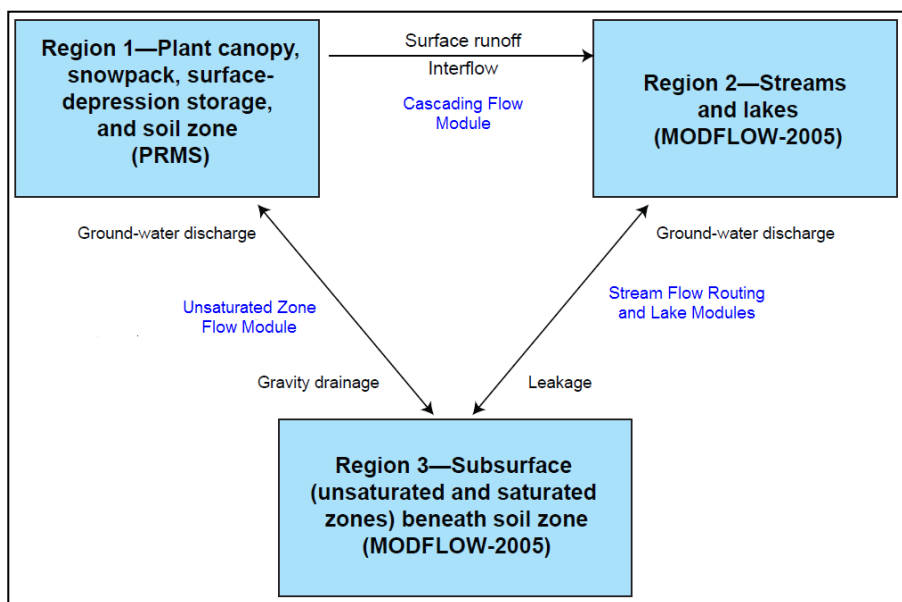


Figure 6.3: GSFLOW process flowchart.

### 6.3.3 Inter-Region Movement of Water

The PRMS submodel represents the vegetative canopy, pervious and impervious surfaces, and the soil zone as a series of reservoirs with finite capacity. The reservoirs are filled and depleted by different hydrologic processes and discharge to one or more reservoirs when the capacity is exceeded. For example, vegetation intercepts rainfall at rates dependent on the plant type and percent of vegetative cover under winter and summer conditions. Intercepted water is subject to evaporation. Water in excess of canopy interception capacity is passed to land surface reservoir or to the snow pack (if present) as “throughfall” or net precipitation. Net precipitation that falls on impervious soils is held in the depression storage reservoir and subject to evaporation. Water in excess of depression storage is routed as overland runoff through the Cascade Flow module in GSFLOW and, if it does not re-infiltrate along the pathway, it passes from PRMS to SFR2 or the LAK3 modules and routed through the stream/lake network.

In a similar manner, net precipitation on pervious soils can infiltrate into the soil zone. If the infiltration capacity is exceeded, the water is discharged as overland runoff (Hortonian runoff) and routed downslope to other cells and ultimately to the stream/lake network. Excess water above field capacity is partitioned between interflow (which is also routed to downslope cells) and gravity drainage to the unsaturated zone represented with the UZF module. Percolation is directed to the saturated zone as groundwater recharge or returned to the soil zone as rejected recharge if the percolation capacity is exceeded. MODFLOW-NWT simulates the saturated flow system that moves groundwater from recharge areas to points of discharge to streams, lakes, wetlands, and wells.

Groundwater can discharge to the soil zone occurs when the water table rises to intersect the base of the soil zone. Discharging groundwater is passed from MODFLOW to PRMS through the UZF module and added to the capillary zone. Excess soil moisture (above saturation) and any rain falling on the cell will discharge as Dunnian runoff.

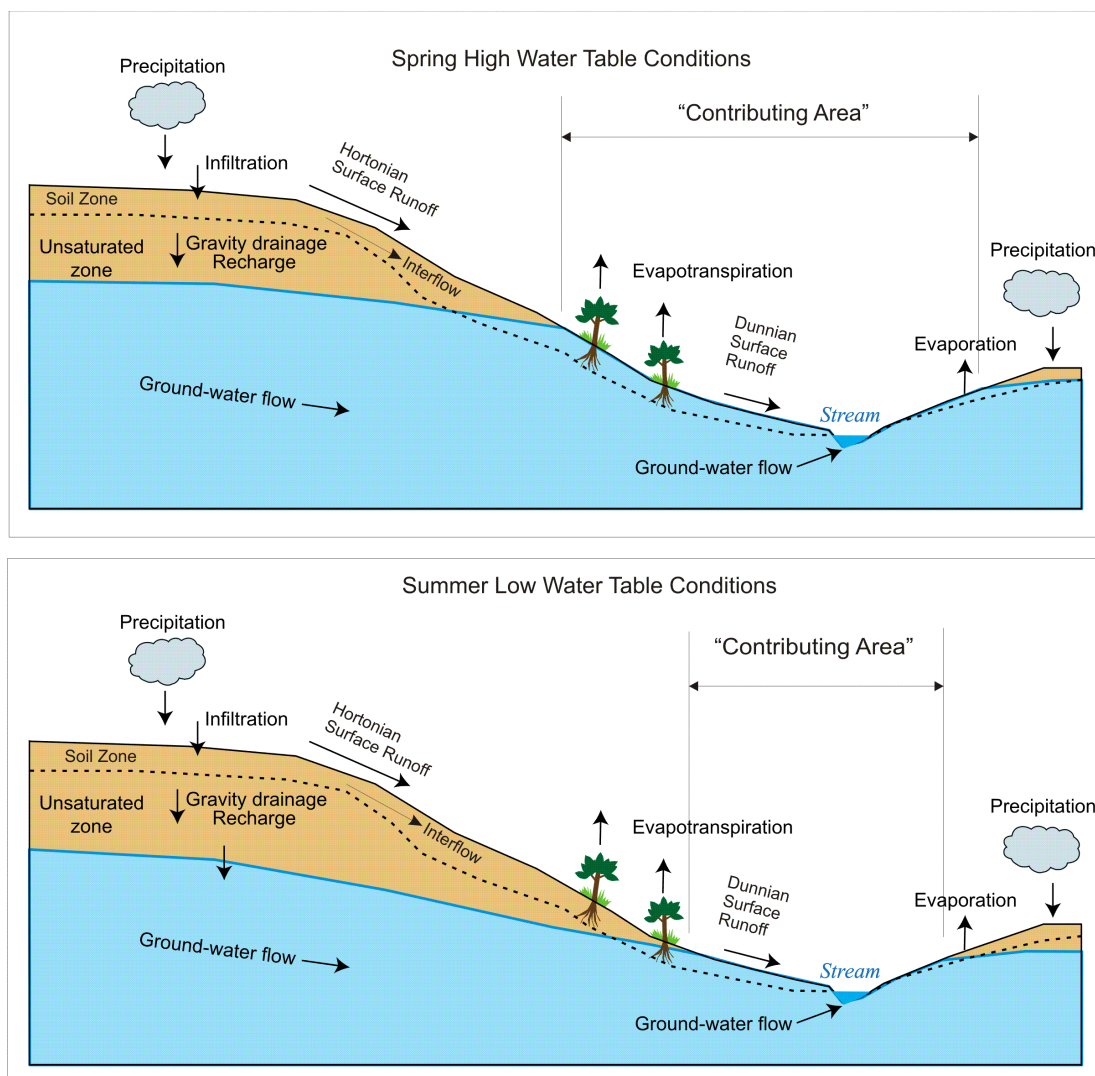


Figure 6.4: Changes in the spring and summer position of the water table increasing Dunnian runoff and the size of the "Contributing Area" (from Markstrom *et al.*, 2008).

The portion of the model area where direct feedback from the groundwater system occurs can change with seasonal fluctuations in the water table or in response to rainfall events. The portion of the watershed where the water table is near surface and contributes to Dunnian runoff has been referred to as the “contributing area” (Dickinson and Whiteley, 1970). Figure 6.4 shows a schematic drawing illustrating the change in contributing area due to the shift in the position of the water table between spring and summer. Rainfall and snowmelt events generate more runoff during the spring because the “contributing area” is larger and saturation excess (Dunnian runoff) is more prevalent. This dynamic process cannot be simulated well in independent surface models which often assign a constant average depth to groundwater for each catchment.

**Stream/aquifer interaction** occurs in the hyporheic zone where water is exchanged between the stream and the groundwater system. This exchange is represented in the GSFLOW model as head-dependent discharge or leakage with the assumption that the rate of water movement between the aquifer system and the stream is proportional to (1) the difference between the head in the aquifer and the stream stage, and (2) the permeability of the intervening streambed. The exchange of water can occur in either direction. Similar exchange can occur between a lake and the underlying aquifer across the lake bed materials as lake levels and groundwater heads change over time. The larger wetlands are represented as shallow lakes in the LSR model.

In many groundwater models, only the exchange of water across the streambed is represented. Studies with the GSFLOW model have shown that considerable amounts of water are exchanged as groundwater discharge to the soil zone in riparian area which subsequently emerges as Dunnian overland runoff. It is also important to recognize that groundwater discharge across the streambed is locally suppressed or even reversed as stream stage temporarily rises after precipitation or snowmelt events. Groundwater then seeps back out to the stream as the stage subsides (bank storage). While the representation of the groundwater discharge to streams in GSFLOW is more physically correct, it is more difficult to separate the surface water components and groundwater components of discharge to streams in an integrated model.

#### 6.3.4 Temporal Discretization and Submodel Coupling

During a GSFLOW simulation, each submodel receives a set of inputs, such as daily climate data for PRMS and changes in recharge and pumping for MODFLOW. The PRMS submodel calculates a new water balance for each cell in response to the climate inputs and passes updated estimates of groundwater recharge, overland runoff to streams, and residual ET demand to the MODFLOW submodel. In turn, the MODFLOW submodel with the UZF module solves the groundwater flow equations to compute new groundwater levels and the resulting changes in storage, groundwater ET, and groundwater discharge to the soil zone, lakes, and streams. Surface water flows, based on inputs including direct precipitation, evaporation, overland runoff, and groundwater gains or losses, are routed downstream and new stage values in lakes and streams are calculated using the SFR2 and LAK3 modules. The process is repeated in an iterative manner until the exchange of water calculated by the two submodels converges. The final soil water balance, groundwater recharge rates, change in discharge to streams, stream flows, lake stages, groundwater heads (including the updated water table position) are then computed and saved and the model progresses to the next daily time step. A schematic showing the iterative computations executed as the model progresses through time is presented in Figure 6.5.

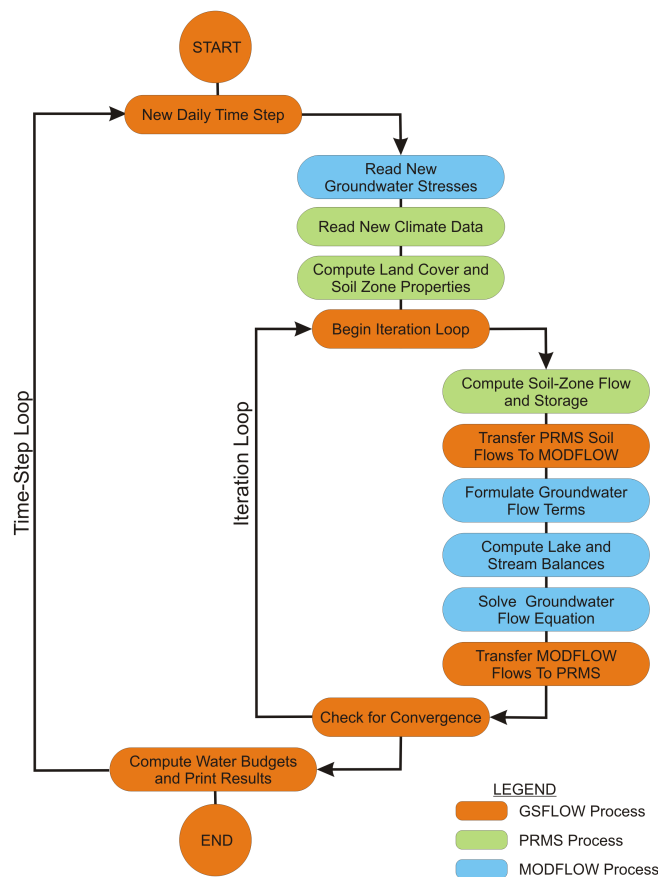


Figure 6.5: Computational sequence for an integrated PRMS/MODFLOW simulation in GSFLOW (modified from Markstrom *et al.* (2008)).

#### 6.4 GSFLOW Model Development Process

Developing an integrated watershed model is more complicated than building an independent hydrologic model or groundwater model. However, many of the basic model development steps and procedures are similar. Model development begins with the collection of available data and reports to capture observations as well as insights from earlier work. The next steps, as documented in Sections 2 through 5, include describing and assessing the features and critical processes active in the study area. Information on the topographic, physiographic, hydrologic, geologic, and hydrogeologic settings is synthesized and used to formulate conceptual models of the soil zone, surface water flow system (lakes, wetlands, and streams), stratigraphy, and hydrostratigraphy.

With data compilation and conceptualization completed, the next step involves converting the conceptual model and data into input data and parameter values for the PRMS and MODFLOW submodels. This translation is described in Sections 7 and 8. For this study, the submodels were tested, “pre-calibrated” independently, and, very early on in the study, the integrated model was constructed and calibrated, as described in Section 9.

It is important to note that the overall process of data assimilation, conceptual model development, and integrated model calibration is also iterative. Analysis of preliminary model results often pointed to gaps in the previous analyses. The gaps were addressed by obtaining additional data or re-evaluating the data analysis and assumptions made in the conceptualization phases. The model extent and model grids, as well as the underlying conceptual geologic model, were revised several times during the course of the study as our understanding of the study area grew.

## 7 Hydrologic Submodel Development

### 7.1 *Introduction*

Hydrological processes in the integrated model were simulated using the USGS Precipitation-Runoff Modeling System (PRMS) code. The original version of the code is documented in Leavesley *et al.* (1983); a modified version of the code was implemented as a submodel in GSFLOW (Markstrom *et al.*, 2008). The PRMS submodel in GSFLOW can run in a stand-alone mode or in a fully-integrated manner, which links the PRMS submodel with the MODFLOW-NWT groundwater submodel. Integration of PRMS into the GSFLOW model was done fairly early on in this study because of the high degree of interaction observed between the two systems.

The following sections present a brief description of the PRMS submodel, a summary of the climate inputs required to drive the model, and an outline of the parameterization process employed in this study. Some of the hydrologic processes were pre-calibrated in the stand-alone submodel. For example, processes such as snowpack accumulation or calculation of potential evapotranspiration proceed in a similar manner whether or not the submodels are linked.

### 7.2 *Submodel Description*

PRMS is an open-source code for calculating all components of the hydrologic cycle at a watershed, subwatershed, or cell-based scale. PRMS is a modular, deterministic, physically-based, fully-distributed model developed to evaluate the impacts of various combinations of precipitation, other climate inputs, topography, soil properties, and land cover on streamflow and groundwater recharge. The modular design provides a flexible framework for model enhancement. The PRMS code has been used recently in many applications across the US (e.g., Ely and Kahle, 2012) and in Canadian watersheds (e.g., Earthfx (2010, 2013, and 2018)). Version 1.1.6 of GSFLOW was used in this study which integrates PRMS version 3.0.5 and MODFLOW-NWT version 1.0.7.

#### 7.2.1 **Spatial and Temporal Discretization**

To use PRMS as a fully-distributed model, the study area was first discretized into a grid of square cells. Square cells, 250 ft on a side, were found to adequately represent the distribution of land cover, topography, and soil properties within the model boundary while minimizing the number of model cells. A portion of the study area represented with 250 ft grid is shown in Figure 7.1.

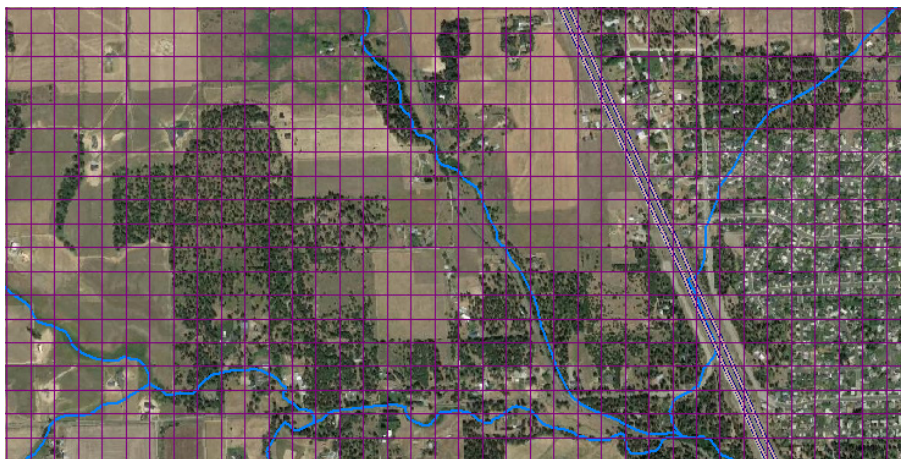


Figure 7.1 Portion of the PRMS grid showing the 250 ft mesh.

The PRMS grid contained 850 rows and 636 columns with 306,816 active cells covering an area of 688 mi<sup>2</sup>. Cells located outside of the MODFLOW submodel boundaries were designated as inactive and were not included in the water balance computations. The origin of the PRMS grid was aligned with the groundwater submodel grid. Each cell was then assigned a unique set of hydrologic properties. Property values and methods for assigning properties are discussed further on. The PRMS cell size does not need to correspond to the area of the MODFLOW cells, allowing for finer representation of the shallow soil zone processes including overland runoff and interflow across the study area (see Figure 6.2).

The PRMS submodel in GSFLOW and the groundwater submodel are integrated on a daily basis, as shown in Figure 6.3. Daily climate data (precipitation, minimum/maximum temperature, and solar radiation) distributed to each cell serve as key inputs to the model. Using the distributed climate inputs, PRMS computes individual water and energy balances for every cell on a daily basis.

### 7.3 Hydrologic Processes

A flow chart describing the physical processes simulated by the PRMS code is shown in Figure 7.2. A more complete description of the program code and underlying theory can be found in Leavesley *et al.* (1983), Markstrom *et al.* (2008), and Markstrom *et al.* (2015). The PRMS model tracks volumes of water for each cell in multiple storage reservoirs. These include interception storage, depression storage, snowpack storage, capillary soil moisture zone storage, gravity soil moisture zone storage (water in excess of field capacity), preferential flow storage, and groundwater storage (when GSFLOW is run in the PRMS-only mode).

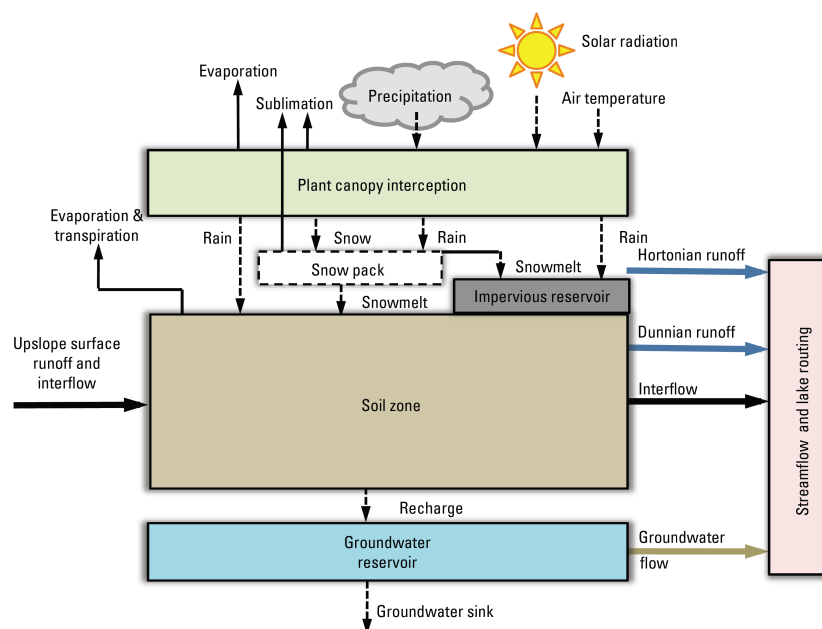


Figure 7.2: Hydrological processes simulated by the Precipitation-Runoff Modeling System (from Markstrom *et al.*, 2015)

#### 7.3.1 Imperviousness, Canopy Interception, and Imperviousness

Each cell can contain both pervious and impervious sub-areas (Figure 6.2). Separate water balance computations are done for each sub-area each day. For both subareas, the model first computes interception by vegetation. The amount of rain and snow intercepted depends on vegetation type, the specified interception storage capacity for the dominant vegetation type in the cell, precipitation type (rain, snow, or mixed) and winter/summer vegetation cover density. When interception storage capacity is exceeded, the surplus is allowed to fall through onto the snowpack, if present, or directly

onto the ground surface, a process termed throughfall or net rainfall. The model computes the capture of precipitation by depression storage in impervious areas. When depression storage capacity is exceeded, the surplus is discharged as overland runoff. Water is removed from the depression storage reservoir in each cell by evaporation.

### 7.3.2 Snow Pack

Snow accumulation and subsequent melting is a key source of spring runoff and groundwater in the spring. Rain-on-snow events and sudden warming can also trigger large runoff events mid-winter. PRMS contains a two-layer, energy-balance model, shown schematically in Figure 7.3, to accurately simulate snowpack and compute snowpack depth, density, albedo, temperature, sublimation, and melt on a daily basis using maximum and minimum air temperature, solar radiation, and precipitation data. The linear, energy-balance snowpack model is combined with an areal snow depletion curve to simulate the sub-cell spatial distribution of snowmelt at shallow snowpack depths (DeWalle and Rango, 2008).

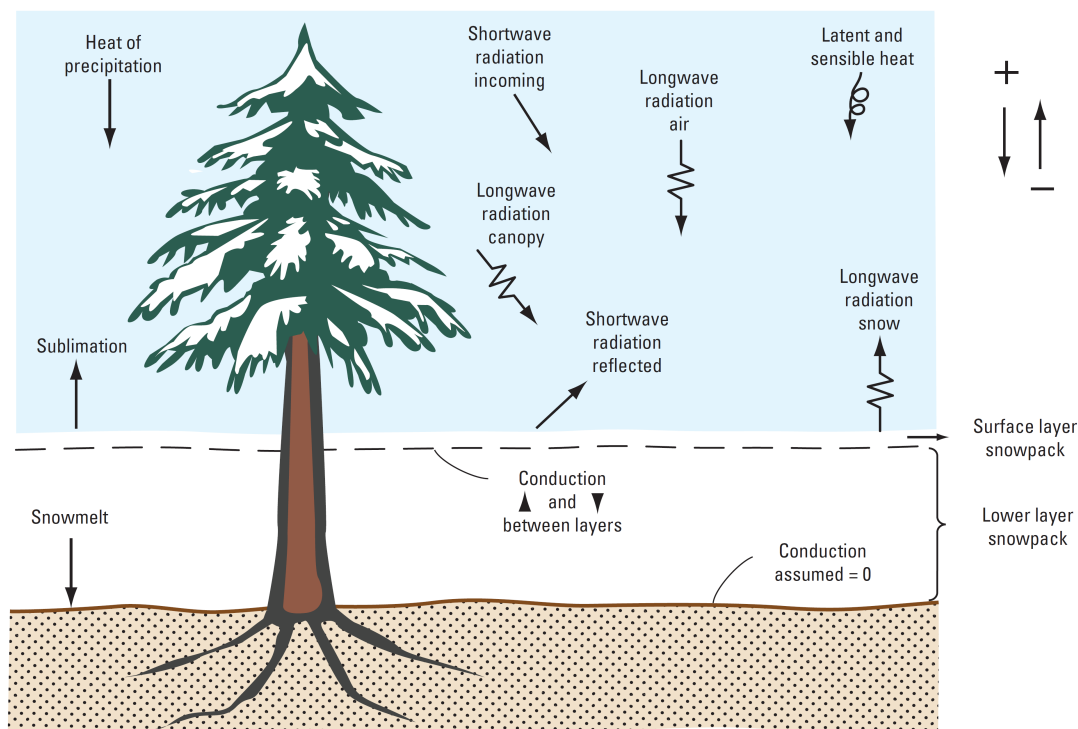


Figure 7.3: PRMS two-layer snowpack conceptualization and the components of the snowpack energy balance, accumulation, snowmelt, and sublimation algorithms (from Markstrom *et al.*, 2015).

The snowpack energy balance model determines the amount of snowmelt on pervious and impervious surfaces on a sub-daily basis to account for differences in the night and day energy flux. Detailed descriptions of the energy balance model can be found in Leavesley *et al.* (1983). The snowpack is treated as a porous medium, where liquid water can be stored and potentially re-freeze.

During precipitation events, the model first checks whether a snowpack exists. If the temperature is below a user-defined base (or critical) temperature ( $T_c$ ), the throughfall is added to the snowpack as new snow. If the temperature is higher than  $T_c$ , the throughfall is added as rain to the snowpack and the temperature of the snowpack is raised through sensible and latent heat exchange. If the energy input is high enough and the snowpack becomes isothermal, all or part of the snowpack can melt.

Water remaining in the snowpack can refreeze based on air temperature change. The albedo (reflectivity) of the snow decreases over time allowing the snowpack to absorb more energy as it

ages. The albedo is reset every time there is a new snowfall event. The snowpack is also subject to evaporative losses through sublimation. Sublimation rates are specified as a fraction of the Potential ET rate.

### 7.3.3 Overland Runoff, Infiltration, Interflow, and Evapotranspiration

The model first computes the capture of throughfall and snowmelt by depression storage on impervious surfaces. When depression storage capacity is exceeded, the surplus is discharged as overland runoff and routed down the cascade flow network (described below). Water is removed from the depression storage reservoir in each cell by evaporation.

Throughfall and snowmelt on the pervious area of each cell is partitioned between infiltration and Hortonian (infiltration-excess) runoff. The original PRMS code included a “contributing area” (or “partial-area”) method (Dickinson and Whiteley, 1970) to partition these flows on a daily basis. Because the “contributing area” was originally intended to account for Dunnian (saturation excess) runoff, Earthfx added the SCS Curve Number method, which partitions infiltration and runoff based on land cover, soil type, and antecedent soil moisture conditions. Water not infiltrating the soil is added to overland runoff and routed down the cascade flow network.

Water infiltrating into the soil zone underlying pervious areas is held in the “capillary zone” reservoir where it is subject to evapotranspiration (ET). Conceptually, the capillary zone reservoir is the volume of water that can be held in the soil when the moisture content is between wilting point and field capacity (as shown schematically in Figure 7.4). Water below the wilting point cannot be extracted by ET.

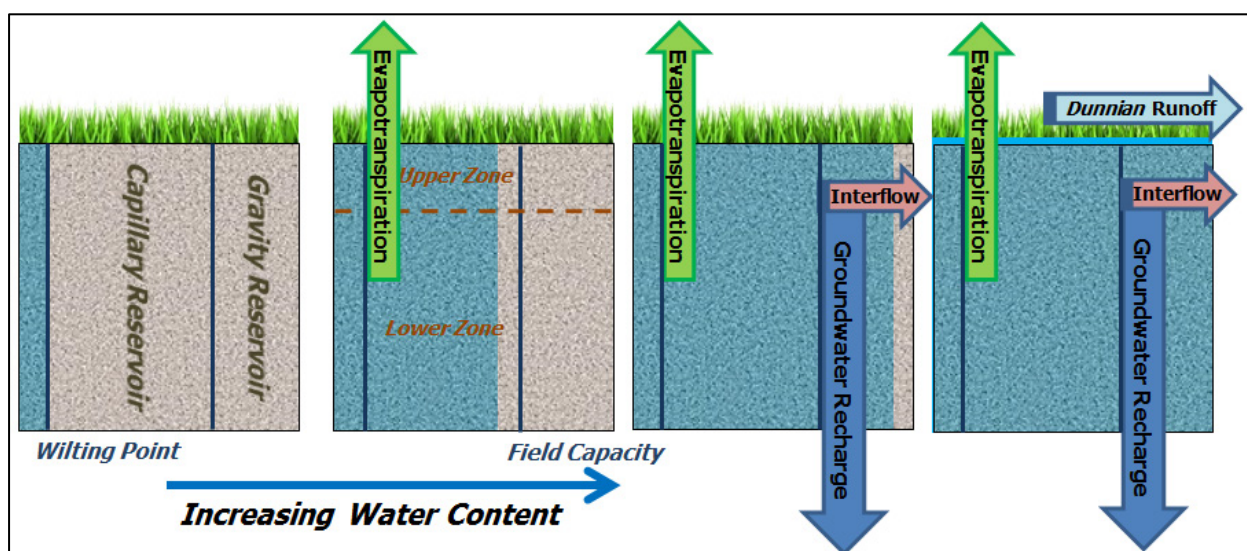


Figure 7.4: Runoff, ET, and interflow processes in the soil zone as a function of increasing moisture content.

The PRMS code has several methods for calculating potential evapotranspiration (PET). The modified Jensen-Haise method (Jensen and Haise, 1963) was used in this study to estimate daily PET and only requires values for daily temperature, incoming global solar radiation, and a few other user-specified parameters. Actual evapotranspiration (AET) depends on available water and is assumed to follow a hierarchy whereby ET is first extracted from interception storage and then depression storage on impervious. Any unmet PET demand is extracted from the capillary reservoir.

A two-layer root zone is used in PRMS, where water is extracted first from the upper (recharge) zone (Figure 7.4) which is assumed to be subject to evaporation and root uptake. The amount extracted depends on the type of soil, vegetation type, vegetation cover density, and the ratio of available

water currently in the soil zone to its maximum available water-holding capacity. Any remaining ET demand is extracted from the lower zone at a rate also dependent on soil, vegetation, and available water.

#### 7.3.4 Gravity Drainage, Interflow, Groundwater Recharge, and Groundwater Discharge

When soil water exceeds field capacity, it is assumed to be held in the gravity reservoir where it is partitioned between interflow and gravity drainage (percolation) to the groundwater reservoir (Figure 7.4). Interflow is routed down the cascade flow network. Percolation is limited to a daily maximum value. For this study, the rate was set to be dependent on the vertical hydraulic conductivity of the surficial soils. Groundwater recharge in winter months is reduced to simulate the effect of partially frozen ground; this is done by scaling the maximum daily percolation rate on days when a snowpack is present. Water retained in the gravity zone is used to refill the capillary zone after ET.

If infiltration exceeds the gravity and capillary storage reservoir capacities, the excess moisture above saturation can be retained “above” the soil zone (to simulate standing water) or discharged as overland runoff. This form of saturation-excess runoff is termed “Dunnian” runoff in the GSFLOW modelling framework (Markstrom *et al.*, 2008).

During PRMS-only simulations, percolation is fed to a linear groundwater reservoir associated with every cell. Lateral groundwater movement can be approximated using a separate groundwater reservoir cascade network or it can be treated as a single groundwater reservoir that contributes to a gaged subwatershed. The latter option was used in preliminary calibration. Discharge from the groundwater reservoirs to streams occurs at a rate dependent on the volume of water stored in the groundwater reservoir and a linear decay coefficient that can be determined using gage discharge records (Linsley *et al.*, 1975). When combined with MODFLOW (GSFLOW mode), groundwater recharge is directed to the underlying MODFLOW cell and MODFLOW simulates the groundwater flow processes. In addition, MODFLOW calculates the volume of water transferred back to the soil reservoirs when the infiltration capacity is exceeded (rejected recharge) or when the water table intersects the soil zone. In the latter case, groundwater fills the soil reservoirs and can contribute to another form of Dunnian runoff. This feedback mechanism is significant in low-lying areas such as stream valleys and wetlands. Any remaining PET demand after soil-zone ET is passed from PRMS to MODFLOW where it can be extracted as groundwater ET from the saturated zone (GWET) at a rate dependent on the depth to the water table.

#### 7.3.5 Cascade Flow

In lumped-parameter models, runoff generated within the subcatchment is routed directly to stream channels. For distributed models, water must be routed to downslope cells and to the nearest stream channels. In GSFLOW, outflows (overland runoff and interflow) from one or many upslope cells are directed to downslope cells. Overland runoff and interflow are routed along this cascade flow network which is determined by basin topography.

Overland runoff (Hortonian) from upslope cells (also referred to as run-on) is added to snowmelt and throughflow for the downslope cell, thereby allowing the run-on to re-infiltrate and/or contribute to the runoff to the next cell. Interflow and Dunnian runoff from upstream cells is added directly to the capillary zone for the downstream cell where it can contribute to groundwater recharge, interflow, and/or more Dunnian runoff. Overland runoff and interflow that does not re-infiltrate eventually reaches a stream or lake. Accumulation of runoff from upstream cells and the convergence of the generally dendritic flow network results in more realistic patterns of ET, runoff to streams, and enhanced recharge in the downslope areas.

## 7.4 Climate Inputs

As discussed in Section 4.1.3, daily PRISM data for WY2003 to WY2017 were obtained and resampled to a grid covering the study area. A subset of the data for WY2009 to WY2013 was selected for model calibration as this corresponded to a time with a maximum number of climate stations and a high number of operational streamflow gages.

Climate inputs required for the hydrologic submodel include daily precipitation, maximum and minimum air temperature, intensity, and solar radiation. The PRMS code internally partitions the daily precipitation into all-snow, all-rain, or mixed events based on the temperature data. The development of the solar radiation input dataset and the hourly intensities are discussed below.

### 7.4.1 Solar Radiation

Solar radiation serves as one of the primary drivers of the ET module within the hydrologic submodel. Incoming solar radiation is controlled primarily by the number of possible hours of sunshine per day and the percent cloud cover. Solar radiation data are collected at few stations in Washington State and data had to be compiled from nearby locations. Figure 7.5 shows the monthly-averaged daily solar radiation for Spokane using data from 1952-1976 (Knapp *et al.*, 1980).

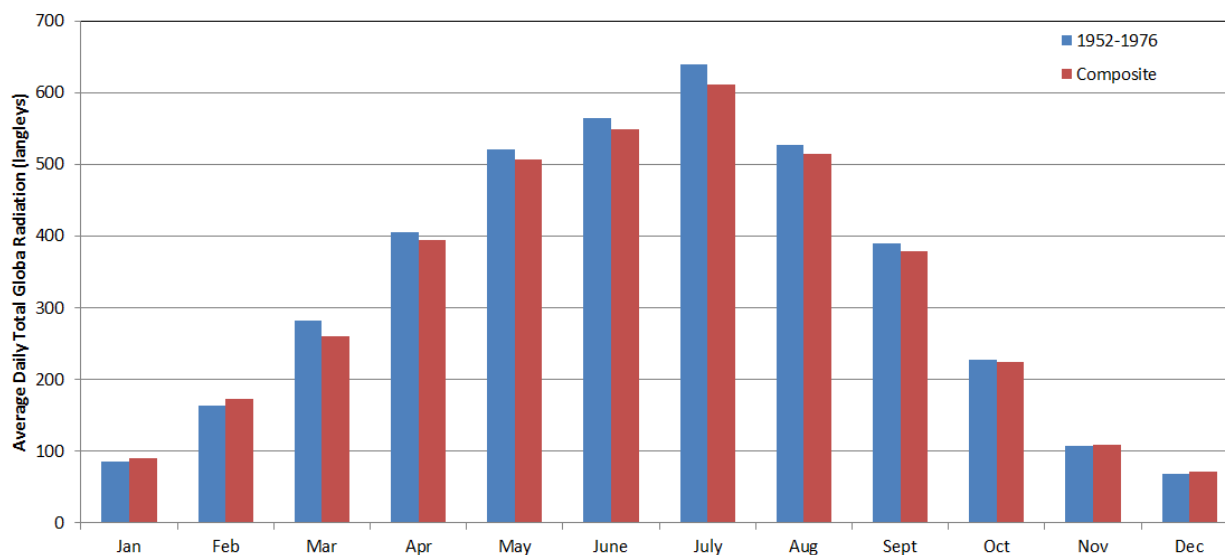


Figure 7.5: Average daily global solar radiation for Spokane (1952-1976) (data from Knapp, *et al.*, 1980) and composite (2001-2017) data.

Data from Deer Park were available from July 2014 onward. Data were obtained from Chamokane, WA for December 2007 onward and from Cheney, WA for prior years. Linear regression analysis was applied to the periods overlapping the Deer Park data. The solar radiation stations exhibited good inter-station correlation ( $r^2 > 0.9$ ). Slight shifts to the daily values for the other stations were applied based on the analysis. Data are specified in langleys per day (one ly/d = 1 cal/cm<sup>2</sup>/d or 41.84 kJ/m<sup>2</sup>-day), the input units required by PRMS. Month average daily values for the composite data were compared against the 1952-1976 data. Values are slightly higher during the winter months and lower during the summer, but no significant deviation was noted.

## 7.5 Parameter Assignment for the Hydrologic Submodel

Initial estimates of model parameters were defined prior to starting PRMS submodel runs and the calibration process. For parsimony, consistent assumptions and parameter values were applied

across the study area, where possible. Discussion of model parameters is grouped into five sub-sections, including:

1. topography-related parameters
2. land-cover related parameters;
3. soil parameters derived from soils mapping;
4. recharge parameters derived from surficial geology mapping; and,
5. other parameters related to hydrological processes, such as snowmelt.

The software package VIEWLOG (Kassenaar, 2013) was used to create, view, re-sample, and/or interpolate most gridded data sets (such as land surface elevations) and to assign parameters using lookups for tabulated values and cell-based indices. Additional gridded data sets were created using VL-GSFLOW, a pre-processor written by Earthfx to generate input data for use in GSFLOW runs. Post-processing of model results and preparation of figures were mostly done using VIEWLOG. VL-GSFLOW was used to post-process time-series data and perform subbasin analyses. It should be noted that for the sake of clarity, model parameters presented in this section of the report refer to values used in the final, calibrated GSFLOW model.

### 7.5.1 Topography-related Parameters

Topographic data for the study area were obtained from the 23.75 ft DEM (Figure 2.4) and were re-sampled to the 250 ft PRMS cells (

Figure 7.7). Slope (Figure 7.8) and slope aspect (Figure 7.9) values were calculated from the DEM using a nine-point planar regression technique that fits a plane to every cell and its eight surrounding cells (see Moore *et al.*, 1991). Slope and slope aspect affect the amount of shortwave solar radiation arriving at land surface. For example, a north-facing valley slope will get less solar radiation than the south-facing slope and will therefore have lower potential ET rates and a longer-persisting snowpack. PRMS corrects the solar radiation inputs for each cell, based on its slope and slope aspect as well as for time of year, before these data are used in snowmelt and ET calculations.

As noted earlier, the PRMS code incorporates a cascading flow algorithm that routes overland flow and interflow from one cell to adjacent cells (Markstrom *et al.*, 2008). Topographic data and terrain analysis techniques were used to define the cascade overland flow routing network. An 8-direction steepest-descent method was selected because it generates an efficient many-to-one cascade network (i.e., only one outflow path per cell is defined) and it avoids undesirable upslope numerical dispersion (see Seibert and McGlynn, 2007).

A portion of the cascade flow network within the Eloika Lake area is shown in detail on Figure 7.10 along with the resampled land surface topography. A cascade pathline goes from cell to cell until a stream reach, lake, or a closed depression ("swale") is encountered.

It should be noted that the USGS DEM appears to have been generated using digitized contours from earlier topographic sheets. The interpolation technique created large uniformly flat zones in area of low relief (Figure 7.8). This, in turn, created a large number of swales when generating the cascade network, and overland flow in these areas did not reach the appropriate streams. Minor adjustments were made to the topography over the course of the study to eliminate some of the swales, but a better DEM with hydraulically-correct topography would produce better results.

### 7.5.2 Land Cover Related Parameters

The NLCD land cover mapping played a large role in assigning key land cover parameters in the hydrologic model. For the sake of parsimony and to simplify property assignment, these were assigned to model cells using a look-up table with parameter values for each classification category. An underlying assumption was that properties for a particular land-use class, such as "Evergreen

Forest", were the same in one part of the model area as another. The NLCD parameterization grid was shown in Figure 2.8 and represents the land use data with 30 m pixels (98.4 ft) resampled to the 250 ft grid. Some minor loss of fidelity may have occurred in the resampling.

Hydrological properties that were spatially distributed based on the NLCD mapping included:

- **Vegetation index:** dominant vegetation type in the cell. It should be noted that PRMS allows only four classifications: bare soil, grass, shrub, or trees.
- **Vegetative cover density** is the fraction of the HRU covered by vegetation and/or tree canopy. Two values are provided: one for the growing season (Figure 7.11) and one for winter (Figure 7.12). Tree canopy was estimated from a separate NLCD tree canopy coverage produced for the U.S. Forest service. The predominant tree coverage is evergreens and winter and summer cover densities were assumed to be similar. For areas with thin or no tree canopy (e.g., agricultural areas and open development), the cover density values were estimated from book values (Chang, 2006), aerial photography, and previous studies.
- **Interception storage:** represents the amount of precipitation retained on vegetative surfaces and/or tree canopy. Three values are specified: interception storage for summer rain (Figure 7.13), winter rain (Figure 7.14), and winter snow (Figure 7.15). Values were estimated for each category from book values (e.g., Chang (2006), Winkler *et al.* (2009), and Komatsu *et al.* (2011)) and for conifers by the method described by Ellis *et al.* (2010). Effective interception capacity is the product of vegetative cover density and interception storage.
- **Soil Depth** is typically represented as mean vegetation rooting depths. Values were derived from book values (e.g., Strong and Roi (1983), Van Rees (1997); Kohzu *et al.* (2003); and Chang (2006)) and from studies in the western US and Canada (e.g., Klepper *et al.* (1985) Horton (1958), and Foxx *et al.* (1985)) and assigned to the PRMS grid based on land cover classification (Figure 7.17).
- **Evaporation extinction depth** is the depth below the soil surface where evaporative loss becomes negligible. A uniform depth of 6 inches was assumed. Transpiration losses can still occur below this depth. The maximum storage available in this zone was calculated as the evaporation extinction depth multiplied by the difference between field capacity and wilting point. It was assumed to be 30% filled at model startup.
- **Percent Imperviousness** is the proportion of the cell area assumed to be impervious. The data were obtained from another NLCD coverage and resampled to the PRMS grid (Figure 7.18).

The PRMS code expects inputs in a mix of imperial and metric units. Conversions were applied to the tabulated values in the data pre-processor. Parameters were refined where needed during the model calibration process to improve the match between observed and simulated flows. A lookup table of final model hydrological parameters by land cover class is provided in Table 7.1.

### 7.5.3 Soils Mapping Related Parameters

Soil properties have a significant influence on hydrological processes and water budget because they control the amount of water that can infiltrate and be transmitted to the water table, as well as the amount of water lost to evaporation and transpiration by plants (actual ET). In PRMS, the soil zone is divided into two conceptual reservoirs: the capillary reservoir and the gravity reservoir (Figure 7.4 and Figure 7.6). Soil water-holding capacity in the capillary and gravity reservoirs (see Markstrom *et al.*, 2008) were input as model parameters that were assumed to be functions of soil zone thickness, porosity, field capacity, and wilting point. Parameters that control the partitioning of flow between interflow and percolation were also specified as soil-type properties.

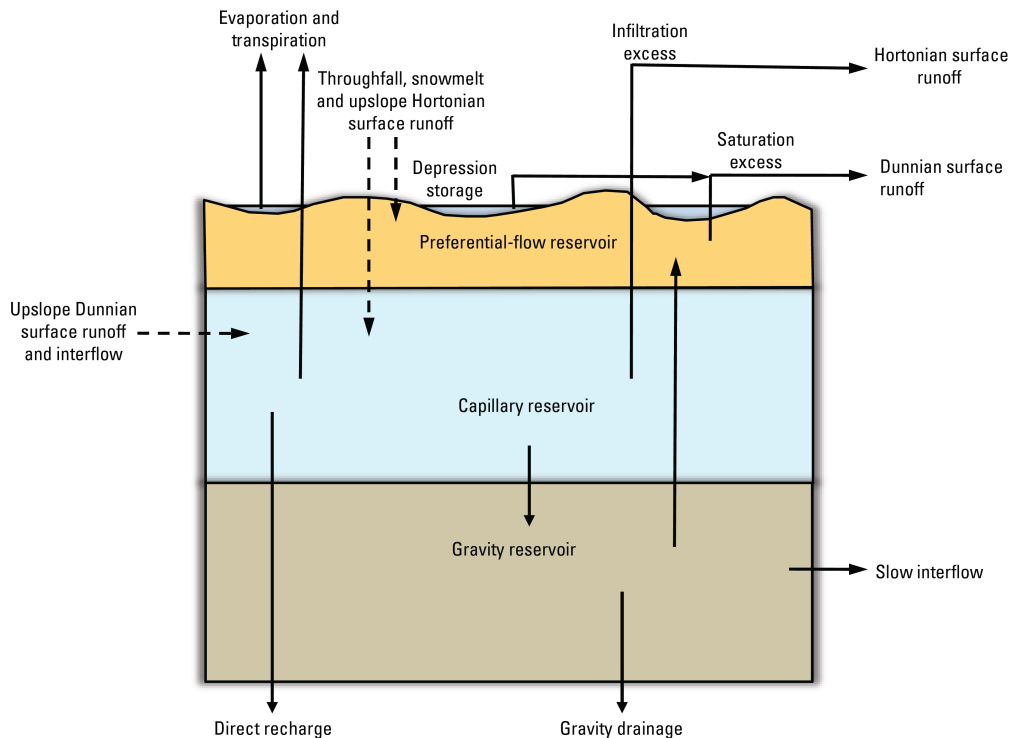


Figure 7.6: Soil water zones in PRMS and GSFLOW (modified from Markstrom *et al.*, 2015).

Agricultural soils data are available from the SSURGO database maintained by U.S. Department of Agriculture – Natural Resources Conservation Service (USDA-NRCS). The database contains a compilation of County-level soil mapping along with extensive tables of soil properties (e.g. thickness of each soil horizon, average grain-size distribution, wilting point, field capacity, and porosity) as well as associated land use and land cover data. Earthfx spent a considerable effort working with the SSURGO database to extract consistent coverages for the study area.

Unfortunately, there was poor agreement between the soil mapping and property data for Spokane County and Stevens and Pend Oreille Counties. For example, the active soil zone thicknesses were interpreted to be very small in the north and west of the study area leading to exaggerated rates of Dunnian (saturated excess) overland runoff and interflow. Some edge matching had been done in creating a Washington State soils map that aggregated many of the soil subtypes, however, large differences in properties seemed to still exist between the counties. As an alternative, the USGS surficial geology maps (Kahle *et al.*, 2013) were extended to cover the entire study area and served as a basis for assigning soil properties based on the parent geologic material. Other properties, such as groundwater seepage rates and interflow properties were also assigned using this approach. Parameters values were chosen largely to be consistent with the SSURGO data for Spokane County and include:

- **Specific soil zone properties:** Porosity (Figure 7.19), field capacity (Figure 7.20), and wilting point (Figure 7.21) were determined based on soil texture. These are not input directly into the model, instead they are specified as auxiliary parameters used in the pre-processor to calculate the following model parameters:
  - **Soil moisture reservoir capacity:** This is the product of soil depth (assigned by land cover type) and the difference between field capacity and wilting point, also known as Plant Available Water (Figure 7.22). An initial soil moisture content must be specified at model startup and was assigned uniformly as 30% of the maximum storage capacity.

- **Subsurface reservoir capacity:** This is the volume of drainable porosity in the soil column equal to the product of soil depth and the difference between porosity and field capacity (Figure 7.23). Markstrom *et al.* (2015) refer to this term as the “saturation threshold”.
- **PRMS soil types:** Soils were classified as one of the three types: sand, loam, and clay (Figure 7.24). Separate moisture profiles are included within PRMS for these soil types to control ET rates when soil moisture levels approach the wilting point.
- **SCS Soil Class:** Soils were assigned soil classes ranging from A to D for use in partitioning infiltration and runoff using the SCS Curve Number (CN) technique. For example, coarse glacial deposits were specified as type A soils; while lacustrine sediments were assigned as type C, as shown in Figure 7.25. This information was not input directly into the model; instead it was used in the pre-processor to assign CN values through a lookup table (Table 7.3). It should be noted that open water and wetlands (that were not explicitly treated as lakes in the model) were assigned high CN values so that precipitation falling on these areas was routed to the cascade network.
- **Slow Interflow Coefficients:** As noted earlier, water in the soil zone gravity reservoir is partitioned between interflow and gravity drainage. Interflow is given precedence and the discharge rate is computed based on the volume of water in the gravity reservoir. Rates can be specified using a linear and a non-linear discharge coefficient. For simplicity, the non-linear term was set to 0.0. The linear term was assigned a lower rate for well-draining soils and a higher rate for poorly draining soils.

Parameter values were modified during submodel and GSFLOW model calibration. The surficial geology classes and associated final parameter values are listed in Table 7.2.

**Maximum Daily Percolation Rates:** The rate of downward percolation from the soil zone to the groundwater reservoir in stand-alone PRMS (or to the UZF unsaturated zone in GSFLOW) is controlled by a rate term (*ssr2gw\_rate*) that multiplies the volume stored in the reservoir raised to an exponent (*ssr2gw\_exp*). Setting the exponent to 1.0 creates a linear reservoir, while setting it to 0.0 allows the water to drain at a constant rate. For this study, we set the exponent to 0.0 and the rate to equal to an estimated average unsaturated hydraulic conductivity of the soil. Initially, the unsaturated hydraulic conductivity was set using a look-up to the surficial geology index. However, problems arose when these values exceeded the values selected for the hydraulic conductivity of the upper groundwater model layer, causing the groundwater model to reject recharge sent by PRMS. In later model runs, maximum daily percolation rates were scaled from the Layer 1 hydraulic conductivities. The spatial distribution of the final calibrated values is shown on Figure 7.27.

A related parameter is “maximum snowmelt infiltration per day”. The factor limits infiltration of snowmelt into the soil zone on days when there is a snowpack and the capillary zone is at field capacity. When the soil zone is below field capacity, the infiltration rate is unlimited. Although not stated in the model documentation, this factor may be meant to account for the rate of movement of meltwater from the top of the snowpack to the base. For this study, we used the parameter to represent limited movement of meltwater through the frozen soil surface. Values were assigned by dividing the maximum daily percolation rates by a factor of 3. Water not able to infiltrate the soil is discharged as “infiltration excess” to the cascade network.

#### 7.5.4 Hydrologic Process Parameters

The PRMS model contains several process submodels, such as the energy balance snowpack model and the PET submodels. The process submodels have numerous parameters, of which many can be assigned on a cell-by-cell basis. For simplicity and consistency, uniform (basin-wide) values were used where appropriate. Independent testing of the process submodels was done to determine optimal values for the parameter, when possible.

**Snow Pack Parameters:** The GSFLOW model employs a snowpack model that estimates the rate of snow accumulation and snowmelt using an energy balance (Section 7.3.2). There are 14 parameters that need to be defined, each with varying degrees of sensitivity.

The performance of the snowpack model was evaluated against snow depth data collected at the two stations in the study area: Elk 5.6 NE (US1WAP00001) and the SNOTEL station at Quartz Peak (707) (locations shown on Figure 7.28). The dataset is relatively complete, with daily measurements starting after the first fall snowfall. Early PRMS model simulations were conducted to pre-calibrate the snowpack process model using observed rain and snow data. A good match was achieved. The parameters were not updated when the model was switched to using PRISM precipitation data. Figure 7.28 shows the simulated snow depth on one day, December 30, 2005, of a 15-year GSFLOW simulation. The results show the higher snow depths versus elevation. The blockiness is an artifact of the PRISM data which are generated on an approximately 2 mi by 3 mi grid. Figure 7.29 plots the simulated snow depths against the observed values at the Elk and Quartz Peak sites. There is generally good agreement at Elk but less so at Quartz Peak. The latter can be explained because the cell sampled (closest to the site) has 85% forest cover while the site is in a clearing outside the model boundary (a cell was locally modified during the pre-calibration to have no forest cover).

**Estimates of Precipitation Form:** Precipitation form is an important input to the snowmelt and snow accumulation process submodels. Form is required to accurately simulate rain-on-snow events which often correspond to annual streamflow peaks in rural catchments (Dickinson *et al.*, 1992). Rain and snow data were available at a few stations. Unfortunately, the PRISM data only provide measurements of total precipitation.

PRMS estimates the rain versus snow fractions from the daily observed precipitation and the daily maximum and minimum temperatures. Two critical temperatures are defined, the maximum daily temperature above which all precipitation is rain ( $T_{max\_all\_rain}$ ) and the minimum daily temperature below which all precipitation is snow ( $T_{max\_all\_snow}$ ). Precipitation is all snow when the maximum daily air temperature is less than or equal to  $T_{max\_all\_snow}$ . Precipitation is all rain when the minimum air temperature is either greater than  $T_{max\_all\_snow}$  or when the maximum air temperature is greater than or equal to  $T_{max\_all\_rain}$ . When the maximum daily air temperature is between  $T_{max\_all\_snow}$  and  $T_{max\_all\_rain}$  and the minimum daily air temperature is less than or equal to  $T_{max\_all\_snow}$ , precipitation is assumed to be a mixture of rain and snow.  $T_{max\_all\_snow}$  and  $T_{max\_all\_rain}$  can be estimated for the study area from climate stations where both snow and rain data are available.

Figure 7.30 and Figure 7.31 present daily precipitation form observations plotted against daily maximum and minimum temperatures respectively. While mixed form events occur across a 15°C (27°F) range, precipitation generally falls as snow when the maximum daily air temperature is below 0°C (32°F). Similarly, when the minimum temperature is above 0°C (32°F) or the maximum daily air temperature is above 4°C (39.2°F), all precipitation falls as rain. These critical temperatures were employed to modify precipitation inputs for the PRMS submodel when using the PRISM data.

**Evapotranspiration:** Potential evapotranspiration (PET) in the PRMS model is approximated using the modified Jensen-Haise equation (Jensen and Haise, 1963). It calculates potential evaporation (PET) in terms of daily temperature and incoming solar radiation and two coefficients that can be estimated using regional air temperature, altitude, vapor pressure, and plant cover as discussed in Markstrom *et al.* (2008). The first term is a monthly adjustment factor used to better fit observed PET. The second term depends on (1) the difference in saturation vapor pressure at the mean monthly maximum temperature in August and the saturation vapor pressure at the mean monthly minimum temperature in August and (2) an elevation term. The second term essentially acts as an elevation correction factor with less ET at higher elevations.

PET calculated by PRMS was compared against PET calculated by the Penman method at stations in Chamokane and Deer Park. The Chamokane data covered the WY2009-WY2013 calibration period and correlated well to the Deer Park data starting in July 2014 (Figure 7.32).

## 7.6 Tables

Table 7.1: Hydrologic submodel lookup table for parameters based on land cover (NLCD (2011)).

NLC ID	Class Name	% of study area	Vegetation Index	Summer Cover Density (0 to 1)	Winter Cover Density (0 to 1)	Summer Rain Inter-ception Storage (in)	Winter Rain Inter-ception Storage (in)	Snow Inter-ception Storage (in)	Winter Radiation Transmission Factor (0 to 1)	Soil Depth (in)
11	Open Water	1.12	Bare	0	0	0	0	0	1	1
21	Developed, Open Space	1.88	Grass	0.85	0.4	0.08	0.04	0.08	0.7	18
22	Developed, Low Intensity	2.31	Grass	0.75	0.45	0.08	0.04	0.08	0.7	18
23	Developed, Medium Intensity	0.43	Grass	0.65	0.35	0.08	0.04	0.08	0.7	18
24	Developed High Intensity	0.02	Grass	0.5	0.2	0.08	0.04	0.08	0.8	18
31	Barren Land (Rock/Sand/Clay)	0.03	Bare	0.1	0.1	0	0	0	0.95	9
41	Deciduous Forest	0.05	Trees	0.85	0.35	0.08	0.04	0.12	0.8	30
42	Evergreen Forest	54.87	Trees	Mapped	Mapped	0.16	0.16	0.39	0.2	30
43	Mixed Forest	>0.01	Trees	0.85	0.5	0.12	0.12	0.2	0.4	30
52	Shrub/Scrub	16.35	Shrub	0.8	0.45	0.08	0.08	0.08	0.6	25
71	Grassland/Herbaceous	10.79	Grass	1	0.85	0.08	0.04	0.04	0.8	15
81	Pasture/Hay	1.29	Grass	0.85	0.04	0.08	0.04	0.04	0.9	6
82	Cultivated Crops	9.29	Grass	0.85	0.04	0.08	0.04	0.04	0.9	12
90	Woody Wetlands	0.38	Shrub	1	0.85	0.12	0.08	0.12	0.4	48
95	Emergent Herbaceous Wetlands	1.20	Shrub	0.75	0.5	0.06	0.04	0.08	0.6	48

Table 7.2: Hydrologic submodel lookup table for parameters based on surficial geology mapping.

Geologic Unit	Description	Index	% of Study Area	PRMS Soil Type	CN Soil Class	Wilting Point (wp)	Field Capacity (fc)	Porosity (n)	Slow Interflow (in/d)
Qs	Recent non-glacial	1	3.8	Loam	B	0.07	0.21	0.40	0.05
Qmw	Mass-wasting deposits	2	2.2	Sand	B	0.1	0.24	0.40	0.05
Qe	Eolian deposits	3	3.1	Sand	A	0.1	0.24	0.35	0.05
Qgf	Fine-grained glacial	4	27.6	Loam	BC	0.09	0.22	0.40	0.30
Qgc	Coarse-grained glacial	5	17.2	Sand	A	0.05	0.16	0.35	0.05
Qgt	Glacial till	6	1.6	Clay	CD	0.07	0.21	0.40	0.30
Mw	Wanapum Basalt	7	0.87	Loam	B	0.08	0.20	0.30	0.15
Mgr	Grande Ronde Basalt	8	0.75	Loam	B	0.08	0.20	0.30	0.15
MI	Latah Formation	9	0.48	Loam	C	0.08	0.20	0.30	0.30
Tkg	TKg Intrusive igneous	10	32.7	Loam	C	0.05	0.15	0.30	0.15
pEm	Metamorphic rocks;	11	7.8	Loam	C	0.05	0.15	0.30	0.15
Lac	Other lacustrine	12	2.0	Clay	C	0.1	0.24	0.40	0.30

Table 7.3: Lookup table to assign CN values based on land cover and soil classes.

Land Cover Class		Soil Class						
		A	AB	B	BC	C	CD	D
<b>11</b>	Open Water	99	99	99	99	99	99	99
<b>21</b>	Developed, Open Space	68	75	80	83	86	88	90
<b>22</b>	Developed, Low Intensity	68	75	80	83	86	88	90
<b>23</b>	Developed, Medium Intensity	72	75	82	86	88	90	91
<b>24</b>	Developed High Intensity	77	83	85	88	90	91	92
<b>31</b>	Barren Land (Rock/Sand/Clay)	74	82	84	89	90	91	92
<b>41</b>	Deciduous Forest	30	39	55	64	70	74	77
<b>42</b>	Evergreen Forest	30	39	55	64	70	74	77
<b>43</b>	Mixed Forest	30	39	55	64	70	74	77
<b>52</b>	Shrub/Scrub	45	58	66	73	77	81	83
<b>71</b>	Grassland/Herbaceous	39	52	61	69	74	78	80
<b>81</b>	Pasture/Hay	49	61	69	75	79	82	84
<b>82</b>	Cultivated Crops	63	70	75	80	83	85	87
<b>90</b>	Woody Wetlands	90	92	94	96	98	99	99
<b>95</b>	Emergent Herbaceous Wetlands	99	99	99	99	99	99	99

## 8 Groundwater Flow Submodel Development

A groundwater flow model is a simplified representation of the complex physical, hydrologic, and hydrogeological processes that affect the rates and direction of groundwater flow. These processes relate primarily to features and physical characteristics of the study area including:

- stratigraphy (i.e., the bedrock and overburden stratigraphic layers, their top and bottom surface elevations, lateral extent of the formations, and unit thickness);
- hydrostratigraphy (i.e., lateral extents of the aquifers and aquitards in the study area, their top and bottom surface elevations, thickness, and degree of continuity);
- aquifer and aquitard properties (e.g., estimated hydraulic conductivity, anisotropy, saturated thickness, transmissivity, porosity, and storage properties);
- inputs to the hydrologic system (i.e., rates of groundwater recharge and discharge and the underlying processes that affect these rates, such as precipitation, ET, overland runoff, infiltration, and baseflow);
- properties of the surface-water system and factors controlling groundwater/surface water interaction; and
- anthropogenic inputs and outputs from the groundwater system (e.g., pumping rates and return flows).

### 8.1 *Groundwater Flow Equation*

Groundwater flow is governed by Darcy's Law, which states that flow is proportional to the hydraulic gradient and to the hydraulic conductivity of the aquifer material. Darcy's Law can be written as:

$$q = -K \frac{dh}{dx} \quad \text{Eq. 8.1}$$

where  $q$  is the specific discharge or rate of flow per unit area,  $K$  is the hydraulic conductivity, and  $dh/dx$  is the hydraulic gradient (change in hydraulic head per unit length). Groundwater flow is also governed by the Law of Conservation of Mass which states that all inflows to an area must be balanced by outflows and/or by a change in aquifer storage. When the mass balance equation is combined with Darcy's Law, it yields the governing equation for three-dimensional groundwater flow.

$$\frac{\partial}{\partial x} \left( K_{xx} \frac{\partial h}{\partial x} \right) + \frac{\partial}{\partial y} \left( K_{yy} \frac{\partial h}{\partial y} \right) + \frac{\partial}{\partial z} \left( K_{zz} \frac{\partial h}{\partial z} \right) = S_0 \frac{\partial h}{\partial t} \quad \text{Eq. 8.2}$$

where:

$K_{xx}$	=	hydraulic conductivity in the x direction;
$K_{yy}$	=	hydraulic conductivity in the y direction;
$K_{zz}$	=	hydraulic conductivity in the z direction;
$h$	=	hydraulic head;
$S_0$	=	specific storage

Hydraulic conductivity is a measure of how easily water can pass through the pores in the geologic unit. Specific storage is a measure of how much water is released from aquifer storage per unit decline in aquifer head per unit volume of aquifer. Water is released from storage due to expansion of the water and due to compression of the pore structure by the increase in intergranular stress.

The intergranular stress increases as the water pressure decreases because total stress due to the weight of the overburden remains constant.

In the hydraulic approach to aquifer flow (see Bear, 1979), Eq. 8.2 can be simplified by integrating over the thickness of the aquifer. The resulting equation for two-dimensional flow in a confined aquifer of thickness B with recharge, discharge, and leakage from above and below can be written mathematically (Bear, 1979) as:

$$\frac{\partial}{\partial x} \left( T_{xx} \frac{\partial h}{\partial x} \right) + \frac{\partial}{\partial y} \left( T_{yy} \frac{\partial h}{\partial y} \right) + \left[ \frac{K'_U}{B'_U} (H_U - h) \right] + \left[ \frac{K'_L}{B'_L} (H_L - h) \right] + R - \sum_{k=1}^{N_{well}} Q'_k = S \frac{\partial h}{\partial t} \quad \text{Eq. 8.3}$$

where:  $T_{xx}$  = transmissivity in the x direction (where  $T_{xx} = K_{xx}B$ );  
 $T_{yy}$  = transmissivity in the y direction;  
 $h$  = hydraulic head;  
 $K'$  = vertical hydraulic conductivity of an overlying (or underlying) confining unit  
 $B'$  = thickness of the upper (or lower) confining unit;  
 $H_L/H_U$  = head in the aquifer layer overlying/underlying the confining unit;  
 $R$  = rate of groundwater recharge;  
 $Q'_k$  = pumping rate (per unit area) at well k  
 $S$  = storativity or storage coefficient (where  $S = S_0B$ )

Eq. 8.3 can be written for each aquifer in a layered sequence of aquifers and confining units. When the upper aquifer layer is unconfined, the transmissivity terms  $T_{xx}$  and  $T_{yy}$  are replaced by the effective transmissivity, equal to  $K_{xx}(h-b)$  and  $K_{yy}(h-b)$ , where  $b$  is the elevation of the base of the aquifer layer. The storage coefficient for an unconfined aquifer is usually replaced with the specific yield,  $S_y$ , represents water "released from storage" due to the draining of the pore space above the water table as the water table drops.  $S_y$  is generally several orders of magnitude larger than compressive storage.

Eq. 8.3 is the partial differential equation that forms the basis of the mathematical model developed for the study area. The equation is "solved" to determine aquifer heads at a point in the model area. Information in the form of aquifer properties, recharge and discharge rates, and conditions along the study area boundaries, are provided as input to the model to make the solution unique to the study area. Numerical methods are used to solve Eq. 8.3 when study area boundaries are irregular and/or aquifer/aquitard properties, aquifer geometry (stratigraphy), and rates of recharge and discharge vary spatially within the study area.

## 8.2 Submodel Description: MODFLOW-NWT

Several different numerical techniques and computer codes have been written to solve the groundwater flow equation and simulate groundwater flow. The groundwater flow model used in this study was built with the USGS MODFLOW computer code. The basic MODFLOW-2005 code is documented in Harbaugh (2005). The MODFLOW code uses the finite-difference method to solve Eq. 8.3. The code is well suited for modelling transient groundwater flow in multi-layered aquifer systems and can easily account for irregular boundaries, complex stratigraphy, and spatial variations in hydrogeologic properties. A newer version of the MODFLOW code, MODFLOW-NWT (Niswonger *et al.*, 2011), is especially well suited for representing thin aquifers and sharp changes in model layer stratigraphy, such as those occurring in areas with steep topography and thin, discontinuous units. MODFLOW-NWT is incorporated as a submodel in Version 1.1.6 of the GSFLOW, which was used in this study.

### **8.3 Model Discretization**

The finite-difference method requires that the study area be subdivided into a grid of small square or rectangular cells and multiple layers. Optimal grid design is a balance between achieving the highest resolution possible (i.e., smaller cells) and minimizing model run times, which increases proportionally to the square or cube of the number of cells. Several grid designs and model extents were tried during the course of model development. The final grid design uses 500 ft square cells in the center of the study area and 1000 ft cells in the model periphery. Rectangular cells, 1000 by 500 ft are used in transition zones. The model grid is shown in Figure 8.4 and consists of 380 rows and 230 columns for a total of 87,400 grid cells for each of the model layers.

MODFLOW works in a local, grid coordinate system based on row and column numbers. The VIEWLOG-GIS preprocessor (Kassenaar, 2013) was used to help translate geo-referenced map data into MODFLOW coordinates. The local origin for the model grid is at 2413,000 E and 281,500 N in the Washington North NAD-83 state plane coordinate system (SPCS). All digital data for the study area were georeferenced to the same SPCS coordinate system.

Numerical model layers were used to represent the 12 hydrostratigraphic layers discussed in the hydrogeological conceptualization (Section 3.3). An important consideration when translating the hydrostratigraphic model layers to numerical model layers is that MODFLOW requires continuity for the simulated numerical layers; whereas the hydrostratigraphic model has layers that pinch out to zero thickness. The hydrostratigraphy of the study area presented a unique challenge because of the discontinuous nature of all units except the unweathered bedrock.

To meet the layer continuity requirements for the numerical model, the model was built from the top down. For each grid location (e.g., row 1, column 1), all hydrostratigraphic layers were checked to see whether they exceeded a minimum 1 ft thickness. If a hydrostratigraphic layer did not meet this minimum, the unit was not represented at that location and the thickness was absorbed into the overlying layer. Thus, only units that were present in the vertical sequence are represented. This process is illustrated in Figure 8.6 for a Section C-C'. A map of the units represented in each model layer was prepared so that the output could be post-processed to determine the heads in each hydrostratigraphic unit. Although this method created a more discontinuous representation of the hydrostratigraphic layers (compared to methods that assign a minimum thickness to each layer whether present or not), it resulted in a dramatic reduction in the number of active cells. As well, there were no active cells below numerical model layer 10, so only 10 numerical model layers were needed to represent the flow system. The assignment of aquifer and aquitard properties was done by unit number. Figure 8.7 shows the assignment of hydraulic conductivity values by unit to each layer in Section C-C'.

### **8.4 Model Boundary Conditions**

The focus of this study is on the Little Spokane River watershed above the Dartford gage. The boundaries of the LSR model area were selected to correspond to natural physical boundaries; primarily the watershed divides in the granitic bedrock highlands. Because of possible groundwater exchange across the northern watershed boundary, the model boundaries were extended northward to the Pend Oreille River. In this way, groundwater inflows and outflows across the watershed boundary could be assessed to determine how much they contribute to the overall water balance and to groundwater and surface water flow. The model boundary encompasses 688 mi<sup>2</sup> (1,780 km<sup>2</sup>), as shown in Figure 1.1. and Figure 8.5.

As was noted earlier, flows at the USGS gage below Dartford are known to be strongly influenced by groundwater discharge from the Spokane Valley Rathdrum Prairie (SVRP) aquifer, which underlies the Spokane River. Modeling of groundwater flow within this regional aquifer was beyond the scope of the current study. The significance of groundwater exchange between the SVRP and the aquifers

in the study area was examined during the course of the study and it was concluded that the bedrock outcrops and subcrops in the Dartford area likely restrict groundwater movement across most of the southern boundary. This is consistent with the geologic analysis and geophysical testing conducted by CH2M-HILL (2000) at the north end of the Hillyard Trough as part of their development of a wellhead protection plan for the Spokane area. It is also consistent with recent hydrogeologic analysis completed for water right consolidations done by Ecology for the Whitworth Water District. Boundary conditions were modified in the gaps, as described below.

#### 8.4.1 Constant Head and No Flow Boundary Conditions

Boundary conditions are specified for cells that lie along lines corresponding to the physical boundaries of the groundwater flow system. Three general types of boundary conditions were used in the groundwater flow model: constant head, no-flow, and head-dependent discharge boundaries. As can be seen in Figure 8.5, constant head cells were applied along the northern model boundary corresponding to the Pend Oreille River. Control elevations for the constant head boundaries were estimated from the 10-m DEM for the study area.

Gaps in the bedrock outcrops/subcrops along the southern model boundary may allow some exchange of groundwater between the aquifers in the Little Spokane River watershed and the SVRP aquifer. To account for this flow, the boundary was represented as a MODFLOW variable head boundary. Time-dependent heads in the SVRP were estimated based on results of the USGS SVRP model (Hsieh *et al.*, 2007). Base heads were interpolated to the boundary cells from those provided in Figure 42 of Hsieh *et al.* (2007). These were allowed to vary over time as:

$$H_t = H \cdot 2.5 * \sin\left(\frac{2\pi \cdot \text{JulianDate}}{365}\right) \quad \text{Eq. 8.4}$$

where:  $H$  = Baseline interpolated head at the variable head cell

The simulated heads peak in April of each year and vary with an amplitude of 2.5 ft consistent with the transient results of the SVRP model for locations in the Hillyard Trough.

No-flow boundaries were imposed along most of the remaining external boundary assuming that cross watershed flow across these boundaries was insignificant and did not affect flows within the Little Spokane River watershed. A no-flow boundary was imposed along the base of the model assuming that the amount of fracturing in the bedrock below that depth was minimal and that inflow from the deeper portion of the unweathered bedrock would also be negligible. Selecting an appropriate depth for cutting off the bedrock zone was a subject of investigation during the early part of this study. The bottom of the Chamokane model (Ely and Kahle, 2012) was set at a constant 800 ft above sea level; resulting in the active bedrock layer thicknesses ranging from 226 to 3,466 ft. The variable thickness, however, introduces spatial variation of the layer's transmissivity which can, in turn, influence groundwater flow. For this study, a final constant layer thickness of 1000 ft was assigned to the active bedrock zone resulting in a constant transmissivity for the unit.

#### 8.4.2 Head-Depended Discharge Boundary Conditions

**Streams:** Head-dependent flux boundaries were used extensively to represent groundwater/surface water interaction between streams, lakes, and larger wetlands within the model area. Flow between the streams and the underlying aquifer was assumed to be exchanged as "leakage" across lower-permeability streambed material. The rate of leakage is determined based on Darcy's Law where:

$$Q_L = \frac{K'}{B'} A_L (H_L - h) \quad \text{Eq. 8.5}$$

where:  $Q_L$  = volumetric flow rate between aquifer and stream;

- $K'$  = vertical hydraulic conductivity of the streambed;  
 $B'$  = thickness of the streambed;  
 $A_L$  = wetted area of the streambed;  
 $H_L$  = stream stage (in masl); and  
 $H$  = head in the aquifer

Leakage between the stream and the aquifer is calculated on a cell-by-cell basis using the SFR2 module (Niswonger and Prudic, 2005). A dendritic stream network was first created by defining stream "segments" and junctions as in the sketch below (Figure 8.1). Stream segments are numbered from upstream to downstream. In SFR2, a stream "reach" is defined as the portion of a stream segment within a model cell. For example, stream Segment 1 in the northwest corner of Figure 8.1 has three reaches (1,1; 1,2; and 1,3).

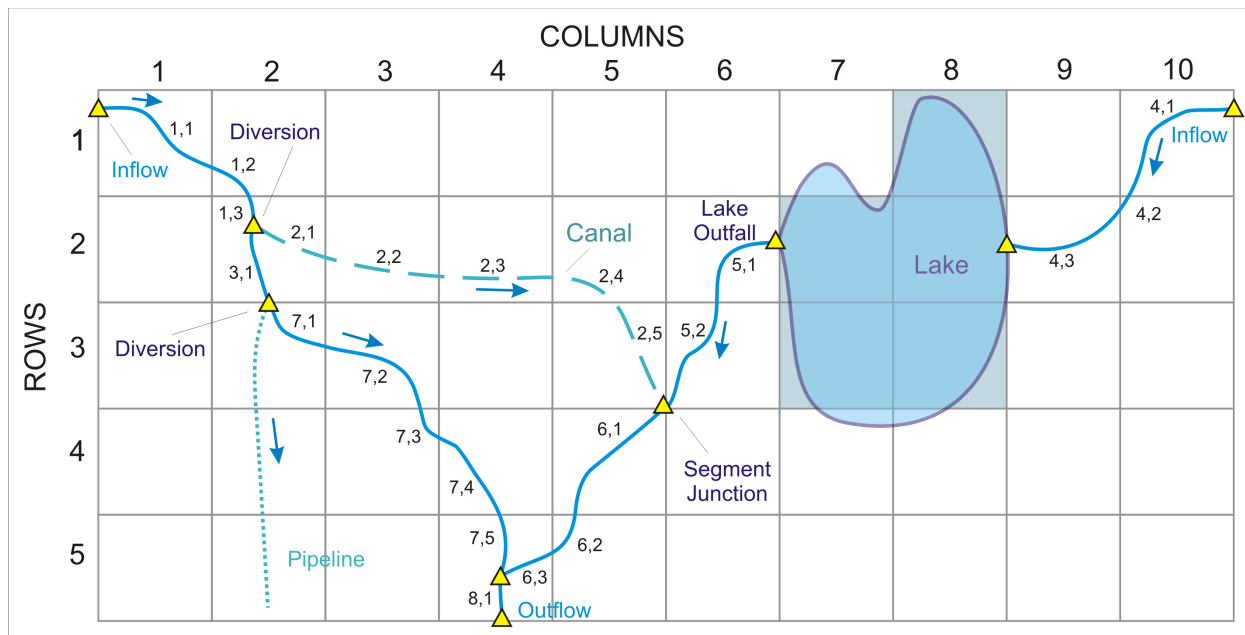


Figure 8.1: Stream network and lake representation in the SFR2 and LAK3 modules (modified from Markstrom, *et al.*, 2008).

Stream reaches were defined by overlaying the model grid on the mapped streams segments shown in Figure 8.5. Over 858 miles of stream channels were simulated in the submodel and included all stream segments classified as perennial and all stream segments classified as intermittent in the central basin. There were a large number of intermittent stream segments mapped in the granitic bedrock highlands that had no evident channel visible on aerial photographs. The intermittent flow in these stream segments was assumed to be dominated by overland runoff processes which were simulated by the PRMS submodel instead of SFR2. In total, the study area contained 3129 stream segments broken into 13,349 stream reaches.

Stream properties, including cross-sectional geometry and streambed elevation, roughness (Mannings  $n$ ), thickness, and hydraulic conductivity, were defined for each segment. To assign reasonable stream properties to all the reaches, streams segments were first characterized by their Strahler order (a classification scheme whereby headwaters are assigned an order of 1; the order increases downstream of the confluence of two similar-order streams). The hydraulic conductivity of the streambed material was set to 0.1 times the hydraulic conductivity assigned to the material in Layer 1 and ranged from  $4.5 \times 10^{-4}$  to 36 ft/d. Bed thickness was set to 1 ft for Class 1 and intermittent streams and 2 ft for higher order streams. Mannings  $n$  was set to 0.030. Stream slope and streambed elevation were estimated for each segment from the DEM.

There are few surveyed channel sections compared to the number of reaches simulated. Typical 8-point stream cross sections and streambed conductance were assigned to each stream order. Following Ely and Kahle (2012), average stream depth, top width and bottom widths for the cross sections were assigned based on mean annual streamflow and regression equations determined by Magirl and Olsen (2009) for Washington State streams given by:

$$D_h = 0.23 Q^{0.37} \quad \text{Eq. 8.6}$$

$$W_t = 4.85 Q^{0.45} \quad \text{Eq. 8.7}$$

$$W_b = 2.14 Q^{0.46} \quad \text{Eq. 8.8}$$

where:  $D_h$  = Hydraulic depth (cross-sectional area divided by top width) [ft]  
 $W_t$  = Channel top width [ft]  
 $Q$  = Average flow [cfs]  
 $W_b$  = Channel bottom width [ft]

Average flows for the gage at Chattaroy and at Dartford were used to set the section properties for the Strahler Class 5 and 6 streams, respectively. Average flows for the other stream orders were estimated from the spot flow data. Sections for the stream classes using these data are shown in Figure 8.2. A small slope to the channel bottom was needed for numerical stability.

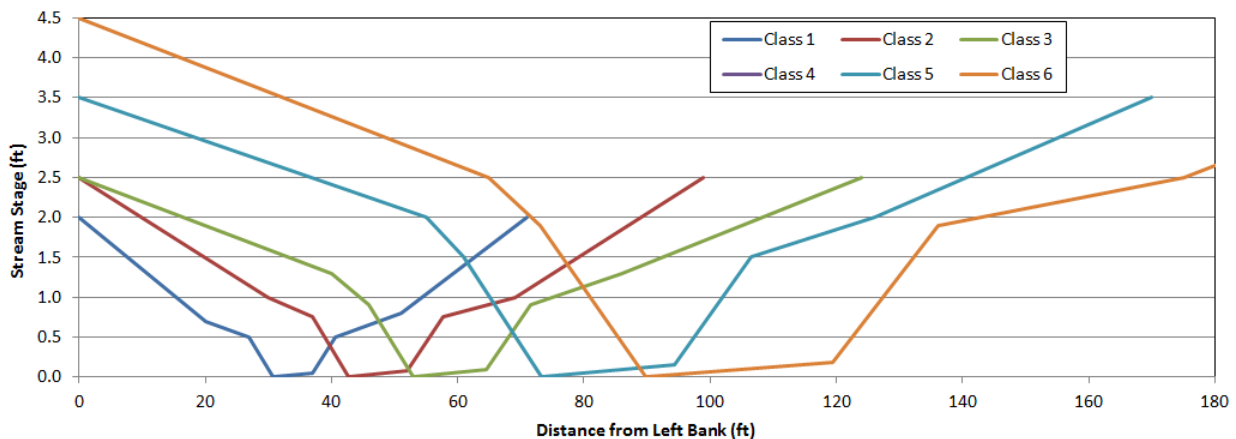


Figure 8.2: Estimated cross-sections for the six Strahler classes.

Flow at the midpoint of each reach is calculated based on the sum of upstream inflows (as calculated by SFR2), precipitation, evaporation, and overland flow to the reach (as calculated by PRMS). Stream stage is then determined from the stream roughness, slope and the cross-sectional geometry. Leakage to or from the aquifer is then calculated based on Eq. 8.5 and the difference between stream stage and the head in the underlying aquifer. Multiple reaches can occur within a single cell and most cells are small enough such that the head in the center of the cell is a reasonable approximation to the head in the aquifer beneath the streambed.

Net outflow from the reach is routed to a downstream reach segment. Because leakage can affect aquifer levels, and in turn, streamflow; the streamflow routing and the groundwater flow equations are non-linear and must be solved in an iterative manner for each time step until convergence is achieved (i.e., changes in simulated flows and heads between successive iterations fall below threshold levels). Stream segments can terminate in a lake or wetland (as shown in Figure 8.1) or exit the model area.

**Lakes and Wetlands:** Leakage between lakes or other standing bodies of water and the aquifer is also governed by Eq. 8.5 and is calculated on a cell-by-cell basis using the LAK3 module in MODFLOW (Merritt and Konikow, 2000). In LAK3, a cell can represent all or a portion of a lake (see Figure 8.1). The area  $A_L$  in Eq. 8.5 is equal to the cell area. Head in the aquifer,  $h$ , is the head in the cell underlying the lake and  $H_L$  is the lake stage. Lake stage is calculated from specified stage-volume relationships. Lake volume is calculated in a separate water budget analysis for each lake based on the sum of upstream inflows (as computed by the SFR2 module); precipitation, evaporation, and overland flow to the lake (as calculated by PRMS); and outflow from the lake (also calculated by SFR2 based on lake stage). Lakes can penetrate multiple model layers and leakage can occur to cells adjacent to or underlying the lake. Larger wetlands that were observed to have standing water in aerial photographs were treated as shallow lakes in Layer 1.

The location and outline of lakes within the study area were based on the USGS High Resolution National Hydrography Dataset Plus (NHDPlus HR) dataset. A total of 46 MODFLOW lakes were simulated in the model, and included 26 lakes and 20 of the larger wetlands. Smaller ( $<0.05 \text{ km}^2$ ) ponds were not explicitly represented in the model at this time. The effect of smaller wetlands, in terms of intercepting runoff and recharging groundwater, was represented by the depression storage feature of PRMS. Bathymetry data were available from the Washington State Department of Fish and Wildlife for Davis, Diamond, Eloika, Fan, and Sacheen Lakes. Other lakes were assigned to have an average depth of 15 ft. The bathymetry data were used to incise the lakes into the upper model layers. Wetlands (e.g., fens, marshes, bogs, and swamps) were assumed to have a uniform depth of 5 ft.

#### 8.4.3 Flow across Top Model Boundary

Groundwater recharge and groundwater ET (i.e., the loss of water from a shallow water table below the soil zone) were simulated using the UZF module (Niswonger *et al.*, 2006). The UZF module was also used to apply a head-dependent discharge boundary across the top surface of the model. When run as a stand-alone submodel, this boundary simulates groundwater discharge from the aquifer to land surface. The discharge is then routed directly to nearby SFR2 stream segments. Assignment of stream reaches to model cells was based on an analysis of land surface topography.

In stand-alone MODFLOW mode, estimated rates of recharge must be specified and then adjusted as part of the model calibration process. Interim results from long-term PRMS runs were used as initial estimates of the spatially-variable annual average recharge rates in the pre-calibration MODFLOW simulations. In this way, reasonable values for the other model parameters (e.g., hydraulic conductivities) could be obtained by pre-calibrating the submodel.

The models were run in an integrated mode early on in calibration process. As discussed in Section 6.3.4, the PRMS submodel is run on a daily basis to calculate the amount of recharge to be supplied to the groundwater system, direct precipitation on lakes and streams, ET demand for lakes and streams, and any unsatisfied ET demand from the soil zone. The MODFLOW submodel is run for the same time step, and computes heads; streamflow and lake stage; and ET from the saturated zone, rejected recharge, and groundwater discharge to the soil zone. This information is passed back to PRMS where the head-dependent discharge is added to the soil water zone where it can then contribute to cascading runoff and interflow. The process is repeated until the two submodels converge.

### 8.5 Simulated Surface Water and Groundwater Withdrawals

A key task in this study was to obtain the best estimates of groundwater and surface water use within the study area for use in the integrated model. Water rights are discussed in Section 5. Withdrawals were simulated in the model as either groundwater withdrawals or surface water diversions. All withdrawals were represented on a daily basis from data generally reported on a monthly basis. Average withdrawals were computed from reported usage for municipal wells.

Agricultural withdrawals for irrigation and residential self-supply were estimated on a monthly basis by Spokane County staff using their Water Demand Model and were aggregated to model cells. It should be noted that while return flows were provided for self-supplied and agricultural water use, all withdrawals were assumed to be 100% consumptive.

### 8.5.1 Groundwater Withdrawals

The distribution of groundwater and surface water withdrawals are presented in Figure 8.9, and consist of 7,480 cells containing wells. Groundwater withdrawals were represented in the MODFLOW submodel using the WEL7 module in MODFLOW-NWT. Wells were assigned to the proper hydrostratigraphic unit based on the well depth and well screen setting, if available. In the case where the well screen depth was not known, it was assigned to the most commonly screened unit within surrounding wells found in the state database. The sum of simulated groundwater withdrawals, on an annual average basis, was 2,154,681 ft<sup>3</sup>/d (49.5 af/d), with about 39% for municipal supply, 23% for agricultural use, and 38% for self-supply, as summarized in Table 8.1.

Table 8.1: Summary of monthly average simulated groundwater pumping.

Month	Groundwater Pumping in af/yr			
	Municipal/ Commercial <sup>[1]</sup>	Agricultural	Self-Supplied	Total
January	2,163	-	1,867	4,030
February	2,198	-	1,850	4,048
March	2,148	-	1,867	4,014
April	2,643	-	1,867	4,510
May	8,371	3,212	9,122	20,705
June	11,447	10,369	11,718	33,534
July	18,432	15,416	15,591	49,439
August	17,635	12,343	15,602	45,580
September	12,534	7,803	11,243	31,580
October	3,720	434	7,225	11,379
November	2,125	-	1,867	3,992
December	2,123	-	1,867	3,990
<b>Annual Average</b>	<b>7,128</b>	<b>4,131</b>	<b>6,807</b>	<b>18,067</b>

[1] Municipal commercial data presented as the average from 2005 to 2015.

The data show a clear seasonal pattern with the highest withdrawals occurring in the summer months, particularly for the agricultural withdrawals, which occur only from May to October. Inter-annual variability could only be assessed for municipal/commercial withdrawals, which were provided as specific monthly averages for 2005 to 2015. A graphical summary of the cumulative average monthly withdrawals (in millions of gallons per month, (MGM)) is presented for 2005 through 2015 in Figure 8.3. Very little inter-annual variability occurred during the fall and winter, with the exception of 2014 and 2015, during which time a large withdrawal for landfill remediation was turned off. Inter-annual variability in monthly withdrawals is higher from late spring to fall owing to differences in domestic irrigation demands during wetter or dryer years. Withdrawals vary from 30 to 60 MGM in the late fall and winter to 600 MGM in midsummer.

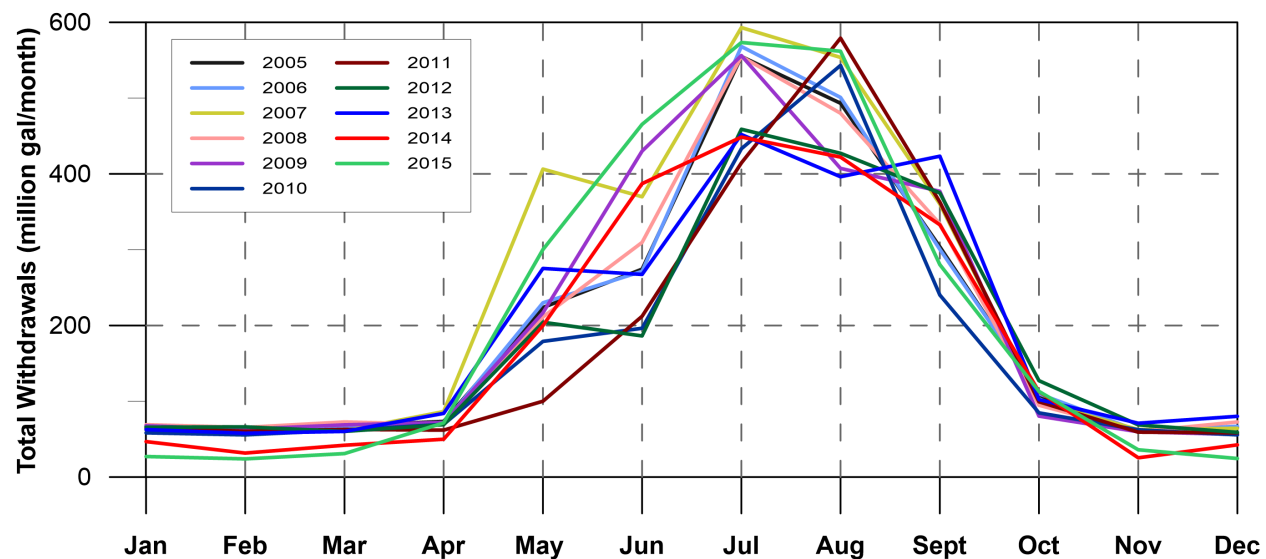


Figure 8.3: Cumulative municipal/commercial monthly withdrawals from 2005-2015.

### 8.5.2 Surface Water Diversions

Seven of the larger surface water withdrawals for agricultural use were simulated as diversions from the nearest stream reach using the SFR2 module in MODFLOW-NWT. The locations of these permits are shown in Figure 8.9. Surface water diversions totaled 126,416 ft<sup>3</sup>/d (2.9 af/d) based on annual average reported values. Surface water diversions were simulated from May to October, as summarized in Table 8.2.

Table 8.2: Summary of monthly average simulated surface water diversions.

Month	Surface Water Diversions, in af/yr			
	Municipal/ Commercial	Agricultural	Self-Supplied	Total
May	-	824	-	824
June	-	2,661	-	2,661
July	-	3,957	-	3,957
August	-	3,168	-	3,168
September	-	2,003	-	2,003
October	-	111	-	111
<b>Annual Average</b>	-	<b>1,060</b>	-	<b>1,060</b>

## 8.6 Model Parameterization

The properties of the model layers, such as the top and bottom elevations, hydraulic conductivity, and storage properties, were assigned to each model cell. Layer tops and bottoms were assigned based on the geometry of the hydrostratigraphic model developed for this study.

Initial estimates for hydraulic conductivity were made based on previous hydrogeologic investigations. Estimated values of hydraulic properties of the hydrostratigraphic units in the study area model are presented in Kahle *et al.* (2013) and were discussed in Section 3.2 of this report.

These values are presented in the first three columns of Table 8.3. Results from the two-layer Mike-SHE model of WRIA-55 (Golder, 2004) are also shown Table 8.3 along with the calibrated hydraulic conductivities from the Chamokane GSFLOW model (Ely and Kahle, 2012) for similar types of hydrostratigraphic units.

The values presented by Kahle *et al.* (2013) were determined by analysis of drawdown/discharge data from testing by the drillers at the time of well installation. A Theis method was applied to wells with screened intervals and a method by Bear (1979) was used for open-hole wells in bedrock. The values are recognized to be biased towards producing higher estimates because of violations of the simplifying assumptions made in the analysis, and the zones tested are biased towards the more productive zones in the formations (see Kahle *et al.* (2013) for a detailed description of the test method and limitations). Despite these biases and limitations, the median values were used to establish initial estimates for hydraulic conductivity values assigned to the groundwater model layers and provided a good starting point for model construction.

It is also noted that the range in hydraulic conductivity for many of the materials vary over several orders of magnitude. The variability may be attributed to natural heterogeneity in addition to uncertainty in the analysis method. For the bedrock units, an equivalent porous medium (EPM) was assumed even though some units may have properties that locally depend on fracture occurrence, aperture, orientation, and connectivity.

Table 8.3: Representative ranges of hydraulic conductivity.

Hydrostratigraphic Unit	Hydraulic Conductivity (ft/d)				
	Min.	Median	Max.	Mike-SHE Model	Chamokane Model
Upper Aquifer	4.4	900	410,000	Zone 1: 2.6 to 23.7 Zone 2: 23.7 to 358	100 to 345
Upper Confining Unit	0.5	8.2	5600		4
Lower Aquifers	8.2	340	8700		135
Lower Confining Unit		0.2			
Wanapum Basalt		0.4		15.9	
Latah	0.19	0.56	15		
Grande Ronde	0.03	2.9	13		0.5
Bedrock	0.01	1.4	5000		Upper: 0.5 Lower: 0.32
Note: Zone 2 occurs in the Diamond Lake area and west of the main branch of the LSR between Dry Creek and Little Deep Creek. The Chamokane units are similar but do not directly correspond to units in the LSR.					

Uniform properties were initially assigned to each of the hydrostratigraphic units. Using the principle of parsimony, similar units (e.g., the two basalt units and two Latah units) were assigned similar properties. The Upper Aquifer and Lower Aquifers in the Diamond Lake area were found to have generally higher hydraulic conductivities values and were treated as separate units. This is consistent with the findings of the Mike-SHE model (Golder, 2004). The pre-Latah Sands were also treated as a separate unit.

Maps showing the spatial distribution of the calibrated hydraulic conductivity values for model layers 1 through 10 are presented in Figure 8.10 through Figure 8.19. Table 8.4 lists the calibrated properties for each of the hydrostratigraphic units. The properties listed represent final calibration values for the integrated model.

Storage parameters (specific storage and specific yield) for the hydrostratigraphic units represented in the model are also presented in Table 8.4. Storage values were calibrated through comparison of transient model outputs with continuous groundwater level data. Specific yield values for the bedrock units were due to the assumption that groundwater flow in these units is dominated by secondary permeability associated with small-aperture fractures. Specific storage values are also low (on the order of  $10^{-6}$  ft<sup>-1</sup>), due to the incompressibility of the rock matrix.

Table 8.4: Final calibrated model parameter values.

Hydrostratigraphic Unit	Hydraulic Conductivity [ft/d]	Anisotropy Kh:Kz	Specific Yield	Specific Storage [1/ft]
Soil Zone	Variable	3:1	0.2	0.0001
Upper Aquifer	360	3:1	0.2	0.0001
Upper Aquifer – NE area	480	3:1	0.2	0.0001
Upper Confining Unit	5	10:1	0.1	0.00001
Lower Aquifers	150	3:1	0.2	0.0001
Lower Aquifers – NE area	300	3:1	0.2	0.0001
Lower Confining Unit	5	10:1	0.1	0.00001
Wanapum Basalt	3	3:1	0.05	0.000001
Upper Latah	0.15	50:1	0.1	0.00001
Grande Ronde Basalt	3	3:1	0.05	0.000001
Lower Latah	0.15	100:1	0.1	0.00001
Pre-Latah Sands	75	3:1	0.2	0.0001
Weathered Bedrock	10	3:1	0.05	0.00004
Unweathered Bedrock	0.12	3:1	0.01	0.000002

## **9 Integrated GSFLOW Model Calibration**

### **9.1 Calibration Strategy and Targets**

#### **9.1.1 Sub-Model Pre-Calibration**

The PRMS submodel was pre-calibrated early on in the study to test the submodel's ability to represent the hydrological processes in the study area and to derive reasonable values for many of the model parameters. In particular, process submodels (such as the snowpack model, PET, and precipitation form models) were tested independently. Although the groundwater processes simulated were simplified and with no feedback represented, care was taken so that submodel results and parameter values were generally transferable to the fully-integrated model.

The large difference in model run times between PRMS-only runs and GSFLOW runs precluded calibrating the fully-integrated model at the outset. Simulations for the five-year calibration period (WY2009 to WY2013) period took 45 minutes in PRMS-only mode but 2.7 days in GSFLOW mode. The longer-term simulations used for model validation and in the scenarios (WY2003-WY2017) took 6.5 days to run in GSFLOW mode. A parameter sensitivity/Monte Carlo approach was used in the pre-calibration period to jointly measure model sensitivity and refine the model calibration.

The calibration process shifted to running GSFLOW in integrated model mode after reasonable parameter values were determined for PRMS and it was felt that representing groundwater interaction was critical for improving the calibration. Adjustments to the preliminary PRMS parameters continued up to the final calibration.

In a similar manner, the groundwater submodel was pre-calibrated to determine reasonable values for the aquifer and aquitard properties as well as for parameters in the SFR2 and LAK3 modules used to represent streamflow and lake/wetland water balances. The model was initially run in steady-state mode to derive reasonable values for the hydraulic conductivity values. Groundwater recharge for the steady-state runs was estimated based on average annual recharge rates from the stand-alone PRMS model. Rejected recharge and groundwater discharge to land surface in areas of shallow water table can occur in the steady-state model. A simplified routing scheme was used in which a receiving stream segment was assigned to each MODFLOW cell. The GSFLOW pre-processor was used to examine the cascade flow network and identify the MODFLOW cells within the contributing area to each stream reach.

The parameter estimation code, PEST (Doherty, 2015), was used to help refine the initial estimates of the groundwater submodel parameter values by minimizing the sum of the squares of the residuals between simulated and observed groundwater levels. The automated calibration procedure had limited success because of noise in the static water level data due to positional errors, elevation errors, and seasonal and inter-year differences. PEST requires multiple runs to determine optimal parameter values and was impractical to use to calibrate the transient GSFLOW model because of the long model run times.

#### **9.1.2 GSFLOW Calibration**

Once the PRMS and MODFLOW submodels were reasonably well pre-calibrated, the focus shifted to the integrated GSFLOW final calibration and updating aquifer/aquitard storage properties and properties that were most sensitive to transient groundwater/surface water interaction processes. The PRISM climate data sets provided the key input for the transient GSFLOW simulations. Water use data for the study area, discussed in Section 5 and Section 8.5, was used to build input data sets of daily surface water and groundwater withdrawals.

The integrated model was found to be stable and simulation results indicated that a long model "start-up", prior to the calibration period, was not needed for the soil zone and upper aquifers

(although the unweathered bedrock showed slower response to start-up conditions). Early on in the process, the model started with an initial steady-state MODFLOW simulation prior to the transient integrated runs. Later simulations used the last day model heads as starting heads and no steady-state run was used. The starting heads were updated periodically during the calibration process.

### 9.1.3 Calibration Targets

The GSFLOW model was calibrated to match available streamflow and groundwater level monitoring data for the 5-year period from October 2008 to September 2013 (WY2009 to WY2013). The relatively short calibration period was a compromise necessitated by the long model run times and the need to do multiple runs. The period covers a dry year, an average year, and three wet years to test the model response across a range of climate conditions.

Although the calibration concentrated on matching the gage at Dartford, the calibration strategy was to regionalize as many of the input parameter values as possible across the model area and reasonably match flows at all the other gages active during the calibration period. Initially, a calibration period starting in WY2006 was selected because seven of the nine gages were active for all or part of the five-year period. However, because of the paucity of climate data, the calibration period start was shifted to WY2009 when only five gages were active. A summary of the gage properties and streamflow characteristics for the available stations was provided in Section 4.2. The contributing area to each gage is shown in Figure 9.1. Stage data were also available from Eloika Lake on a continuous basis for non-winter months.

Three objective functions were used to drive the manual calibration of the model with respect to matching observed streamflow: Nash-Sutcliffe (1970) efficiency (NSE), log-transformed Nash-Sutcliffe efficiency (log NSE), and the volumetric efficiency between the observed and simulated streamflow. The NSE is given by:

$$\text{Nash Sutcliffe Efficiency} = 1 - \frac{\sum_{n=1}^{nobs} (Q_o - Q_s)^2}{\sum_{n=1}^{nobs} (Q_o - \bar{Q}_o)^2} \quad (\text{Eq. 9.1})$$

where  $Q_o$  is the observed flow and  $Q_s$  is the simulated flow. The NSE can range from 1 to minus infinity, with 1 being a perfect fit. A Nash-Sutcliffe efficiency of 0.6 is considered a reasonable value (Chiew and McMahon, 1993). It must be recognized that the model simulates flow on a daily basis and would not be expected to achieve a perfect match to observed mean daily flows. Because of the importance of matching low flows in this study, the Log NSE, which is considered a better measure of the model calibration to low flows (Krause *et al.*, 2005), was given similar emphasis.

Ely and Kahle (2012) used the “volumetric efficiency” (Criss and Winston, 2008) as a way to examine goodness of fit between simulated and measured streamflow volumes, where:

$$\text{Volumetric Efficiency} = 1 - \frac{\sum |Q_s - Q_o|}{\sum Q_o} \quad \text{Eq 9.2}$$

Similar to NSE, the VE ranges from 0 to 1 and represents the fractional volumetric mismatch between the measured and simulated values. Percent volumetric difference or bias, normalized root mean difference, mean error, index of agreement, Kline-Gupta efficiency, and  $r^2$  statistics were also considered as secondary metrics during calibration.

The static groundwater level data and average water levels at wells with transient data were used as a primary target to match the overall range in water levels and groundwater flow patterns. The data were filtered to remove wells with obvious errors, such as water levels below the bottom of the monitoring interval, or wells with obviously incorrect spatial coordinates. The remaining 3,043 observed static water levels made up the final calibration dataset, and were assigned to the model aquifers and aquitards based on their screened/open hole intervals.

Aquifer and aquitard properties were refined during the GSFLOW model calibration to improve the match. Three statistics were used to assess the quality of the model calibration: the mean error (ME), mean absolute error (MAE), and root mean squared error (RMSE). These are given by Anderson and Woessner (1992) as:

$$\text{Mean Error} = \frac{1}{n} \sum_{i=1}^n (h_o - h_s)_i \quad \text{Eq. 9.3}$$

$$\text{Mean Absolute Error} = \frac{1}{n} \sum_{i=1}^n |(h_o - h_s)_i| \quad \text{Eq. 9.4}$$

$$\text{Root Mean Squared Error} = \sqrt{\frac{1}{n} \sum_{i=1}^n (h_o - h_s)_i^2} \quad \text{Eq. 9.5}$$

where:

$h_o$  = observed head;  
 $h_s$  = simulated head; and  
 $n$  = number of observations.

Other spatial and statistical analyses were applied to the results, as described below.

#### 9.1.4 Surface Water Calibration Results

Figure 9.2 through Figure 9.16 present the results of the GSFLOW calibration efforts at the five calibration gauges for the period WY2009 to WY2013. Hydrographs, log-transformed hydrographs, and flow duration curves are presented for each gauge to demonstrate the quality of the current calibration. The FDC curves developed for the gages are based on observations from the calibration period, not the full period of record. Figure 9.17 to Figure 9.23 present hydrographs for the seven gages active during the WY2003-WY2008 validation period.

The observed flows are reasonably well correlated to the simulated rainfall and snowmelt events and the timing of the peak flows in the simulated response generally match the observed events. There are exceptions, most likely due to limitations in the precipitation monitoring network that would cause events to be missed or lead to “phantom” events created by extrapolating data from distant stations. There are also simplifications in the snowmelt model and limits in the temperature data inputs to the process model.

Calibration statistics for the calibration and validation periods are listed in Table 9.1. The model achieved reasonable NSEs of 0.597 and 0.449 for the calibration and validation periods, respectively, at the Dartford gage, and log-NSEs of 0.636 and 0.657. Daily results were aggregated over each month and compared with monthly averaged observed values. Monthly NSEs at the Dartford gage were 0.648 and 0.571. The log-NSEs were slightly higher, 0.650 and 0.668, compared to the non-transformed factors. The volumetric efficiencies were 0.675 and 0.683, respectively, for the calibration and validation periods.

The calibration appears to improve as the catchment area increases, likely due to averaging local underpredictions and overpredictions over larger areas. For example, the model consistently overpredicts the volume of flows at the Elk gage and for the limited record at the TMDL-1 gage. The

NSE and log-NSE values are extremely poor for this gauge due to the offset even though the patterns produced by the model are consistent with gage hydrographs. Additional data collection in this area and further refinements to the model may help improve the results. The model matches the high flows below Eloika Lake but is missing the low flows; Figure 9.6 shows that the model does not allow flow to drop below 20 cfs while the gage shows that flows can drop to 4 cfs at times. Refinements to the method for representing the uncontrolled discharge from the lake may improve results. The model appears to do a reasonably good job of matching flow magnitudes and recessions for Dragoon Creek especially during the validation period although it is not that evident from the NSE and Log-NSE statistics. The model also matches the limited data for TMDL-2 closely during this period.

The model matches fall, winter, and early spring flows at the Deadman and Dartford gages reasonably well. There are late spring and/or summer increases in flow at these two gages that the model generally misses. One possible explanation is that there is some interaction with the SVRP that affects these basins with the peaks in these flows offset in time. Further investigation of the possible interaction and possible expansion of the model is recommended for future studies.

Simulated streamflow for the long-term baseline simulation period (WY2003-WY2017) was also compared against the observed data for gauges with long-term record. A flow hydrograph at the Dartford gage for the period is shown in Figure 9.24 and a flow duration curve is shown in Figure 9.25. As can be seen in the flow duration curve, the model provides a reasonably good match to net streamflow volume at the high and low ranges. Calibration statistics are presented for the long-term simulation in Table 9.1. Model statistics are slightly reduced in quality relative to the model calibration period. The log-NSEs values, in particular, are lower because the model seems to consistently overpredict the summer flows in the later years.

Golder (2004) also had difficulty matching flows with their model even though they were able to “capture the form and magnitude of the LSR hydrographs”. Specifically, they found that their early winter flows were too high and “peaky” although the peaks occurred at the correct time in response to storm events, and that some peaks were not simulated or were too high. No calibration statistics were provided in their report. Ely and Kahle (2012) were able to achieve a much better fit to observed streamflow in the Chamokane watershed, especially in the lower flow range, although there were also noted undershoots and overshoots in the higher flow range. It should also be noted that the Chamokane watershed was much smaller (about one-fourth the size of the LSR), had a dedicated AgriMet station, and only one gage to match.

Spotflow measurements are collected by Ecology at gaged and ungaged streams across the subwatershed. Data are collected on a monthly basis year-round at some stations and more irregularly at others. Figure 9.26 presents a visual comparison of the average of these observations at 38 locations against simulated streamflow for the long-term simulation period. A good visual match is achieved for most reaches, with a slight overprediction in a southern tributary to Deadman Creek and the upper reach of Otter Creek. Simulated and average observed values are presented in Table 9.2.

Finally, Figure 9.27 shows a comparison of simulated stage in Eloika Lake versus observations. There appears to be a consistent 2 ft shift in the results with the model tending to underpredict stage. The lake response is reasonably well matched although lake levels drop further than the model allows. As noted earlier, refinements to the method for representing the uncontrolled discharge from the lake may improve results.

### 9.1.5 Groundwater Calibration Results

As discussed earlier, the static groundwater level data and average water levels at wells with transient data were used as targets to match the overall range in water levels and groundwater flow patterns. To obtain long-term average values, daily simulated heads for each layer were averaged over the WY2003-WY2017 simulation period. Because of the way the model was constructed, the

aquifer units could be present in any of the numerical model layers. A post-processing code was run to create potentiometric surfaces from the average daily heads and the layer index files.

Figure 9.28 to Figure 9.31 show the average simulated heads in the Upper Aquifer, Lower Aquifers, Grande Ronde basalt aquifer, and bedrock aquifer. The bedrock aquifer heads represent an average of the heads in the pre-Latah Sands (where present), weathered bedrock, and unweathered bedrock. Also posted are color-coded dots showing the observed groundwater levels in wells. Differences between the color inside and that surrounding the dots indicate a deviation from the observations. A visual comparison of the observed and simulated values shows that reasonably good matches were achieved. A good match was also achieved across the model with the regional groundwater flow patterns (discussed in Section 3.1.2).

Scatterplots comparing the static water levels to the simulated steady-state heads are shown in Figure 9.32 for each of the aquifers. Ideally, all data points should fall on the 1:1 line shown on the plot and clustered around or clustered within a reasonable error interval. As can be seen, the model tends to underpredict groundwater levels in the Upper and Lower Aquifers and overpredict levels in the bedrock aquifer. The simulated values in the Grande Ronde Basalt aquifer are better distributed.

Figure 9.33 through Figure 9.36 show the spatial distribution and relative magnitude of the residuals within each aquifer. The red dots indicate areas where the simulated heads are high relative to the observed values. The distribution of the residuals generally does not appear to be biased high or low in any specific area although there are two clusters of low values in the residuals for the basalt aquifer east of Deer Park and southeast of Chattaroy and a cluster of high values in the bedrock aquifer north of Colbert.

A quantitative analysis of the quality of the calibration was conducted using the statistics in Eq. 9.3 through Eq. 9.5. Statistics were compiled for each of the major aquifers and for all 2658 aquifer measurements, as shown in Table 9.3. A negative Mean Error (ME) for the overall results indicates that simulated values are generally higher than the observed values by 7.52 ft. The Mean Absolute Error and the Root Mean Squared Error (RMSE) provide a good estimate of the average magnitude of the difference and variance between observed and simulated values. The groundwater submodel had a MAE of 37.8 ft and a RMSE of 56.4 ft.

Generally accepted guidelines indicate that the model is well calibrated when the RMSE is less than 10% of the range of water levels (Spitz and Moreno, 1996). The model RMSE expressed as a percentage of the range in water level observation data was 3.86%, which is less than this calibration guideline. It should also be noted that the observations have data quality concerns (discussed in Section 3.1.2) that add a degree of intrinsic error to the observation data; a perfect calibration to these data is therefore unattainable.

Observed and simulated groundwater levels were compared at the nine locations with continuous measurements as well as at monitors with shorter term records. Offsets in the average observed and simulated values varied in magnitude between wells. The shifts are noted but the focus of the transient calibration was on replicating the timing and the magnitude of the water level fluctuations. Hydrographs for wells in each of the four major aquifers are presented in Figure 9.38 through Figure 9.40. Figure 9.38 shows groundwater levels at the DOE-Chattaroy monitor, completed in the bedrock. While the magnitude and timing of the annual fluctuations are comparable, there is a noticeable rising trend in the simulated values (starting in WY2003 and stabilizing by WY2013) that indicates the model may still be responding to initial conditions.

Figure 9.38 shows simulated and observed groundwater levels at the Deer Park Monitor, completed in the Grand Ronde basalt. The model simulates the timing of the annual changes but the more drawn-out response in the wells to seasonal pumping indicates that the storage properties assigned to the aquifer, while already very low, are likely too high. Conversely, the hydrograph for the Whitworth Water–Shady Slope well in the Lower Aquifers (and immediately adjacent to Whitworth

Pumping Well 8) shows a more muted response to pumping indicating that, locally, the hydraulic conductivity of the aquifer is too high. The borehole log for the well noted the presence of some clay stringers and lenses and some fine-sands in the profile. The degree of connection between the Shady Slope well and the Lower Aquifers in which the municipal wells are completed is unclear from the available borehole data.

Figure 9.40 shows the hydrograph for the Water District 3 – River Estates well screened in the Upper Aquifer and located close to the main branch of the Little Spokane River north of Chattaroy. The model matched the magnitude of the sharp increases in water levels that occur in the spring followed by a slow decline through the summer. The recovery in the fall was too rapid compared to observed and indicates that soil water depletion by ET may be underestimated.

The results of the comparisons to transient data highlight that there is room for continued local improvement to the model calibration. A key goal of this study was to build the integrated model and obtain reasonable parameter values that could be applied consistently across the study area. It is felt that reasonable average values were obtained in the regional calibration. This approach was not intended to deprecate the role of heterogeneity in the local response of the wells. Rather, the model is intended to serve as a framework for local studies in which the knowledge of the geology will be improved and where variable model parameters will be assigned based on the results of local aquifer testing and matching to observed response. The scenarios described in Section 10 illustrate that the model is useful for analyzing watershed and subwatershed response. Further local-scale calibration using additional observation data should be conducted before applying the model to local-scale investigations (e.g., predicting drawdowns in wells or well interference).

## 9.2 GSFLOW Outputs

GSFLOW model outputs include daily streamflow and groundwater heads. The PRMS submodel also provides daily values for all components of the water budget including precipitation, interception, snowmelt, evapotranspiration, overland runoff, infiltration, and groundwater recharge. The daily outputs are best visualized with hydrographs or animated maps, the latter cannot be provided in printed reports, unfortunately. The GSFLOW code contains routines to sum many of the daily values over the basin. Earthfx added additional components to the output and aggregated other flow components so that local (cell-based) and subcatchment-based water balances can be readily produced.

Additional groundwater submodel outputs include the flows across constant head boundaries; groundwater recharge and groundwater ET; lateral and vertical flows between each cell; well discharge; groundwater discharge to streams and lakes; and groundwater discharge to the soil zone (also referred to as surface leakage). The VL-GSFLOW post-processor takes daily values and aggregates them over time to provide monthly, seasonal, and annual water budgets. Values can also be aggregated spatially to provide water budgets at the subwatershed scale and for particular areas of interest.

As an example, Figure 9.41 shows the cell-based average daily precipitation for the long-term simulation averaged over each gaged catchment. As another example, Figure 9.42 presents the average March simulated heads in the bedrock and simulated streamflow (in cfs). Groundwater levels and streamflow are at or near their highs for the year. Figure 9.43 shows the average August simulated heads and streamflow which are at or near their lows for the year. Many of the lower-order streams have negligible flow and do not show on the figure.

### 9.3 Water Budget Assessment

After final calibration, the PRMS submodel was run from WY2003 through WY2017 to quantify components of the long-term average water budget under current (baseline) conditions. PRISM climate data was used as input for this period.

Model results were saved for each MODFLOW and PRMS cell on a daily basis. The VL-GSFLOW post-processor was used to aggregate these outputs at different time scales and for each subwatershed. Net precipitation over the model area, presented in Figure 9.44, was calculated as the average of the daily values for each PRMS model cell over the study period. Values range from 16.9 in/yr at the southern end of the LSR Valley to 43.9 in/yr around Mt. Spokane. The blockiness of the results is due to the 3 mile by 2 mile grid resolution of the PRISM data

Average annual evaporation from interception storage in the canopy is shown in Figure 9.45. The interception term includes sublimation from snow intercepted by vegetation. The results are strongly influenced by land cover type (Figure 2.8), vegetative cover density (Figure 7.11 and Figure 7.12), interception storage (Figure 7.13 to Figure 7.15), as well as the distribution of precipitation. Values range from 0.0 for open water to 7.1 in/yr over forested land in the Mt. Spokane area; the average over the basin is 3.3 in/yr.

Figure 9.46 shows the average annual Hortonian runoff from impervious surfaces. The results are strongly linked to the distribution of impervious land cover (Figure 7.18). The maximum values occur within the cities of Newport and Deer Park and in north Spokane. Total Hortonian runoff, shown in Figure 9.47, includes runoff from impervious areas and infiltration-excess runoff from pervious area as computed using the SCS curve number (CN) method. Values range from 0.0 to 26.4 in/yr. It should be noted that the values shown are for runoff generated within the cell and does not include run-on from saturated-excess runoff from upslope cells.

The PRMS code does not output the Dunnian flow generated in each cell, although the Dunnian flow contributions to streams and lakes are saved. Dunnian flow is also a component of several other output terms. For example, Figure 9.48 shows the average annual upslope Dunnian runoff entering each cell from cells higher up on the cascade flow path. A log-scale is used for the color ramp to highlight results. Upslope Dunnian flow is added directly to the capillary reservoir and is not partitioned (whereas upslope Hortonian is partitioned the same way as snowmelt and net precipitation on the cell). In PRMS-only simulations, Dunnian flow is mainly generated in areas where upslope interflow and Dunnian flow exceed the storage capacity of the gravity reservoir. In GSFLOW simulations, Dunnian flow can also be generated where significant groundwater discharge to the soil zone occurs, such as in areas of shallow water table. The figure shows that Dunnian flow occurs mainly in low-lying areas that generally correspond to the location of intermittent stream segments that were not simulated with SFR2.

Similarly, Figure 9.49 shows average annual upslope interflow entering each cell from cells higher up on the cascade flow path. Interflow occurs over the entire study area and is influenced by the slow interflow coefficient. As was noted in Section 7.5.3, lower rates were assigned to well-draining soils and higher rates to poorly-draining soils. Upslope interflow is also added directly to the capillary reservoir and is not partitioned. High interflows are generated in areas of shallow water table because groundwater discharge cannot remove water from the gravity reservoir.

Figure 9.50 shows the average annual generated runoff, obtained by subtracting the cascading flow entering the cell from the cascading flow exiting. A log-scale is used for the color ramp to highlight results. Cascading flow defines the average volume of water moving along the cascade flow path at a given location and includes interflow, Hortonian runoff, and Dunnian runoff.

Snowmelt, net precipitation and upslope Hortonian run-on are partitioned into Hortonian runoff and infiltration. Figure 9.51 shows the simulated average annual infiltration for the study area. This

water enters the capillary reservoir and is subject to ET. The ET demand is based on the distribution of PET, shown in Figure 9.52, which was computed on a daily basis from temperature and solar radiation (corrected for slope aspect). Annual PET values range from 34.6 to 40.2 in/yr and average 37.4 in/yr over the basin. The ET demand is equal to the PET minus any evaporation from the canopy and sublimation from the snowpack and snow stored in the canopy.

The distribution of total actual evapotranspiration (AET) is presented on Figure 9.53. This includes interception and sublimation but not lake evaporation or losses from impervious areas. The distribution of actual ET from the soil zone is presented on Figure 9.54. Total ET values averaged about 16.5 in/yr over the basin which is lower than determined in the simplified flow analysis (Section 4.2.2) and may be a contributor to the overestimation of low flows at the Dartford gage. Further refinement of soil zone properties, by increasing the active soil zone depth (to store more water through the summer) and/or lowering CN values to allow more infiltration, may improve results.

AET from the soil zone is often rate limited by the amount of water available. It can exceed infiltration where upslope Dunnian runoff, upslope interflow, and groundwater discharge to the soil zone occur. Model results predict AET rates vary between 1.8 to 59.3 in/yr (averaging 11.8 in/yr) over the study area. [The exceedance of PET was noted in a few cells where the water-table was close to surface. The exceedances were close in value to the groundwater ET rate which is supposed to be limited to the residual PET demand. There could be an accounting error in the way AET is calculated in these areas or an error in the PET demand transferred. Further investigation is warranted, but as noted, the number of cells affected was small and the impact on the overall water budget for the study area and subwatersheds is not significant]. The soil AET distribution is affected by runoff patterns where areas at the downstream end of the cascade network have more run-on and infiltration, and therefore, more soil water available for ET compared to uplands.

Figure 9.55 shows average annual net groundwater recharge for the study area, which is affected by all the factors noted previously. A log-scale is used for the color ramp to highlight results. The value is calculated as the groundwater recharge sent by PRMS to the groundwater model minus groundwater discharge back from MODFLOW. Generally, groundwater recharge is higher in the uplands due to increased rainfall and lower PET. Within the lowland basin, higher rates occur in areas of more permeable surficial soils. Localized patterns within the lowland basin can also be seen where the ridges separating subbasins have lower recharge whereas cells further down the cascade network have higher rates. Negative net recharge rates (white areas) occur where groundwater discharge exceeds the recharge rates calculated by PRMS. A few cells representing swales at the end of long cascade flow paths had extremely high recharge rates (> 120 in/yr). As discussed earlier, the swales can be eliminated by manually adjusting topography to convey the water to nearby streams. A better approach would be to use improved topographic mapping. LIDAR data are available for parts of the basin and would need to be processed, but were not used in this study.

### 9.3.1 GSFLOW Water Budgets

Daily values for components of the groundwater budget, output by the MODFLOW submodel, were aggregated over the study area to produce simulation period, annual, monthly, and average monthly water budgets. Major water budget components for the groundwater system include net recharge, surface leakage (i.e., groundwater discharge to the soil zone), groundwater discharge to lakes and streams, boundary flows, and pumping.

A balance for the simulation period is presented in Table 9.4. The first year of the simulation was not used in this or the other analyses presented in this section because these results may be affected by model start-up.

Inflows to the subwatershed area are dominated by recharge, which makes up more than 34% of the water entering the area. Within the model area, water moves in and out of the storage reservoir and should balance over the long term, but there is an excess of water “coming out” of groundwater and

going into storage in this simulation period. There is also a significant amount of stream flow loss recharging the aquifer but this is balanced by the combination of water discharging directly to the stream channel and discharge to the soil zone mainly in riparian areas. Figure 9.56 shows areas where streamflow is lost to the aquifer (in red) and areas where the aquifer discharges to streams (in blue) based on the long-term simulation. Most of the main tributaries are gaining reaches but losing reaches are widely distributed among the many smaller tributaries. Figure 9.57 shows areas where groundwater discharge to the soil zone (surface leakage) occurs, mainly along the stream reaches in the lowlands and where intermittent streams are mapped in the uplands. Not all the surface leakage makes it into streams, however. Some of the water entering the cascade network may re-infiltrate and be lost to ET, interflow or groundwater recharge. Together, streamflow out and surface leakage account for more than half (60.3%) of the outflow from the watershed.

The remainder of the inflows (approximately 1.9%) are composed of lakebed losses (0.3%) to the groundwater system and inflows at the constant head boundaries (1.6%). Remaining outflows (8.5%) occur at the lakes (2.0%) which are mostly areas of groundwater discharge, wells (1.4%), outflow at constant head boundaries (0.9%), and groundwater ET (4.2%). It should be noted that although the water budget closes within 1.5%, there is some double counting of flows, because water discharging to the stream can re-infiltrate downstream and get counted again as inflow.

An annual groundwater budget for the LSR watershed is shown in Figure 9.58. The graph shows how inflows and outflows are affected by wet and dry years. The key changes are the volumes of water “going into” storage (light green) as heads rise in response to increased recharge in wet years and the volumes coming out of storage (and “going into” the aquifer) the heads drop in dry years. Streamflow and surface leakage volumes are reduced in dry years. The other components change as well, but do not significantly contribute to the water budget.

The daily flows were averaged to create an average monthly water budget (Figure 9.59) that illustrates seasonal trends in the water balance. Water goes into storage during the winter and early spring and comes out of storage during the drier summer months. The rate of recharge also decreases significantly in the late spring and summer as do groundwater discharge to the soil zone and to streams.

A more complete budget can be obtained from the daily GSFLOW basin-wide summary, which outputs a set of 62 budget terms. Select values were aggregated over the study area to produce simulation period, annual, monthly, and average monthly water budgets. The budget includes many of the groundwater components but also includes key hydrologic components including evaporation and ET terms; Hortonian and Dunnian runoff; and interflow. The average values for the simulation period (WY2004 to WY2017) are provided in Table 9.5. Figure 9.60 shows the annual average budget with precipitation plotted on the right y-axis and 17 other items plotted on the left y-axis. Only the last six years are shown for clarity while the average is for the whole period. One key item to note in the graph is that, although groundwater recharge in and groundwater discharge out balance over the long term, there are significant differences on a year-by-year basis.

Some more useful analyses can be obtained from these basin wide summaries. For example, Figure 9.61 shows a water budget for the area streams showing the variability in the components contributing to streamflow. Figure 9.62 shows an annual budget for the components contributing flow to study area lakes. Similar water budgets can be done on a subwatershed basis or for individual lakes and streams of interest.

## 9.4 Limitations

As with all models, it must be recognized that there are inherent simplifications in the model conceptualization of distributed hydrologic and hydrogeologic processes and in the simplified assignment of parameters. There are also limitations and uncertainty in the input and calibration

target data and potential for erroneous data or inputs to affect results. Accordingly, it is unlikely to achieve a perfect and/or unique integrated groundwater/surface water model.

With regards to the intrinsic uncertainty in the input data, the data used to describe the geologic, hydrogeologic, and hydrologic setting of the study area is presented in Sections 2 through 5. Data from a wide variety of sources, including climate records, streamflow measurements, static and transient groundwater levels, geologic logs, and pumping data were collected, reviewed, and synthesized. In general, the data coverage for the study area is quite high, however some limitations were noted in the soils mapping, topographic mapping, and the number of transient groundwater monitors. It should be recognized that the area went through an extremely complex depositional history with basalt flows, catastrophic flooding, submersion under glacial lakes, and glaciation. Previous studies have helped to interpret the geologic data but geologic mapping is subject to uncertainty in areas of poor borehole coverage.

There are a good number of stream gages with current or historic data. Lake stage is monitored at Eloika Lake; however, monitoring of stage in other lakes and the larger wetlands would be of benefit. The climate data coverage has improved over the last 10 years but is sparse in the preceding period. Good estimates of water use were obtained from the Spokane County. Despite these considerations, it is acknowledged that there is always a degree of uncertainty with regards to hydrogeologic properties and model assumptions needed to extrapolate available data.

There are nine locations with continuous record and many of these are in the vicinity of well fields. This is a large study area and the density of transient data is considered to be very sparse. Observation points are needed in the vicinity of the wellfields, because their response to changes in pumping provides direct information on local hydraulic conductivity values and storage properties. A sufficiently long period with a number of events (e.g., well shutdown or change in pumping rate) to analyze the data for calibration purposes is ideal. Continuous data are also needed in many more areas, away from the wellfields, to better understand the natural shallow aquifer response to recharge events. Long-term record is needed to understand seasonal response in dry and wet years. More observation points will also aid in applying automated calibration techniques.

With regards to uncertainty due to inherent simplifications in the model conceptualization of distributed hydrologic and hydrogeologic processes, the LSR model represented a refinement of the hydrologic, geologic, and hydrogeologic setting compared to the Golder (2004) study and incorporates new information and insights gained since that time. In particular, it was important to create a contiguous coverage of the area, subdivide the hydrostratigraphic units, incorporate the weathered and unweathered bedrock, represent lakes and wetlands, and simulate the system on a daily rather than weekly time frame. We also built on the work by Kahle *et al.* (2013) and created continuous 3-D hydrostratigraphic surfaces across the study area.

The integrated modelling approach applies a physically-based approach to quantifying groundwater recharge and groundwater/surface water interaction rather than using simplifying assumptions and an automated calibration approach to estimate these components of the groundwater flow system. By integrating the PRMS and MODFLOW submodels in GSFLOW, feedback mechanisms between the groundwater and surface water systems are better represented. The reasonableness of submodel outputs (e.g., groundwater recharge values from the hydrologic submodel and groundwater discharge to the soil zone from the groundwater submodel) and the overall water budget were tested much more rigorously than possible with separate, non-integrated models. Although no model can perfectly match the observed behaviour due to inherent simplifications and incomplete information, it is felt that the model results are reasonable, physically-based, and scientifically sound.

With regards to the uncertainty related to the model calibration, the results obtained with the PRMS-submodel appear reasonable and the observed streamflow was matched reasonably well. The GSFLOW model was calibrated to a wide range of conditions, including wet and dry-year conditions,

and validated over extended simulation periods to increase the degree of confidence in model results. Improvements can always be made, however, through additional data collection and refinement of model parameters.

The results of the groundwater model calibration yielded a reasonably good match to the static groundwater levels and groundwater flow patterns. The integrated model and obtain reasonable parameter values that could be applied consistently across the study area. The calibration to transient data highlighted that, although reasonable parameter values were obtained that could be applied consistently across the study area, there is still room for continued local improvement to the model calibration. It is hoped that this model will serve as a framework for local studies in which the knowledge of the geology will be improved and where variable model parameters will be assigned based on the results of local aquifer testing and matching to observed response.

The scenarios described in Section 10 illustrated that the model is useful for analyzing watershed and subwatershed response. Further local-scale calibration using additional observation data should be conducted before applying the model to local-scale investigations (e.g., predicting drawdowns in wells or well interference).

A number of areas were highlighted for further investigation that should lead to improved matches to the observations, including possible interaction with the SVRP aquifer, refinements to the method for representing discharge from Eloika Lake, further investigation of soil parameters and PET rates, improvements in soil mapping and assignment of soil properties, improvements in the topographic mapping, and improvements in the assigned locations and elevations to wells, improvements in measuring stream discharge under ice conditions, and improvements in simulating decreases in groundwater discharge to streams and riparian areas under winter conditions.

With respect to quality assurance/quality control in developing the models, it is recognized that building the conceptual and numerical models required a large amount of data analysis and preparation. Care was exercised in setting up, documenting, and conducting the model calibration and subsequent scenario analyses. Automated processing was done using pre- and post-processors, where possible, to eliminate the potential for human error. Internal reviews were conducted to ensure that the input data preparation programs produced correct input files. All model outputs were saved and reviewed through visual inspection of hydrographs, digital mapping, and animation of results.

## 9.5 Tables

Table 9.1: Streamflow calibration statistics for the GSFLOW model.

Gauged Basin	Daily		Monthly		
	Nash-Sutcliffe	Log Nash-Sutcliffe	Nash-Sutcliffe	Log Nash-Sutcliffe	Volumetric Efficiency
Calibration Period (October 1983 – September 1986)					
Elk	-3.69	-1.40	-3.27	-1.62	0.538
TMDL-23	0.475	0.149	0.460	0.131	0.309
Dragoon Creek	0.377	0.571	0.471	0.646	0.565
Deadman Creek	0.352	0.624	0.477	0.648	0.528
LSR at Dartford	0.597	0.636	0.648	0.650	0.675
Validation Period (October 2002 – September 2008)					
TMDL-1	-4.45	-1.22	-4.04	-1.39	0.713
TMDL-23	0.530	0.488	0.252	0.339	0.340
TMDL-2	0.576	0.650	0.688	0.689	0.709
Dragoon Creek	0.368	0.479	0.592	0.623	0.650
DR9	0.298	-0.148	0.432	0.059	0.624
Deadman Creek	-0.094	-0.035	0.260	0.099	0.419
LSR at Dartford	0.449	0.657	0.571	0.668	0.683
Baseline Period (October 2002 – September 2017)					
Dragoon Creek	0.101	0.482	0.435	0.636	0.586
Deadman Creek	0.231	0.317	0.448	0.399	0.481
LSR at Dartford	0.524	0.578	0.608	0.585	0.636

Table 9.2: Summary of spot flow measurements and average simulated flow.

Name	Description	No. of Observations	Average Flow (cfs)	Simulated Average Flow (cfs)
12429500		45	72	
Beaver Creek	at Horseshoe Lake Rd	36	1.81	5.14
Buck Creek	at Horseshoe Lake Rd	36	6.31	15.6
Chattaroy	Little Spokane River	76	124	185
Deadman Creek 1	at N. Holcomb Rd.	21	14.2	29.5
Deadman Creek 2	at Heglar Rd.	20	10.4	36.9
Deer Creek	near mouth at N. River Terrace Rd.	12	16.8	3.90
DR1	Dragoon Creek	25	5.46	7.89
DR2	Dragoon Creek	25	18.6	19.2
DR9	Dragoon Creek Mouth	35	31.5	60.2
DRT3	Spring Creek	25	3.22	19.1*
DRT4	Beaver Creek	25	3.24	5.04
DRT5	West Branch Dragoon Creek	24	10.3	15.1
DRT6	Mud Creek	25	2.48	2.79
DRT7	Wethey Creek	25	2.55	4.11
DRT8	Huston Creek	25	1.38	1.2
LS5(LSPOK)	near N. LSR Dr. and N. Meadow View Dr.	12	357	270
LSRTMDL-1	at Scotia Rd.	12	39.3	37.0
LSRTMDL-2	at Bridge Crossing on E. Deer Park Milan Rd.	12	234	163
LSRTMDL-20	Upstream of Trout Lake	17	16.5	19.6
LSRTMDL-22	at Fan Lake Rd. Crossing	41	20.1	56.4
LSRTMDL-23	Outlet of Eloika Lake	27	80.5	67.8
LSRTMDL-3	at N# LSR Dr. near Shady Slope Rd	15	185	281
Ltl_Deep_1	at Black Rd.	14	1.51	4.24
Ltl_Deep_2	at Big Meadows Rd.	13	1.87	4.79
Ltl_Deep_3	at Big Meadows Rd	13	3.04	5.73
Ltl_Deep_4	at Dunn Rd	13	4.91	15.15
Ltl_Deep_5	near Yale Rd, downstream of RR overpass	13	4.92	9.04
Otter Creek 1	at Fertile Valley Rd	34	1.20	2.61
Otter Creek 2	at Grange Hall	34	0.969	3.24
Otter Creek 3	at Allen Rd.	34	0.808	2.74
Peone Creek	at Peone Rd	12	0.464	3.15
Peone_Ck_2_trb	at Moffat Rd.	12	0.367	1.45
Unnamed Creek 1	At N. Day Mt Spokane Rd	50	0.179	0.008
Unnamed Creek 2	at Day Mt. Spokane Rd.	37	0.076	0.18
Unnamed Creek 3	at Forker Rd	21	1.08	2.97
West Branch LSR	at crossing with Highway 2	28	34.0	68.7
West Branch LSR	Horseshoe Lake Outlet	30	13.8	48.5

Table 9.3: Calibration statistics for the groundwater submodel.

Aquifer Unit	Number of Wells (n)	Mean Error (m)	Mean Absolute Error (m)	Root Mean Squared Error (m)	Range in Observations (ft)	RMSE as Percent of Range (%)
Upper Aquifer	193	50.6	54.0	72.3	960	7.53
Lower Aquifer	71	55.1	57.4	71.7	827	8.67
Grand Ronde Basalt	975	-2.06	26.6	36.51	624	5.85
Bedrock Aquifer	1419	-22.3	42.3	63.9	1701	3.75
<b>All Wells</b>	<b>2658</b>	<b>-7.52</b>	<b>37.8</b>	<b>56.4</b>	<b>1463</b>	<b>3.86</b>

Table 9.4: Groundwater budget for the Little Spokane River watershed, as simulated by the MODFLOW submodel, for WY2004 to WY2017.

Groundwater Budget Component	Inflows (in)	Inflows (cfs)	% of Total Inflows
Inflow from Storage	8.48	429	27.1
Recharge	10.63	538	34.0
Constant Head Inflow	0.50	25	1.6
Stream Leakage In	11.57	586	37.0
Lake Leakage In	0.10	5	0.3
Total Inflows	31.3	1583	100%
Groundwater Budget Component	Outflows (in)	Outflows (in)	% of Total Outflows
Outflow to Storage	9.89	-501	31.2
GW ET	1.33	-67	4.2
Constant Head Outflow	0.30	-15	0.9
Surface Leakage	10.7	-540	33.6
Stream Leakage Out	8.47	-429	26.7
Lake Leakage Out	0.65	-33	2.0
Well Pumping	0.44	-22	1.4
Total Outflows	31.7	1607	100%

Table 9.5: Groundwater budget for the Little Spokane River watershed, as simulated by GSFLOW, for WY2004 to WY2017.

<b>GSFLOW Budget Component</b>	<b>Inflows (in)</b>	<b>Inflows (cfs)</b>	<b>% of Precip- itation</b>
Precipitation	25.818	1306.8	
Evaporation from interception	3.533	178.8	13.7
ET from pervious	10.706	541.9	41.5
Evaporation from impervious	0.070	3.5	0.3
Groundwater ET	1.339	67.8	5.2
Groundwater recharge	10.618	537.4	41.1
Groundwater discharge to soil zone	10.677	540.4	41.4
Groundwater boundary outflow	0.269	13.6	1.0
Groundwater pumping	0.447	22.6	1.7
Groundwater discharge to streams	8.468	428.6	32.8
Groundwater discharge to lakes	0.659	33.4	2.6
Hortonian runoff to streams	0.328	16.6	1.3
Dunnian runoff to streams	8.145	412.3	31.5
Interflow to streams	2.006	101.6	7.8
Stream leakage to groundwater	11.558	585.0	44.8
Lake precipitation	0.216	10.9	0.8
Lake evaporation	0.310	15.7	1.2
Hortonian runoff to lakes	0.015	0.7	0.1
Interflow/Dunnian runoff to lakes	0.179	9.0	0.7
Lake leakage to groundwater	0.073	3.7	0.3
Streamflow out	8.057	407.8	31.2

## 10 Model Scenarios

### 10.1 *Introduction*

Once the GSFLOW integrated groundwater/surface water model was calibrated and validated to an acceptable level, a set of model scenarios were developed in consultation with Spokane County and the stakeholder Technical Advisory Committee to test the model. The scenarios considered included simulating the effect of:

- 1) increased permit-exempt self-supply water use
- 2) water rights retirement,
- 3) aquifer recharge projects, and
- 4) future climate change.

Inputs for the future climate change scenarios were provided by WEST. Parameters for the other scenarios were provided by Spokane County.

The effect of the simulated changes can be relatively small when analyzing streamflow and heads at the watershed scale. The best method for visualizing results was by conducting comparative (“with” and “without”) analyses against the previously described long-term (WY2003-WY2017) simulation. In this way, the changes in streamflow and groundwater levels under the future conditions could be determined. For example, changes in groundwater levels with increased domestic use were highlighted by subtracting simulated heads with increased pumping from the baseline heads at every cell in the model. This yielded maps of drawdowns in each aquifer. Similarly, changes in streamflow could be highlighted by subtracting hydrographs of streamflow under future conditions from the baseline hydrographs.

A consistent approach was followed for each of the scenarios to enable these analyses. The configurations of the model layers and streamflow network were kept constant throughout the duration of the transient assessment. In the first three scenarios, changes were only made to groundwater and surface water withdrawals. Most significantly, the WY2003 through WY2017 daily climate information used in the baseline simulation was used as a consistent input climate data set for the first three future conditions scenarios. This was done because (1) the future climate is unknown; (2) the WY2003 through WY2017 period includes representative wet, dry and average climate years; and (3) a consistent transient climate input facilitated the direct comparison of the effects of water use changes and aquifer recharge projects on the surface water and groundwater systems. With this approach, hydrographs of simulated responses at a gage or monitoring well for the three scenarios could be directly compared to determine the incremental effects of the future changes.

The fourth scenario, simulating future climate change, deviated from this approach. However, the “change field” method employed (discussed further on) modified the magnitude of the temperature and precipitation values in the data set but did not change the timing of the events. In this way, it was still possible to do meaningful direct comparisons of model response under baseline and future climate conditions.

Each transient GSFLOW simulation generated a complete water budget for every cell in the model for every simulation day. A comprehensive analysis on the outputs from each of the scenarios was performed. Specific details for each scenario and results are discussed in the following sections.

## 10.2 Increased Domestic Water Use

This first scenario analyzed the incremental changes to the LSR watershed due to the increase in the permit exempt wells (single-family domestic supply) projected to occur over the next twenty years. Spokane County staff used their Water Demand Model to predict where the demand would occur and aggregated these values to the model cells. The increase in demand was estimated to be on the order of 2,200 acre-feet total annual use, with the highest use during the summer months. A breakdown of monthly withdrawals is provided in Table 10.1. All other groundwater withdrawals and surface water diversions simulated in the baseline run, as presented in Table 8.1 and Table 8.2 were not changed. It should be noted that while return flows were provided for self-supplied water use, all withdrawals were assumed to be 100% consumptive in the simulations.

Table 10.1: Summary of monthly average simulated groundwater pumping.

Month	Self-Supplied Groundwater Pumping		
	Baseline (acre-ft)	Future (acre-ft)	Difference (acre-ft)
January	158.4	208.6	50.12
February	143.1	188.4	45.27
March	158.4	208.6	50.12
April	153.3	201.8	48.50
May	774.2	1021	247.2
June	962.5	1270	307.7
July	1323	1747	423.6
August	1324	1748	423.9
September	923.4	1219	295.2
October	613.2	808.6	195.5
November	153.3	201.8	48.50
December	158.4	208.6	50.12
<b>Annual Total</b>	<b>6,846</b>	<b>9,031</b>	<b>2,186</b>

The distribution of groundwater withdrawals and surface water diversions under baseline conditions were presented in Figure 8.9, and consist of 7,480 cells containing wells. Groundwater withdrawals were represented in the MODFLOW submodel using the WEL7 module in MODFLOW-NWT. Figure 10.2 shows the locations of all cells with future increases in self-supply domestic pumping. The dots are color-coded to show the relative magnitude of the changes. Large changes (between 2000 and 3000 GPD) can be seen in the southeast corner of the Deadman Creek subwatershed and the northwestern part of the Dragoon Creek subwatershed.

Figure 10.3 shows the simulated decrease in long-term average heads within the Upper Aquifer, where present, as a result of the increased domestic self-supply withdrawals. The patterns are difficult to interpret in the Upper and Lower Aquifers and the Grand Ronde Basalt aquifer due to the discontinuous nature of these units. Figure 10.4 shows the decrease in heads (drawdowns) in the bedrock aquifer. The distribution of the drawdowns corresponds to the locations of the increased withdrawals. In general, the drawdowns are less than 2 ft, although there are some areas in the Deadman Creek subwatershed with simulated drawdowns of 10 ft.

Figure 10.5 shows the simulated streamflow at the Dartford gage with the baseline (in blue) and the increased domestic use scenario (in red) for WY2008 to WY2013, a period with a number of dry

years and wet years. The shorter period is shown so that the traces can be enlarged. The upper part of the scale is also cut off. Even so, it is hard to discern the subtle differences in flows. Included on the plot is a trace showing the difference in simulated flow. Most of the changes are negative, indicating that flows have decreased. There are a number of days where flow has increased, often dramatically, mostly under high rainfall/snowmelt conditions. These changes may be due to the non-linear behavior in the model when water levels drop below layer bottoms (i.e., when layers go dry).

Hydrographs are presented for Deadman Creek and Dragoon Creek gages in Figure 10.6 and Figure 10.7, respectively. Similar patterns are seen with more consistent decreases in streamflow in Dragoon Creek.

### 10.3 Water Rights Retirement

This second scenario analyzed the incremental changes to the LSR watershed due to the retirement of selected agricultural water rights. Spokane County provided the location and quantity of four water rights for analysis purposes. The four water rights were all groundwater withdrawals within the Dragoon Creek subwatershed with the monthly withdrawals in acre-feet as listed in Table 10.2. For the retirement scenario, the withdrawals associated with the four water rights were removed from the well input file while all other groundwater withdrawals and surface water diversions were held the same as the baseline conditions. Groundwater levels and streamflow were analyzed to assess the benefits of retiring these water rights.

Table 10.2: Retired Water Rights for Scenario 2.

Month	Water Right 1 (af)	Water Right 2 (af)	Water Right 3 (af)	Water Right 4 (af)	Monthly Total (af)
May	30.6	6.26	3.13	13.6	53.63
June	95.7	19.5	9.79	42.5	167.57
July	147	30.0	15.04	65.4	257.44
August	118	24.0	12.04	52.3	206.13
September	72.0	14.71	7.37	32.0	126.11
October	4.14	0.85	0.42	1.84	7.25
<b>Annual Total (af)</b>	<b>467</b>	<b>95.4</b>	<b>47.8</b>	<b>208</b>	<b>818.14</b>

Figure 10.8 shows the simulated increase in long-term average heads (recovery) within the Upper Aquifer, where present, as a result of retiring the four water rights. The figure is focussed on the Dragoon Creek subwatershed. The greatest recovery is in the northwest part of the watershed where simulated levels rise over 8.6 ft. The patterns of water level change are difficult to interpret in the Lower Aquifers and the Grand Ronde Basalt aquifer due to the discontinuous nature of these units. Figure 10.9 shows the recovery in the bedrock aquifer, where simulated levels rise 9.3 ft in the southeast and 3.5 ft in the northwest.

Figure 10.5 shows the simulated streamflow at the Dartford gage with the baseline (in blue) and the increased domestic use scenario (in red) for WY2008 to WY2013. As in Scenario 1, the shorter period is shown so that the traces can be enlarged. The upper part of the scale is also cut off. Included on the plot is a trace showing the difference in the simulated flows. Most of the changes are positive, indicating that flows have increased slightly relative to baseline. There are a number of days where flow has decreased. These changes may be due to the non-linear behavior in the model when water levels drop below layer bottoms.

Hydrographs are presented for the Dragoon Creek gage in Figure 10.11. Figure 10.12 shows simulated flows at Dragoon Creek and Highway 395 below Deer Park, south of the largest retired

water right. The hydrographs show a consistent increase in simulated flows with the retired rights. Of note is the higher flows in March (or earlier, in some years), indicating that the benefit is not restricted just to the months without pumping.

#### **10.4 Aquifer Recharge Projects**

This third scenario analyzed the incremental changes to the LSR watershed due to managed aquifer recharge projects intended to enhance summer/fall streamflow. The projects analyzed were envisioned to include subsurface infiltration galleries or surface infiltration basins, with a goal of infiltrating about 2 acre-ft/day during the spring months. Water for the recharge projects would come from diverting seasonally-high spring streamflow.

Spokane County provided 10 test locations with streamflow diversion rates based on the analysis of 2015 spotflow observations. Infiltration sites were picked based on the presence of relatively flat topography near streams in areas of mid-range hydraulic conductivity. Diversions were set up in the SFR2 input data set and wells were set up in Layer 1 and assigned equivalent monthly injection rates to represent infiltration below the root zone.

Initial results showed that the infiltration caused groundwater levels to rise quickly, thereby preventing the full amount of the diverted water to be infiltrated. Earthfx developed a simple method for screening potential infiltration sites based on depth to water and the likely rise in water levels. A conservative depth to water was determined at each cell in the model by subtracting simulated baseline water levels on March 1, 2006 (a period of high groundwater levels) from land surface topography. This value was taken as the “available rise”. Next, the change in water level due to injecting 1 cfs for 30 days was calculated using a Theis approximation and the effective transmissivity of Layer 1 and the specific yield. Figure 10.13 shows the percentage of available rise left in each cell, where a high percentage is ideal. White areas are where heads were or would go above land surface.

Ten new test locations were selected close to the original ones but with injection locations in areas of high depth to water and a high percentage of available rise. Figure 10.14 shows the locations of the alternate stream diversion and artificial recharge infiltration sites. Figure 10.15 shows the simulated increase in long-term average heads (recovery) within the bedrock aquifer as a result of operating the ten aquifer recharge projects over the 14-year simulation period. The figure is focussed on the southern part of the study area where the sites are located. High increases in head occur at Site 2 (14.3 ft), Site 3 (16.5 ft), and Site 7 (15.8 ft). These are not indicators of more efficient recharge; rather, the higher levels are related to the injection rates and the local aquifer hydraulic conductivities.

Figure 10.16 shows the simulated streamflow at the Dartford gage with the baseline (in blue) and the recharge projects scenario (in red) for WY2008 to WY2013. As in Scenario 1, the shorter period is shown so that the traces can be enlarged. As can be seen from the trace showing the difference in the simulated flows, most of the changes are small but positive, indicating that flows have increased slightly relative to baseline. There are slight reductions in the February to May flows due to the diversions and a small number of days outside that period where flow has decreased.

Figure 10.17 presents hydrographs for Dartford Creek near Highway 395. The hydrographs show the decrease in flows due to the diversions for Site 3 in February through May and a small increase in flows during the summer through January. Figure 10.18 presents hydrographs for flow in Little Deep Creek near Highway 2. This figure also shows the decrease in flow due to the diversions in February through May. Consistently higher flows are observed from June to January due to the combined effects of recharge at Sites 5, 6, and 7, indicating that groundwater recharge at these sites is effective in increasing summer/fall flows.

## 10.5 Future Climate Change

An assessment of the effects of future global climate change on the surface water and groundwater flow system in the LSR watershed was conducted as part of this study. Climate predictions are done with General Circulation Models (GCMs) that simulate atmospheric and ocean circulation across the globe and the interaction with the land masses and sea ice. The models are built on large grids with cell sizes ranging from 150 to 250 miles. Results of long-term GCM simulations are presented in terms of annual, seasonal, and monthly change in climate variables such as temperature, precipitation, solar radiation, and wind speed. There are many GCM models, developed by different government and/or academic research groups in different countries.

Data from the GCM models must be downscaled for use in regional studies. As an example, the Climate Impact Group (CIG) at the University of Washington used downscaled climate models and hydrologic models to conclude that higher seasonal temperatures will increase fall rain events and decrease spring snowmelt events as freezing levels rise in mountainous areas and precipitation amounts increase slightly. The Climate Impact Group also host a website (<https://cig.uw.edu/resources/-analysis-tools/projections/>) where they provide estimates of air temperature and precipitation increases in the Pacific Northwest, West and East of the Cascades, for the 2050s and the 2080s. Figure 10.1 shows the predicted changes in air temperature and precipitation amounts for the various climate models for a range of emission scenarios from “very low” to “high” for fall 2050, for the part of Washington State east of the Cascades.

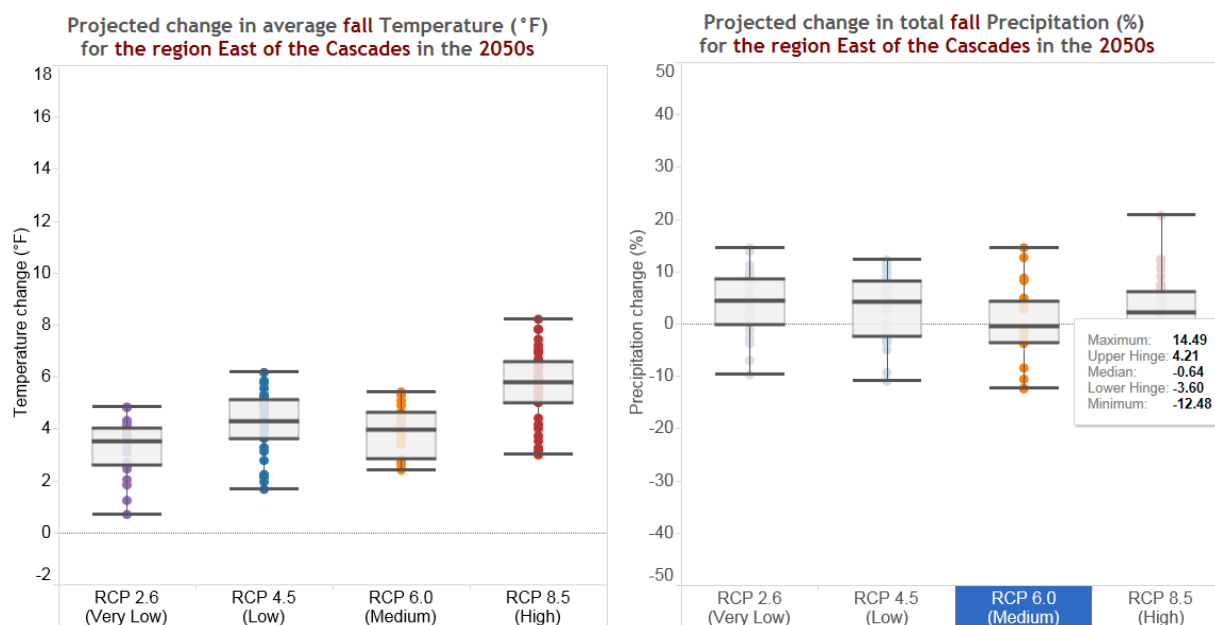


Figure 10.1: 2050 climate change predictions for the fall, east of the Cascades (from the CIG website)

To test the integrated groundwater/surface water model’s ability to simulate a climate change alternative and to determine the likely effects on streamflows and groundwater levels, information from the CIG website was extracted for the 2050s east of the Cascades. Estimates were selected for the “medium” (RCP 6.0) emissions for comparison to baseline conditions representing current climate. Other emission scenarios were also simulated to evaluate sensitivity. Table 10.3 shows the projected increases, by season, for air temperatures and precipitation, respectively. Negative values for precipitation change represent a percent decrease in precipitation.

Table 10.3: Projected 2050 temperature (°F) and precipitation increases (percentage) for RCP 6.0 east of the Cascades.

RCP 6.0	Temperature Increase			Precipitation Increase		
	Median	Low Range	High Range	Median	Low Range	High Range
Fall	3.93	2.82	4.63	-0.64	-3.6	4.21
Winter	3.80	3.05	4.535	5.84	1.06	8.52
Spring	3.94	2.53	4.87	5.89	3.34	13.51
Summer	4.83	3.28	5.25	-5.38	-7.71	-1.08

There are many methods for using the downscaled results in watershed models. The “change field” approach was selected for this study. The method entails calculating mean monthly or seasonal changes in future climate based on output from the downscaled GCM models and applying those changes to local daily climate observations. Accordingly, the shifts to temperature and the percent increases in precipitation for the median values presented in Table 10.3 were applied to the daily PRISM temperature and precipitation data sets for WY2003 to WY2017. This adjusted data set became the input for the WY2043 to WY2057 mean climate change scenario.

The partitioning of the PRISM precipitation data into rain and snow is dependent on temperature. Figure 10.19 compares the distribution of rain and snow as determined by the precipitation-form process submodel in PRMS. As can be seen, significant decreases in snowfall are predicted for the future climate conditions. Also shown is the general increase in winter and spring precipitation and decrease in summer and fall precipitation, as per Table 10.3.

Figure 10.20 compares the simulated average monthly snowpack depth (in inches) for the baseline and mean climate change conditions, and shows that the reduced snowfall and higher temperatures under future climate change lead to a thinner winter snowpack that is essentially gone in April rather than persisting until May. Similarly, snowmelt volumes, a key factor in spring groundwater recharge and streamflows, also decrease significantly. Figure 10.21 shows that the most significant percentage change in the snowpack thickness occurs in the central basin. However, the absolute change in January snowpack depth (up to 11.8 in) increases with elevation as shown in Figure 10.22. The increased temperature also increases the computed PET demand, up to 8 in/yr in the southern part of the study area.

Figure 10.24 shows the basin-wide average monthly groundwater recharge for the baseline and future climate scenarios. The increased precipitation in the winter months and earlier snowmelt increases groundwater recharge significantly in December and January over the baseline conditions. Groundwater recharge decreases during the critical growing months. Figure 10.25 shows the simulated long-term change in groundwater recharge (in/yr) within the study area under future climate conditions. In general, recharge is seen to increase (red shading) in the bedrock uplands, in the Diamond Lake area. Recharge decreases (blue shading) in the inter-stream areas within the central basin. While there is a slight increase in groundwater recharge on average (Figure 10.24), annual average simulated heads in the bedrock aquifer generally decreased within the study area, as shown in Figure 10.26, due to the decrease in summer recharge and increase in groundwater ET. The maximum head decrease was over 10 ft. The white areas in the figure show net increases in bedrock heads. An expected seasonal reversal in heads due to higher precipitation in early winter did not seem to occur.

The average annual basin-wide groundwater budget under future climate conditions is shown in Figure 10.27. Differences in the year-to-year flows (compared to those shown for the baseline climate conditions in Figure 9.58) are present but difficult to discern. An average monthly water budget under future climate conditions is presented in Figure 10.28. This figure can be compared to

Figure 9.59 for the baseline conditions and clearly shows the increased recharge in the winter months and sharp decrease in recharge in March and April. Decreases are also predicted for simulated summer outflows from the watershed.

Figure 10.29 shows the simulated streamflow at the Dartford gage with the baseline (in blue) and the mean future climate scenario (in red) for the simulation period. Figure 10.30 shows a portion of the hydrograph for WY2008 to WY2013 (and the equivalent WY2048-WY2053 future climate period) so that the traces can be enlarged. Also shown is a trace of the difference in the simulated flows (in green). The hydrographs show that there is a consistent increase in late fall to early spring flows and a consistent decrease in late spring to early fall flows under this scenario relative to baseline climate conditions.

Figure 10.31 presents the average daily flow (i.e. average of all Jan. 1's, Jan. 2's, etc. in the simulation). This tends to filter out the variability in the daily flows and shows seasonal trends better. These hydrographs show that flow in the winter months is generally higher relative to the baseline but flows decrease in the remainder of the year. The decrease in summer low flows of about 20 cfs at the Dartford gage would be of concern for water users in the watershed.

Additional analyses were run by WEST to show the sensitivity of model results to the range of climate change parameters. As an example, simulations were done with the low and high ranges for RCP 6.0. Values for the change in temperature and precipitation for these scenarios are provided in Table 10.3. It should be noted that the "low" range in precipitation has the largest decreases in fall winter and winter precipitation.

Figure 10.32 shows the simulated streamflow at the Dartford gage for the baseline, mean climate change, and high range climate change scenarios for WY2008 to WY2013 (and the equivalent WY2048-WY2053 future climate period). Streamflow for the high range scenario is consistently higher than the median change scenario. Similarly, Figure 10.33 shows the simulated streamflow at the Dartford gage for the baseline, mean climate change, and low range climate change scenarios for WY2008 to WY2013. Streamflow for the low range scenario is consistently lower than the median change. These results indicate that streamflow in the LSR is much more sensitive to the change in rates of precipitation than to change in temperature. Average daily streamflows in mid-August were about 1.4 cfs lower for the low range scenario than for the median change scenario. Other combinations of scenarios (e.g., a high range temperature and low range precipitation for RCP 6.0 or other emissions scenarios) can be run to bracket a broader range of possible future climate outcomes.

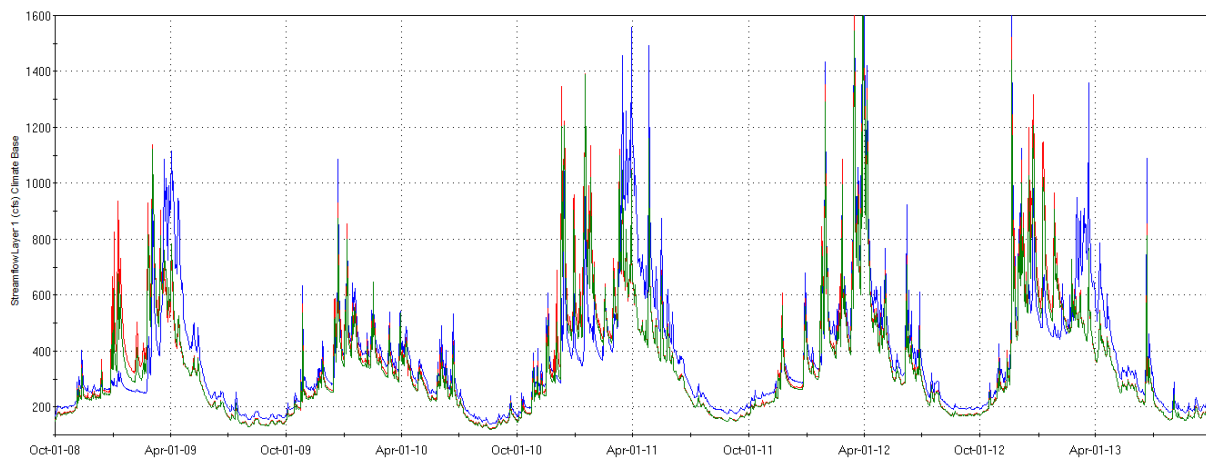
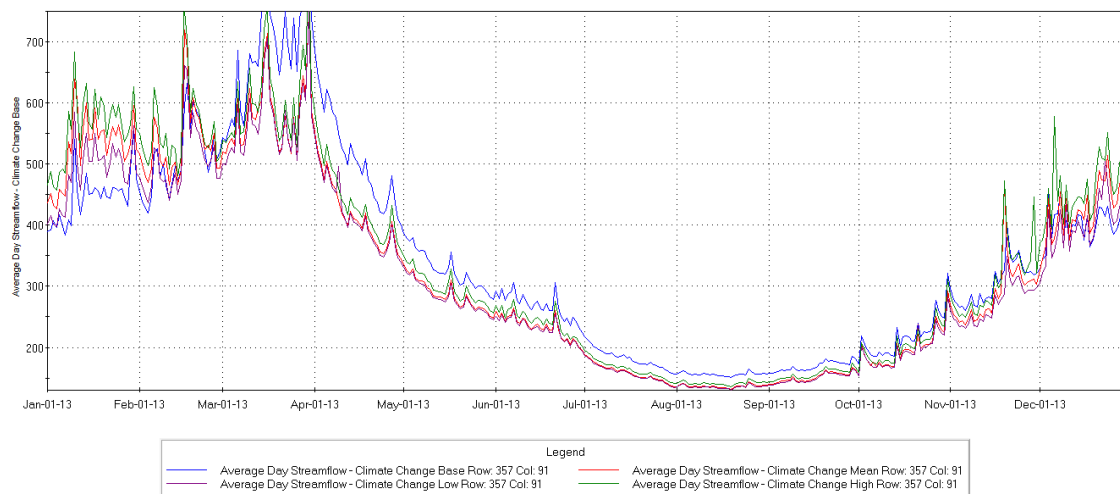


Figure 10.33: Simulated flow at the Dartford gage – baseline (blue) versus mean future (2050) climate change scenario (red) and low range future (2050) climate change scenario (green) for WY2008-WY2013 (WY2048-WY2053).



## 11 Conclusions

The objective of this study was to develop, calibrate, and test an integrated groundwater/surface water model for the Little Spokane River watershed. The model will serve as the scientific framework for better understanding the hydrology and hydrogeology of the Little Spokane watershed and provide support for reallocation of banked water rights and assignment of mitigation value to water storage and retiming projects.

To construct the integrated model, the study team formed by WEST Consultants and Earthfx Incorporated completed an extensive data synthesis and regional characterization. This work included: compilation and analysis of geologic, hydrogeologic, climate, and hydrologic data; development of conceptual geologic and hydrostratigraphic models; preparation of three-dimensional model surfaces; and assignment of initial estimates for hydrologic and hydrogeologic parameters. The hydrologic and hydrogeologic conditions in the Little Spokane River watershed are known to be highly variable owing to the complex geologic history of the area. Previous studies have also indicated that there is significant interaction between the groundwater and surface water systems.

The GSFLOW integrated groundwater/surface water model was constructed to represent hydrologic and hydrogeologic processes in the Little Spokane River watershed with an emphasis on the interaction and feedback between surface and subsurface processes. The GSFLOW code represents the integration of two open-source and well-documented programs, the U.S. Geological Survey codes PRMS and MODFLOW. The PRMS submodel computes a separate soil water balance for each cell on a 250 ft square grid and routes overland runoff to streams and lakes using a cascading flow algorithm. Hydrologic data including streamflow, climate, soil property, land-use, and topographic data were assembled and used to assign initial estimates for model parameters.

The MODFLOW groundwater flow submodel was constructed for the study area incorporating insights and data from the hydrologic, geologic and hydrostratigraphic conceptual model. Key features of the study area hydrogeology were carried forward into the numerical representation. The groundwater submodel was subdivided vertically into 10 numerical model layers, where each layer was occupied by one or more of the 12 mapped hydrostratigraphic units. Initial estimates of hydrologic properties were based on mainly on previous studies by Kahle *et al.* (2013), Golder (2004), and Ely and Kahle (2012).

Initial estimates for PRMS and MODFLOW submodel parameters were refined to better match observed daily streamflow at multiple gages, groundwater levels, and lake stage over a 5-year period with the best data coverage (WY2008 to WY2013). The model was validated by extending the simulation period back to WY2003 and comparing against observed streamflow, lake levels, and groundwater potentials. The calibrated model was able to provide reasonable matches to the complex patterns in the observed streamflow and groundwater level monitoring data. The quality of the model calibration was assessed through the use of calibration statistics, which indicated a good fit to the available groundwater and surface water data, as well as visual checks using hydrographs and contour maps. Results suggest that the hydrologic and hydrogeologic processes are well represented in the model. Discussions on uncertainty and model limitations, based on the results of these analyses, were provided.

The simulation period was then extended to WY2017 to provide a baseline to compare against additional simulations of future water use management scenarios, including increased withdrawals for domestic self-supply, retirement of selected water rights, implementation of artificial recharge projects, and future climatic change. Model outputs were compared against the baseline simulation to quantify the likely effects on groundwater and surface- water resources for each scenario. Hydrographs and maps were produced to illustrate changes in streamflow and groundwater levels at key locations. Monthly and annual average water budgets were created to show how the changes affected each part of the hydrologic cycle.

The future increase in pumping for self-supplied domestic use had the broadest impact on simulated groundwater levels because of the large number and distribution of increased withdrawals. The magnitude of the drawdowns was relatively small and the change in simulated streamflow at the Dartford gage was also minimal. The retirement of four water rights increased heads more significantly and the magnitude of change depended on the size of the retired water right. Streamflow was affected most notably in close proximity to the larger retired water rights, but only minimally at the Dartford gage. The operation of ten artificial recharge projects had more notable cumulative effect on streamflow at the Dartford gage, both due to the diversions of flow during the spring and due to the increased discharge during the summer and fall. The magnitude of the increases in summer and fall flows depends on many factors including location, hydraulic properties of the shallow aquifer, and infiltration rates. Local refinement of the model and further testing would be needed to select optimal sites and project design parameters.

Simulations of future climate change indicated that the model was most sensitive to predicted decreases in precipitation and less to the change in temperature. A representative emissions scenario (RCP 6.0) and median seasonal temperature and precipitations predictions from a range of GCMs was analyzed and showed that significant decreases in average mid-Autumn streamflow

(about 20 cfs) might be excepted. Other scenarios were simulated to determine model sensitivity to the range in temperature and precipitation changes.

The calibrated GSFLOW model presented in this report represents a solid foundation for undertaking watershed-scale water resources in the Little Spokane River watershed. It is also hoped that as additional data are collected and as time permits, that the model be subject to a program of continual refinement to improve the model calibration and reduce uncertainty in model predictions.

Report prepared by:

E.J. Wexler P.Eng., M.Sc., M.S.E.  
Vice President, Senior Hydrogeologist

Spencer Malott, M.E.Sc.  
Hydrologist

Dirk Kassenaar P.Eng., M.Sc.  
President, Senior Hydrogeologist

Asoka Kodippili, P.Geo.  
Hydrogeologist, Data Analyst

## 12 References

- Ader, M.J., 1996, Hydrogeology of the Green Bluff plateau, Spokane County, Washington: Washington State Department of Ecology Open File Technical Report 96-3, 1 v., 28 p.
- Anderson, A.L., 1927, Some Miocene and Pleistocene drainage changes in Northern Idaho: Moscow, University of Idaho, Idaho Bureau of Mines and Geology Pamphlet 18, 29 p.
- Anderson E.A., 1968, Development and testing of snow pack energy balance equations. Water Resource Research, v. 4, no. 1, pg. 19-37.
- Anderson, M.P. and Woessner W.W., 1992, Applied Ground Water Modelling -- Simulation of flow and advective transport: Academic Press, USA.
- Aspect Consulting LLC, 2015, Little Spokane Water Bank Feasibility Study: prepared for Spokane County, Project No. 140129, June 30, 2015, 193 p.
- Bear, J., 1979, Hydraulics of Groundwater: McGraw Hill International Book Company, New York, 567 p.
- Bjornstad, B., and Kiver, E., 2012, On the trail of the Ice Age floods the northern reaches: Sandpoint, Idaho, Keokee Books, 432 p.
- Boese, R.M., 1996, Aquifer delineation and baseline groundwater quality investigation of a portion of north Spokane County, Washington: Cheney, Eastern Washington University Master of Science Thesis, 223 p.
- Boleneus, D.E., and Derkey, R.E., 1996, Geohydrology of Peone Prairie, Spokane County, Washington: Washington Geology, v. 24, no. 1, p. 30–39. (Also available at [http://www.dnr.wa.gov/Publications/ger\\_washington\\_geology\\_1996\\_v24\\_no1.pdf](http://www.dnr.wa.gov/Publications/ger_washington_geology_1996_v24_no1.pdf).)
- Bolke, E. L., and Vaccaro, J. J., 1981, Digital-model simulation of the hydrologic flow system, with emphasis on ground water, in Spokane Valley, Washington and Idaho: U.S. Geological Survey Water-Resources Investigations Open-File Report 80-1300, 43 p.
- Carrara, P.E., Kiver, E.P., and Stradling, D.F., 1996, The southern limit of Cordilleran ice in the Colville and Pend Oreille valleys of northeastern Washington during the late Wisconsin glaciation: Canadian Journal of Earth Sciences, v. 33, no. 5, p. 769–778.
- CH2M HILL, 2000, Spokane aquifer joint board wellhead protection plan, Volume 1: report prepared for the Spokane Aquifer Joint Board.
- Chang, M., 2006, Forest hydrology -- an introduction to water and forests: CRC/Taylor & Francis, Boca Raton.
- Chiew, F.H.S. and McMahon, T.A., 1993, Assessing the adequacy of catchment streamflow yield estimates: Australian Journal of Soil Research, 31: 665-680.
- Chow, V.T. (ed.), 1964, Handbook of Applied Hydrology -- A Compendium of Water-Resources Technology: McGraw-Hill Book Company, New York, 1418p.
- Chung, S.K., 1975, Water resources management program—Little Spokane River Basin, WRIA 55: Olympia, Wash., Department of Ecology Policy Development Section, Water Resources Division, 83 p.

- Cline, D.R., 1969, Groundwater resources and related geology, north central Spokane and southeastern Stevens Counties, Washington: Washington Department of Water Resources Water Supply Bulletin 27, 195 p., 2 pls.
- Conners, J.A., 1976, Quaternary history of northern Idaho and adjacent areas: Moscow, Idaho, University of Idaho, Ph.D. dissertation, 504 p.
- Dames and Moore, Inc., and Cosmopolitan Engineering Group, 1995, Draft initial watershed assessment Water Resources Inventory Area 55, Little Spokane River watershed: Dames and Moore, Inc., and Cosmopolitan Engineering Group Open-File Technical Report 95-15, 33 p.
- Danish Hydrologic Institute, 2004, MIKE SHE User Manual: Hørsholm, Denmark
- DeWalle, D.R., and Rango, A., 2008, Principles of snow hydrology: Cambridge University Press, Cambridge, U.K., 410 p.
- Dickinson, W.T. and Whiteley, H.Q., 1970, Watershed areas contributing to runoff: International Association of Hydrologic Sciences Publication 96, p. 1.12-1.28.
- Dickinson, W.T., Whiteley, H.R., and Kelly, P.N., 1992, Extremes for Rainfall and Streamflow, How Strong are the Links?: Canadian Water Resources Journal, 17(3), 224-236.
- Doherty, J., 2015, Calibration and Uncertainty Analysis for Complex Environmental Models: Watermark Numerical Computing, Brisbane, Australia. ISBN: 978-0-9943786-0-6.
- Earthfx Incorporated, 2010, Water Balance Analysis of the Lake Simcoe Basin using the Precipitation-Runoff Modelling System (PRMS): prepared for the South Georgian Bay - Lake Simcoe Source Protection Region, October 2010, 106 p.
- Earthfx Incorporated, 2013, Tier 3 Water Budget and Local Area Risk Assessment for the Kelso and Campbellville Groundwater Municipal Systems -- Phase 1 Model Development and Calibration Report: report submitted to Conservation Halton, April, 2013, Toronto, ON.
- Earthfx Incorporated, 2018, Whitemans Creek Tier 3 Local Area Water Budget and Risk Assessment - Model Development and Calibration Report: prepared for the Grand River Conservation Authority and Lake Erie Source Protection Region, March 2018, 485 p.
- Ellis, C., Pomeroy, J., Brown, T., and MacDonald, J., 2010, Simulation of snow accumulation and melt in needleleaf forest environments: Hydrol. Earth Syst. Sci., v. 14, no. 6, p. 925-940.
- Ely, D.M. and Kahle, S.C., 2012, Simulation of groundwater and surface-water resources and evaluation of water-management alternatives for the Chamokane Creek basin, Stevens County, Washington: U.S. Geological Survey Scientific Investigations Report 2012-5224, 74 p.
- EMCON, 1992, Deer Park ground water characterization study, hydrogeologic summary report, v. 1: Bothell, Wash., EMCON Northwest, Inc., project 0622-001.02, 83 p.
- Foxx, T.S., Tierney, G.D., and Williams, J.M., 1985, Rooting Depths of Plants Relative to Biological and Environmental Factors: Los Alamos National Laboratory, NM., 28 p.
- Freeze, R.A. and J.A. Cherry, 1979, Groundwater: Prentice-Hall Inc., 604p
- Golder Associates, Inc., 2003, Little Spokane (WRIA 55) and Middle Spokane (WRIA 57) watershed planning phase II–Level 1 assessment - data compilation and analysis: Seattle, Golder

- Associates, Inc., prepared under grant no. 9800300 from the Washington Department of Ecology, variously paginated.
- Golder Associates, Inc., 2004, Final report to the Little and Middle Spokane watershed WRIA 55 and 57 planning unit, level 2 technical assessment—Watershed simulation model: Seattle, Golder Associates, Inc., prepared under grant no. 9800300, from the Washington Department of Ecology, 51 p., 4 appendixes.
- Harbaugh, A.W., 2005, MODFLOW-2005, the U.S. Geological Survey modular ground-water model—the Ground-Water Flow Process: U.S. Geological Survey Techniques and Methods 6-A16, variously paged.
- Healy, R.W., 2010. Estimating Groundwater Recharge: Cambridge University Press, 256pp.
- Homer, C.G., Dewitz, J.A., Yang, L., Jin, S., Danielson, P., Xian, G., Coulston, J., Herold, N.D., Wickham, J.D., and Megown, K., 2015, Completion of the 2011 National Land Cover Database for the conterminous United States-Representing a decade of land cover change information: Photogrammetric Engineering and Remote Sensing, v. 81, no. 5, p. 345-354
- Horton, K.W., 1958, Rooting Habits of Lodgepole Pine: Forest Research Division, Canada Dept. of Northern Affairs and National Resources - Forestry Branch, Technical Note No. 67, 26 p.
- Hsieh, P.A., Barber, M.E., Contor, B.A., Hossain, Md. A., Johnson, G.S., Jones, J.L., and Wylie, A.H., 2007, Ground-water flow model for the Spokane Valley-Rathdrum Prairie Aquifer, Spokane County, Washington, and Bonner and Kootenai Counties, Idaho: U.S. Geological Survey Scientific Investigations Report 2007-5044, 78 p.
- Hunt, R., Walker, J., Selbig, W., Westenbroek, S., and Regan, R., 2013, Simulation of climate-change effects on streamflow, lake water budgets, and stream temperature using GSFLOW and SNTMP, Trout Lake Watershed, Wisconsin: U.S. Geological Survey Scientific Investigations Report 5159, U.S. Dept. of the Interior, Reston, Va.
- Huntington, J.L., and R.G. Niswonger, 2012, Role of surface-water and groundwater interactions on projected summertime streamflow in snow dominated regions -- An integrated modeling approach: Water Resources Research 48(11): doi: 10.1029/2012WR012319.
- Jensen, M.E., and Haise, H.R., 1963, Estimating evapotranspiration from solar radiation: Proceedings of the American Society of Civil Engineers, Journal of Irrigation and Drainage, v. 89, no. IR4, p. 15-41.
- Kahle, S.C., Olsen, T.D., and Fasser, E.T., 2013, Hydrogeology of the Little Spokane River Basin, Spokane, Stevens, and Pend Oreille Counties, Washington: U.S. Geological Survey Scientific Investigations Report 2013-5124, 52 p., <http://pubs.usgs.gov/sir/2013/5124/>
- Kassenaar, J.D.C., 2013, VIEWLOG (version 4). Microsoft Windows, v.3.1 through 8.1. Toronto, ON: VIEWLOG Systems Inc.
- Kiver, E.P., and Stradling, D.F., 1982, Quaternary geology of the Spokane area: in Roberts, S., and Fountain, D., eds., 1980 Field Conference Guidebook: Spokane, Wash., Tobacco Root Geological Society, p. 26-44.
- Kiver, E.P., and Stradling, D.F., 2001, Ice age floods in the Spokane and Cheney area: Washington Field trip guide, October 20, 2001, Cheney, WA., Ice Age Floods Institute, 48 p.

- Kiver, E.P., Stradling, D.F., and Moody, U.L., 1989, Glacial and multiple flood history of the northern borderlands—Trip B: in Joseph, N.L., and others, eds., *Geologic guidebook for Washington and adjacent areas*, Washington Division of Geology and Earth Resources Information Circular 86, p. 321–335.
- Klepper, E.L., Gano, K.A., and Cadwell, L. L., 1985, *Rooting Depth and Distributions of Deep Rooted Plants in the 200 Area Control Zone of the Hanford Site*: Prepared for the U.S. Department of Energy, Pacific Northwest Laboratory, January 1985, 206 p.
- Knapp, C.L., Stoffel, T.L., and Whitaker, S.O., 1980, *Insolation Data Manual - Long-term Monthly Averages of Solar Radiation, Temperature, Degree-days and Global KT for 248 National Weather Service Stations*: published by the Solar Energy Information Data Bank - Solar Energy Research Institute, SERI/SP-755-789, October 1980.
- Kohzu, A., Matsui, K., Yamada, T., Sugimoto, A., and Fujita, N. 2003, Significance of rooting depth in mire plants -- evidence from natural 15N abundance: *Ecological Research*, 18(3), 257-266.
- Komatsu, H., Kuklohnme, T., and Otsuki, K., 2011, Increasing annual runoff—broadleaf or coniferous forests?: *Hydrological Processes*, 25(2), 302-318.
- Krause, P., Boyle, D. P., and Bäse, F., 2005, Comparison of different efficiency criteria for hydrological model assessment: *Advances in Geosciences*, 5(5), 89-97.
- Landau Associates, Inc., and others, 1991, *Colbert landfill remedial design/remedial action*, Spokane County, Washington, Volume I of III—Final phase I engineering report: Landau Associates, Inc., (under contract to) Spokane County, Washington, 1 v.
- Leavesley, G.H., Lichty, R.W., Troutman, B.M., Saindon, L.G., 1983, *Precipitation-Runoff Modeling System—User's Manual*: USGS Water Resources Investigations Report 83–4238
- Linsley, R.K., Kohler, M.A., and Paulhus, J.L.H., 1975, *Hydrology for Engineers*: 2nd ed., McGraw-Hill Company, 482 p.
- Magirl, C.S., and Olsen, T.D., 2009, Navigability potential of Washington rivers and streams determined with hydraulic geometry and a geographic information system: USGS Scientific Investigations Report 2009–5122, 22 p. (Also available at <http://pubs.usgs.gov/sir/2009/5122/>.)
- Maidment, D.R., ed., 1992, *Handbook of hydrology*: McGraw-Hill. 1424pp.
- Markstrom, S.L., Niswonger, R.G., Regan, R.S., Prudic, D.E., and Barlow, P.M., 2008, GSFLOW-coupled ground-water and surface-water FLOW model based on the integration of the Precipitation-Runoff Modeling System (PRMS) and the Modular Ground-Water Flow Model (MODFLOW-2005): USGS Techniques and Methods book 6, chap. D1, 240 p.
- Markstrom, S. L., Regan, R. S., Hay, L. E., Viger, R. J., Webb, R. M., Payn, R. A., and LaFontaine, J. H., 2015, PRMS-IV, the precipitation-runoff modeling system, version 4: U.S. Geological Survey Techniques and Methods, book 6, chap. B7, 158 p., <http://dx.doi.org/10.3133/tm6B7>.
- McDonald, E.V., and Busacca, A.J., 1992, Late Quaternary stratigraphy of loess in the Channeled Scabland and Palouse regions of Washington State: *Quaternary Research*, v. 38, p. 141–156.
- Merritt, M.L., and Konikow, L.F., 2000, Documentation of a computer program to simulate lake-aquifer interaction using the MODFLOW groundwater flow model and the MOC3D solute-transport model: USGS Water-Resources Investigations Report 00-4167, 146 p.

- Miller, F.K., 1974, Preliminary Geologic Map of the Newport Number 2 Quadrangle, Pend Oreille and Stevens County, Washington: State of Washington, Department of Natural Resources, Division of Geology and Earth Resources.
- Miller, F.K., 2000, Geologic map of the Chewelah 30' X 60' quadrangle, Washington and Idaho: USGS Miscellaneous Field Studies MF-2354, at <http://pubs.usgs.gov/mf/2001/2354/>.
- Moore, I.D., Grayson, R.B. and Ladson, A.R., 1991, Digital Terrain Modelling -- A Review Of Hydrological, Geomorphological, and Biological Applications: in Terrain Analysis And Distributed Modelling In Hydrology: K.J. Beven And I.D. Moore (ed), John Wiley & Sons.
- Nash, J.E. and J.V. Sutcliffe, 1970, River flow forecasting through conceptual models, Part I - A discussion of principles: *Journal of Hydrology* 10, p. 282-290.
- Niswonger, R.G., and Prudic, D.E., 2005, Documentation of the Streamflow-Routing (SFR2) Package to include unsaturated flow beneath streams — A modification to SFR1: U.S. Geological Survey Techniques and Methods 6-A13.
- Niswonger, R.G., Prudic, D.E., and Regan, R.S., 2006, Documentation of the Unsaturated-Zone Flow (UZF1) Package for modeling unsaturated flow between the land surface and the water table with MODFLOW-2005: USGS Techniques and Methods Book 6, Chapter A19, 62 p.
- Niswonger, R.G., Panday, Sorab, and Ibaraki, Motomu, 2011, MODFLOW-NWT, A Newton formulation for MODFLOW-2005: USGS Techniques and Methods 6–A37, 44 p.
- Niswonger, R.G., K.K. Allander, and A.E. Jeton, 2014, Collaborative modelling and integrated decision support system analysis of a developed terminal lake basin. *Journal of Hydrology*: doi: 10.1016/j.jhydrol.2014.05.043.
- Searcy, J.K, 1959, Flow-Duration Curves; Manual of Hydrology: Part 2, Low-Flow Techniques: USGS Water-Supply Paper 1542-A.
- Seibert, J. and B.L. McGlynn, 2007, A new triangular multiple flow direction algorithm for computing upslope areas from gridded digital elevation models: *Water Resources Research*, v. 43, 8 p.
- Sloto, R.A., and Crouse, M.Y., 1996, HYSEP: A Computer Program for Streamflow Hydrograph Separation and Analysis: U.S. Geological Survey Water-Resources Investigations Report 1996–4040, 46 p., <https://pubs.er.usgs.gov/publication/wri964040>.
- Spitz, K., and Moreno, J., 1996., A practical guide to groundwater and solute transport modeling: John Wiley, New York.
- Spokane County, 2006, Watershed Management Plan Water Resources Area 55–Little Spokane River and Water Resources Area 57–Middle Spokane River: Little Spokane and Middle Spokane River Planning Unit, 120 p.
- Spokane County, 2009, WRIA 55 (Little Spokane River) Groundwater Inventory and Mapping Project, June 2009, prepared for WRIA 55/57 Watershed Implementation Team: Spokane, Wash., Spokane County Water Resources, 16 p.
- Spokane County, 2010a, Little Spokane Groundwater Elevation and Stream Flow Monitoring Project, June 30, 2010, prepared for WRIA 55/57 Watershed Implementation Team: Spokane, Wash., Spokane County Water Resources, 52 p.

- Spokane County, 2010b, Spokane County Residential Water Use Survey, prepared for WRIA 55/57 Watershed Implementation Team and WRIA 56 Watershed Implementation Team: Spokane, WA., Spokane County Water Resources, variously paged.
- Spokane County, 2011, Little Spokane Groundwater Elevation and Stream Flow Monitoring Project Technical Memorandum–2011 Project Update, June 30, 2011, prepared for WRIA 55/57 Watershed Implementation Team: Spokane, WA.
- Spokane County Water Resources, 2011, Spokane County Water Demand Forecast Model, pp. 19
- Spokane County Water Resources, 2013, Spokane County Water Demand Forecast Model, Model 3.0 and 2013 Forecast Update, pp. 96.
- Stoffel, K.L., Joseph, N.L., Waggoner, S.Z., Gulick, C.W., Korosec, M.A., and Bunning, B.B., 1991, Geologic map of Washington northeast quadrant: Washington Division of Geology and Earth Resources, Geologic map GM-39, scale 1:250,000.
- Strong, W., Roi, G., 1983, Rooting depths and successional development of selected boreal forest communities: Canadian Journal of Forest Research, v. 13, no. 4, p. 577-588.
- Tanvir Hassan, S.M., M.W. Lubczynski, R.G. Niswonger, and Z. Su, 2014, Surface-groundwater interactions in hard rocks in Sardon catchment of western Spain -- an integrated modeling approach: Journal of Hydrology: doi: 10.1016/j.jhydrol.2014.05.026.
- U.S. Forest Service, 2010, Ice Age floods in the Pacific Northwest [poster]: U.S. Forest Service, modified by the Ice Age Flood Institute and Eastern Washington University.
- U.S. Geological Survey, 2017, National Hydrography Dataset Plus High Resolution (NHDPlus HR) - USGS National Map Downloadable Data Collection
- Van Rees, K., 1997, Rooting Patterns of Boreal Tree Species: final report submitted to the Prince Alberta Model Forest Association, January 1997.
- Waitt, R.B., Jr., and Thorson, R.M., 1983, The Cordilleran ice sheet in Washington, Idaho, and Montana: in Wright, H.E., and Porter, S.C. (eds), Late-Quaternary environments of the United States, v. 1: Minneapolis, University of Minnesota Press, p. 53–70. Washington Department of Ecology, 2009a, Focus on Water Banking, Publication No. 09-11-035.
- Washington Department of Ecology, 2009b, Focus on Little Spokane Watershed, Publication No. 09-11-012.
- Washington Department of Ecology, 2015, Focus on Water Availability: Little Spokane Watershed, WRIA 55, Publication No. 11-11-059.
- Washington Department of Ecology and WestWater Research, 2004, Analysis of Water Banks In the Western States. Publication No. 04-11-011.
- Washington State Division of Geology and Earth Resources, 2005, Digital 1:100,000-scale geology of Washington State, ver. 1.0: Washington Division of Geology and Earth Resources database, at [http://www.dnr.wa.gov/ResearchScience/Topics/GeosciencesData/Pages/gis\\_data.aspx](http://www.dnr.wa.gov/ResearchScience/Topics/GeosciencesData/Pages/gis_data.aspx).
- Winkler, R., Moore, R., Redding, T., Spittlehouse, D., Carlye-Moses, D., and Smerdon, B., 2009, Chapter 6: hydrological processes and watershed response. Compendium of forest hydrology and geomorphology in British Columbia. BC Ministry of Forests and Range, Research Branch, Victoria, BC.